Flexible Regression Models for Functional Neuroimaging

by

Kathakali Ghosh Mukherjee

Submitted in fulfillment of the requirements for the
Degree of Doctor of Philosophy

in the

School of Mathematics and Statistics
College of Science and Engineering
University of Glasgow

May 2016

To The Holy Almighty

UNIVERSITY OF GLASGOW

Abstract

College of Science and Engineering
School of Mathematics and Statistics

Doctor of Philosophy

by Kathakali Ghosh Mukherjee

Current practice for analysing functional neuroimaging data is to average the brain signals recorded at multiple sensors or channels on the scalp over time across hundreds of trials or replicates to eliminate noise and enhance the underlying signal of interest. These studies recording brain signals non-invasively using functional neuroimaging techniques such as electroencephalography (EEG) and magnetoencephalography (MEG) generate complex, high dimensional and noisy data for many subjects at a number of replicates. Single replicate (or single trial) analysis of neuroimaging data have gained focus as they are advantageous to study the features of the signals at each replicate without averaging out important features in the data that the current methods employ. The research here is conducted to systematically develop flexible regression mixed models for single trial analysis of specific brain activities using examples from EEG and MEG to illustrate the models. This thesis follows three specific themes: i) artefact correction to estimate the 'brain' signal which is of interest, ii) characterisation of the signals to reduce their dimensions, and iii) model fitting for single trials after accounting for variations between subjects and within subjects (between replicates). The models are developed to establish evidence of two specific neurological phenomena - entrainment of brain signals to an α band of frequencies ($8-12$Hz) and dipolar brain activation in the same α frequency band in an EEG experiment and a MEG study, respectively.

Chapter 1 gives an overview of these two neuroimaging methods, the neuroimaging phenomena being studied by the experiments, the data collected from the experiments that are used in this research and a discussion of prevalent statistical methods in analysing such data. A specific artefact in neuroimaging signals is that of spikes. In this thesis, spikes in the data due to transcranial magnetic stimulation (TMS) of the brain recorded by EEG are estimated using a flexible additive model framework. This model also simultaneously estimates other artefacts such as a cyclic mains current and long-term trend components that may be present in the signal. This novel *artefact correction* and signal estimation method is described in Chapter 2. A simulation study is also described as a part of this chapter, to validate the additive model framework for estimation of brain signals. MEG and EEG recordings comprise of high resolution signals which have particularly high sampling frequency in time. In order to gain efficiency during model fitting of such data, it is therefore useful to reduce the data dimensionality prior to model fitting. A *data reduction* strategy based on characterisation of the signals is proposed in Chapter 3, in which the 'brain' signals of interest are described in terms of a small number of functional curves with the aim of capturing the variable phase/frequency and amplitude of the signal of interest at each channel/sensor. A subset of these signals are then summarised in terms of the characteristic functions for a channel or set of channels associated with the region where the neurological phenomenon occurs in the brain. Summary results for the remaining subjects are reported in Appendix A. Chapters 4 and 5 propose cutting-edge *mixed effects model fitting* for the neuroimaging data, with an aim to explain the particular neurological phenomenon of interest. Entrainment is modelled from the TMS-EEG signals in Chapter 4. Dipoles during pre-stimulus period in the MEG data are modelled in Chapter 5. Main contributions of the thesis and future work are discussed in Chapter 6.

Contents

List of Figures

List of Tables

Acknowledgements

I thank my supervisors, Prof. Adrian W Bowman and Dr. Claire Miller, both of whom have been tremendous mentors, encouraging and providing many opportunities for me to grow as a researcher. I am immensely grateful for their guidance, insight and support throughout the course of this PhD, helping me not only professionally and academically but also in overcoming my personal barriers and challenges.

I thank the School of Mathematics and Statistics at the University of Glasgow for the Teaching Assistantship, that funded my research and helped me develop my teaching skills. I also thank our collaborators Prof. Joachim Gross and Dr. Gregor Thut of the Centre for Cognitive Neuroimaging (CCNi) at the University of Glasgow for making the experimental data sets used in this thesis available and for the valuable discussions I had with them to aid me in understanding the rich and complex neuroimaging data and the associated statistical problems in the context of neuropsychology. I especially thank Dr. Massimo Ventrucci for his own statistical research with these data which forms the preliminary foundation for much of this thesis and also for sharing his knowledge and expertise about the data and basic concepts in statistical neuroimaging, when I was first introduced to this field of research.

My heartfelt thanks to the academic staff of the School of Mathematics and Statistics, especially Prof. Marian E Scott, Prof. Dirk Husmeier and Dr. Ludger Evers who as the Internal Committee of Examiners, regularly assessed my research for annual progression and provided helpful recommendations to improve my work further. I also thank the Administrative and IT Staff of both the School of Mathematics and Statistics and the College of Science and Engineering, your continual efforts and support in sorting out student travel, administrative paperwork and IT issues on my behalf were imperative in making my life as a doctoral researcher at the university smooth, efficient and enriching.

I extend special thanks to my family and friends without whose sacrifices, well wishes and belief in my abilities, this work would not have come to fruition. I would like to express my heartfelt gratitude to my husband Ankur and son Arko for their unconditional support throughout my entire PhD journey. I would especially like to mention here the contributions of my parents: Maa and Baba, you have

always instilled in me a deep passion for knowledge and constant learning which has inspired me every single day in this path. Thanks also to my family members Anita Mukherjee, Prof. Sib Nath Mukherjee, Amrita and Shantanu for inspiring me to do my best in face of every challenge and propelling me towards a career in research. Thank you, Dr. Shanta Davie, Tuesday Moodie and Cathie Scotchford for your invaluable friendship and help in the last one year.

I thank all my peers and colleagues at the University, especially Alastair, Ruth, Maria, Joanna, Helen, Gary, Kelly, Charis and Khunes - interactions with you during my stay at Glasgow made it much more interesting and enjoyable. I also thank all my friends - especially Dhanyaa, Maggie and Smita who stood by me through especially difficult times.

Largely due to your guidance, encouragement and good wishes, I have reached this stage despite all the odds. Thank you all.

Declaration of Authorship

I, KATHAKALI GHOSH MUKHERJEE, declare that except where explicit reference is made to the contribution of others, this thesis titled, 'FLEXIBLE REGRESSION MODELS FOR FUNCTIONAL NEUROIMAGING' and the work presented in it are my own. I also declare that this work has not been submitted for any other degree at the University of Glasgow or any other institution,

I confirm that:

- This work was done wholly or mainly while in candidature for a research degree at this University.
- Where I have consulted the published work of others, this is always clearly attributed.
- Where I have quoted from the work of others, the source is always given. With the exception of such quotations, this thesis is entirely my own work.
- I have acknowledged all main sources of help.
- Where the thesis is based on work done by myself jointly with others, I have made clear exactly what was done by others and what I have contributed myself.

Signed:

Printed Name: KATHAKALI GHOSH MUKHERJEE

Abbreviations

AM	Additive Models
EEG	Electroencephalography
FDA	Functional Data Analysis
ICA	Independent Component Analysis
LM	Linear Models
MEG	Magnetoencephalography
MEM	Mixed Effects Models
TMS	Transcranial Magnetic Stimulation

Symbols

α	frequency	Hz
ω	angular frequency	rads^{-1}
β	model coefficients for fixed effects	
b	model coefficients for random effects	
ϵ	error term for linear models	
$m(.)$	smooth functions	

"Everything must be made as simple as possible. But not simpler."

Albert Einstein (paraphrased)

Chapter 1

Introduction

1.1 Context

Noisy, high resolution, discrete, spatiotemporal data are a common occurrence in many areas, for example in the fields of signal processing and image analysis. Functional data analysis (FDA), due mainly to Ramsay and Silverman (2002, 2005), provides a powerful theoretical framework to analyse such data. One key assumption of functional data analysis is smoothness, simultaneously allowing discrete data to be represented as a continuous function and reducing noise. Further, high resolution signals create large volumes of data which may be computationally expensive during analysis. Non-parametric smoothing strategies are effective and proven methods of down-sampling without losing much of the relevant information, resulting in computational efficiency. This thesis develops a flexible regression modelling framework to model noisy complex, high resolution data from functional neuroimaging records. It employs non-parametric smoothing methods and flexible regression models to correct for noise, down-sample to characterise data using fewer parameters and describe specific brain activities within this framework.

Functional neuroimaging techniques such as magnetoencephalography (MEG) and electroencephalography (EEG) are widely used for understanding brain function. They measure electromagnetic activity in the brain by recording electric currents

on and magnetic fields outside the head. Fig. 1.1 is a schematic representation of the electric current q generated within the brain, and consequent electric and magnetic fields H and B respectively that are perpendicular to each other. The data are collected at a very high resolution in time and space using a large number of channels or sensors around the scalp. A set of time series, which are spatially correlated, are simultaneously recorded from these channels or sensors. Experimental data using such non-invasive techniques are often collected with a goal of understanding specific neurological phenomena. Further, non-invasive Transcranial Magnetic Stimulation (TMS), first demonstrated by Barker et al. (1985), is used to study the functions of the brain by exposing it to controlled external magnetic stimuli. During a TMS administration, an external magnetic field is applied with the help of a magnetic coil in a pulsating manner, resulting in a current flow inside the brain (Hallett, 2000). This can temporarily excite or inhibit specific areas of the brain, altering brain activation patterns. Recently it has been possible to obtain EEG recordings of the brain while administering TMS in real time leading to experimentation in TMS-EEG (Ilmoniemi et al., 1997, Komssi et al., 2004, Miniussi and Thut, 2009). This generates functional data which provides information on how TMS affects brain function. The two motivating data sets

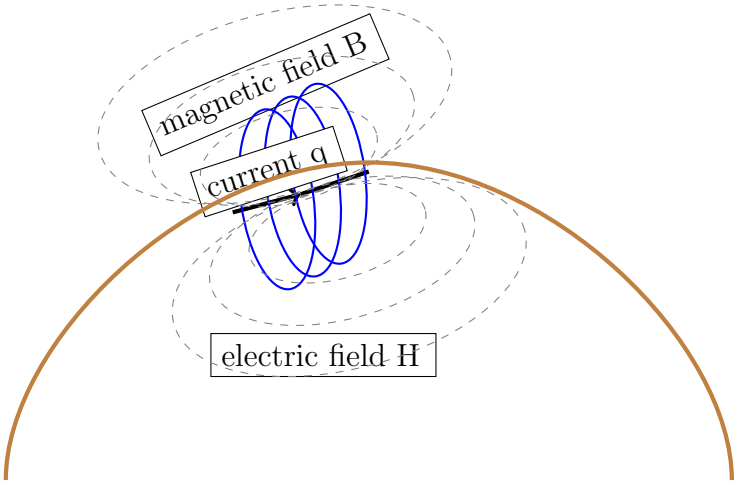

FIGURE 1.1: Electromagnetic field (electric field H denoted by grey dashed lines and magnetic field B denoted by solid blue rings) around the scalp, originating from the electric current q in the brain (solid black line).

for this thesis are from two neuropsychological experiments that are designed to

collect TMS-EEG and MEG recordings in several individual subjects before and after stimulus. Throughout this thesis, data from these two experiments are used to address the statistical problems as well as to demonstrate the application of statistical modelling strategies proposed as novel solutions for these problems. In particular, the goal of statistical modelling of these two data sets is to establish evidence of two distinct brain functions, namely (i) entrainment of brain signals to a specific range of frequencies and (ii) dipolar activation in the brain.

One of the data sets comes from EEG recordings of an experiment to investigate the entrainment of brain signals to a specific frequency band on being exposed to transcranial magnetic stimulation of similar frequencies (Thut et al., 2011a). The other data set comprises of MEG recordings from an experiment that studies the effect of brain state prior to stimulus presentation on reaction time in the motor areas as a consequence of visual stimuli (Schnitzler and Gross, 2005, Ventrucci et al., 2011).

A review of the literature spanning the fields of statistical modelling, functional data analysis, statistical signal processing and functional neuroimaging, which provide the foundation of this research, is expounded throughout this chapter. Section 1.2 describes these two neurological phenomena that are being investigated in the context of two motivating examples. Section 1.3 gives an overview of the currently applied statistical methodology that describes the neurological phenomena of interest. Section 1.4 elucidates the specific statistical problems encountered in investigating the neurological phenomena of interest and methods proposed in this thesis to address these problems.

1.2 Motivation and Data

Entrainment of brain signals to stimuli at regular temporal frequencies in the α band ($8-12$ Hz) is the focus of many neuroimaging studies (De Graaf et al., 2013, Mathewson et al., 2012, Romei et al., 2010, Spaak et al., 2014). It is also well established that the human visual cortex shows the strongest resonance to the 10

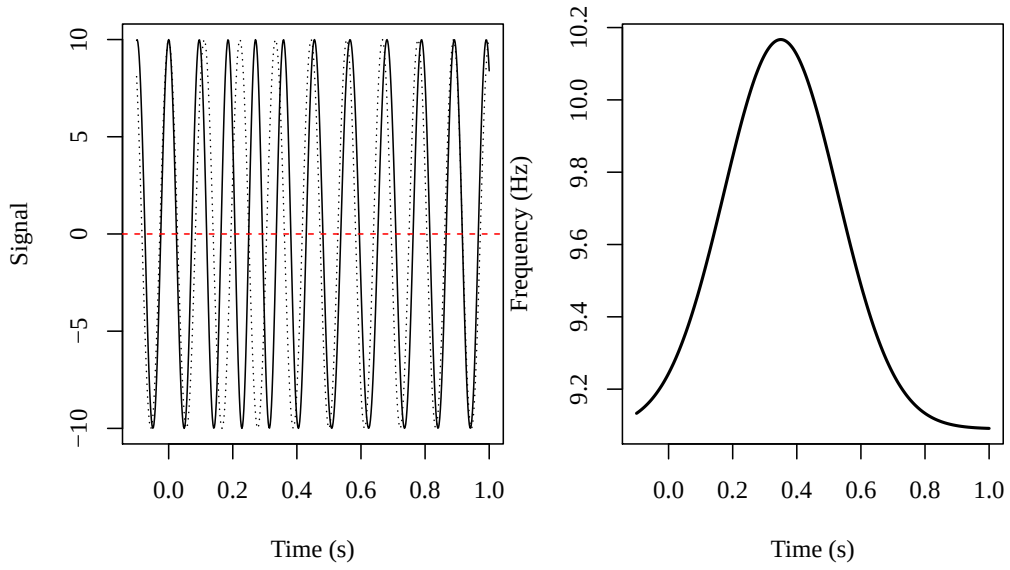

FIGURE 1.2: (Left) Diagrammatic representation of an entrained signal where the frequency changes to $10.2Hz$ gradually as the TMS pulses are applied. The dotted line shows the signal at a constant frequency (slightly below $9.2Hz$) and the solid line shows the entrained signal. (Right) The corresponding variable frequency function of the signal that starts at a pre-stimulus frequency of around $9.2Hz$, reaches the $10.2Hz$ frequency just before 0.4s and then drops down gradually.

Hz visual stimuli (Herrmann, 2001). Entrainment of a signal occurs when either the instantaneous frequency of the signal *changes* to oscillate in the frequency range of interest or the signal *retains* this frequency for at least one complete oscillation if it is already oscillating in that frequency. Further, the degree of entrainment *may be dependent* on the phase of the signal at the onset of the TMS pulses. The amplitude of such signal, if it is in phase with the TMS pulses, may *enhance* over time. Fig. 1.2 is a simulated example of a signal changing frequency to 10.2 Hz after the administering of the stimulus. This feature is clearly demonstrated in the corresponding plot of the frequency function which shows a clear entrainment to the α-band frequency of 10.2 Hz. A signal of constant initial frequency of 9.2 Hz is denoted by the dotted blue line in Fig. 1.2 (Left), to provide a comparison with the entrained signal (solid line). The TMS-EEG experiment, the data from which is analysed here, was designed to investigate evidence of entrainment of brain signals to the specified range of α frequencies. Thut et al. (2011a) present evidence of entrainment of brain signals when TMS pulses are administered in short regular

bursts, perpendicular to the target gyrus. The data comprise of EEG recordings from 8 subjects under 4 conditions, each having 54 trials or replicates. Data are recorded at $S = 60$ channels connected to an EEG cap and $T = 5500$ time points spanning a time span of 1.1 seconds indicating that the data have very high resolution both spatially and temporally, and specifically over time. Fig. 1.3 shows the placement of EEG channels over the scalp projected on a $2D$ surface. In a single replicate for an individual subject, at each of these channels, a time trace is recorded as the EEG signal for the duration of 1.1 seconds. Each trial is repeated 54 times for an experimental condition resulting is a high dimensional array of 8 (subjects) $\times$4 (conditions) $\times$54 (replicates) $\times$60 (channels) $\times$5500 (time points) discrete observations. This complexity poses the problem of high dimensionality that has to be handled while analysing such data. The region encircled by the blue dotted line in Fig. 1.3 is the region which is most predominantly affected by the change in magnetic field as the magnetic coil of the TMS equipment is placed over that region. Hence the data from channels in this region are selectively modelled in this thesis to detect maximum effect due to TMS stimulus. The main condition comprises of 5 TMS pulses, administered at regular intervals in an orientation perpendicular to the gyrus (a portion of the parietal lobe of the brain) with the exact inherent subject specific α frequency. The orientation provides maximum impact of the TMS on the brain activity. The inherent α frequency for each subject is previously determined in an MEG recording. The EEG signals are recorded simultaneously with the administration of the TMS pulses in each channel for several replicates in the subjects at (1) the main condition, (2) when the orientation of the TMS equipment has been rotated by 90°, (3) when the TMS pulses are applied asymmetrically and (4) when the pulses are only sound clicks. It has been shown in Thut et al. (2011a) that under the main condition, brain signals entrain themselves to the α-band frequency that the TMS pulses are applied at. Considering that the inherent α-band frequency of an individual is $10Hz$, the time segment of 0.1s before the presentation of the first TMS pulse is referred to as 'pre-stimulus period' in this work. The next 0.4s when the 5 TMS pulses are administered at the inherent α frequency is known as the 'stimulus period'. The

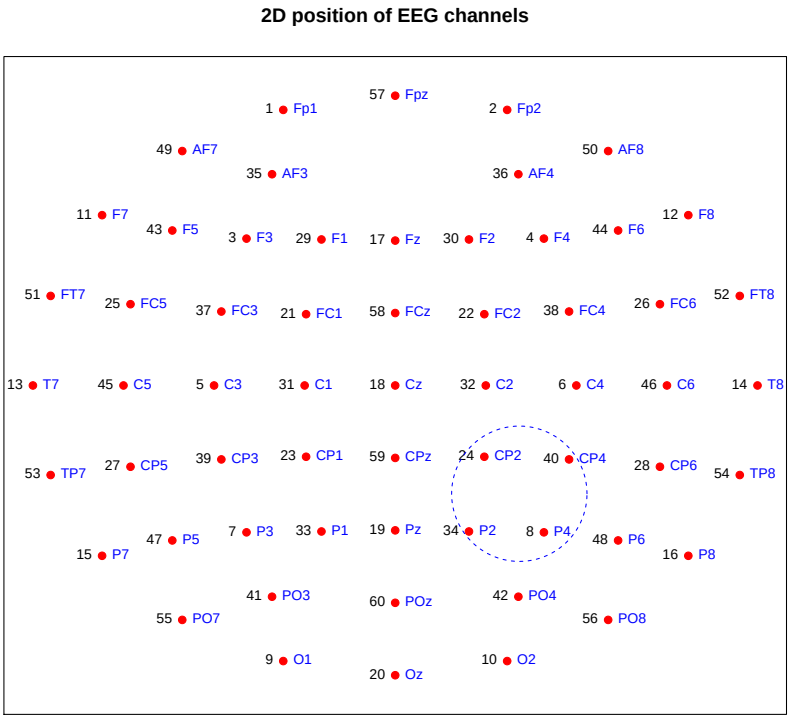

FIGURE 1.3: 2 dimensional spatial map of the brain surface showing EEG channel locations. The dotted circle represents the region of interest where the effect of TMS is maximum.

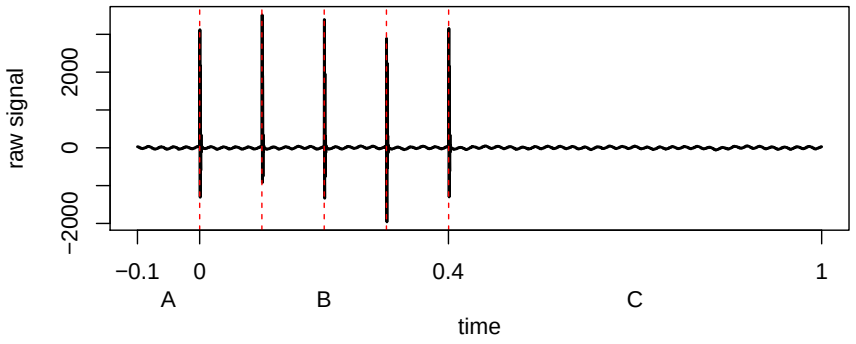

FIGURE 1.4: (A) Pre-stimulus, (B) Stimulus and (C) Post-stimulus time periods in a time trace of the signal at one channel for a replicate of an individual subject from the TMS EEG experiment.

remaining 0.6s of the recording is termed as the 'post-stimulus period'. The break up of the time span into the three time segments is depicted in Fig. 1.4.

When the TMS-EEG data are presented, they have noise and artefacts, which pose problems during single trial analysis. Due to the nature of the experiment considered here, TMS pulses generate spikes at the time they are administered. These spikes are high frequency and high amplitude signals in the data that decay very rapidly, as the TMS pulse stops very quickly. Further, due to the presence of electrical equipments and apparatus where data is collected, a 50 Hz mains current is picked up by the recordings. Sometimes, random long-term artefacts are present in some of the recordings which are similar to non linear trends. The artefacts are further discussed in greater detail in the next section.

Dipolar brain activity is the focus of the other data set investigated in this thesis. In a typical MEG experimental setting, dipolar activity when the adjacent groups of sensors oscillate with similar frequency in an out-of-phase manner, is of interest. This dipolar behaviour can be modelled and simulated as shown for the prestimulus period in Ventrucci et al. (2014).

The data set under investigation results from this MEG setting and comprises of data simultaneously recorded at $S = 264$ magnetic sensors on a helmet around the scalp. A $2D$ representation of the spatial distribution of the MEG sensors from a flattened MEG helmet is shown in Fig. 1.5. Data from all sensors are available for numerous replicates (number of replicates around $80-120$) each on 17 subjects and 4 experimental conditions for $T = 1000$ time points in 1s during which the main stimulus first activates the visual cortex and the response subsequently activates the motor cortex of the brain. A dipolar brain activity can be thought of as a scenario when the polarity of amplitude in adjacent groups of sensors tend to oscillate in an out-of-phase manner within an α range of frequencies for at least one complete oscillation. Fig. 1.6 is a spatial map of the brain at a particular time point based on the MEG data set - where a dipole is illustrated with the white and red regions representing the two opposite poles that oscillate with similar frequency and out of phase.

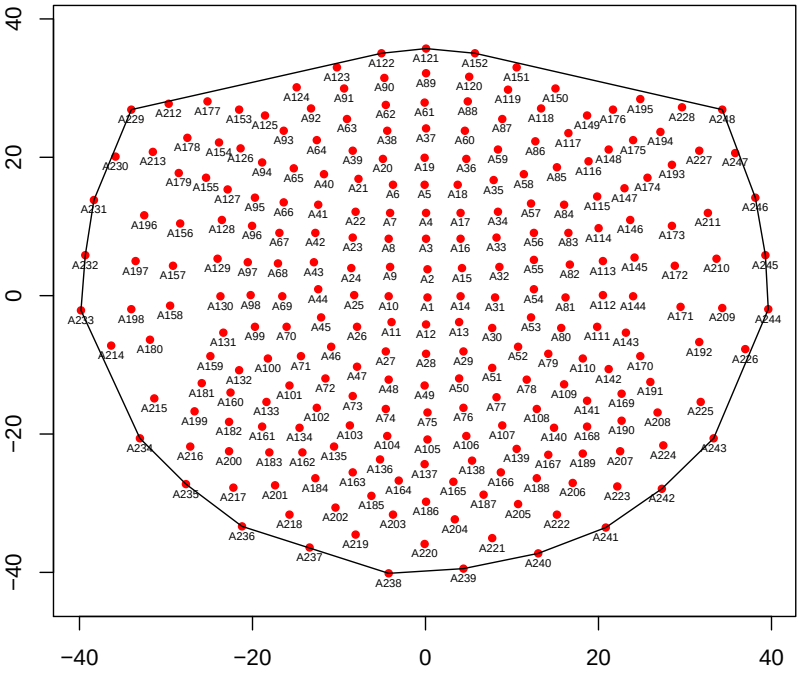

FIGURE 1.5: 2 dimensional spatial map of the brain surface showing MEG sensor locations

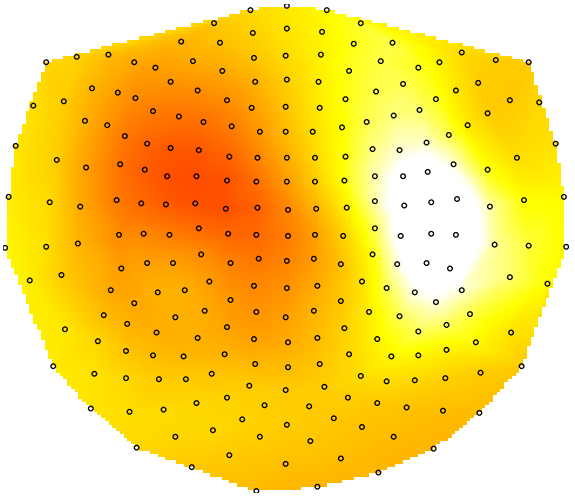

FIGURE 1.6: Spatial map of the brain showing dipolar behaviour of MEG data - the adjacent red and white region represent the two poles

Subsets of these two data sets from the TMS-EEG and MEG experiments are used throughout this thesis to investigate, develop and consequently apply the statistical modelling strategies.

1.3 Current Statistical Approaches

Traditionally neurological data are studied by collapsing the data over many replicates to the mean. However, an increasing number of studies have adopted single trial analysis as it can provide additional meaningful information about brain activity based on the trial to trial variation in the data that is masked when the data are averaged. Pernet et al. (2011) review the relevant brain imaging studies and present a strong case for the need to analyse data at the single trial level by considering the variance between replicates. One of the main drawbacks of single trial analysis is the low signal to noise ratio (SNR) due to the presence of noise and artefacts in the signals. In signal processing, signal to noise ratio is a measure of signal strength power to the power of background noise. Gonzalez-Moreno et al. (2014) present an evaluation of pre-processing methods to improve SNR, and suggest the use of decomposition methods to increase SNR.

The MEG data set has already been preprocessed using the decomposition method based on independent component analysis (ICA) for artefact rejection to optimise SNR before being provided for this research. ICA (Comon, 1994, Hyvärinen, 1999c, Hyvärinen and Oja, 1997) is a linear transformation method for decomposing an observed random vector into statistically independent components. This method is based on principles of blind source separation or BSS (Cardoso, 1998a, Jutten et al., 1988) assuming that the parameters associated with the artefacts are unknown. It then uses the independence property to decompose the signal into components that are as independent from one another as possible. Considering a simple multiplicative model of $n \times 1$ vector of observations $\mathbf{y}$:

$$\mathbf{Y} = \mathbf{As}, \tag{1.1}$$

where $\mathbf{A}$ is a $n \times n$ invertible matrix of vectors $[\mathbf{a_1}, ..., \mathbf{a_n}]$ and $\mathbf{s} = [s_1, ..., s_n]$ are the source signals, a $n \times 1$ vector of statistically independent components. The problem then is to estimate the source signals $\mathbf{s}$ based on the observations y. A trivial but important reparametrisation of the blind source separation model is using the additive model framework (Cardoso, 1998b) where the components y_p are defined as $y_p = a_p s_p$ for $1 <= p <= n$. So the model given as (1.1) can be rewritten as:

$$\mathbf{y} = \sum_{\mathbf{p=1}}^{\mathbf{n}} \mathbf{x_p}. \tag{1.2}$$

Ventrucci et al. (2014) describe a dipole model that ascertains the presence of a dipole based on frequency, amplitude and dipole strength. The dipolar frequency and amplitude of each replicate is the average frequency and amplitude of the two adjacent regions or poles. The functional parameter 'dipole strength' is derived as a curve measuring the degree to which the signals at the two poles are out-of-phase. In this thesis, dipoles are detected and modelled for each replicate using the same methods described in Ventrucci et al. (2014) and the mean characteristics of these three parameters are investigated by fitting a model for all the replicates for the three functional parameters. These models utilise the coefficients from the approximate p-spline fits corresponding to the curves as responses (from which the functional responses may be easily estimated), leading to functional models. Further, smoothing of the data is shown to reduce noise and increase the SNR (Ventrucci et al., 2011).

The EEG data set on the other hand contains spikes due to the TMS, a cyclic mains current and possibly a long-term trend component embedded in the recorded signal as the identified artefacts that need to be removed. The spikes in particular pose a problem because of their very high frequency and amplitude. Fig. 1.7(a) illustrates a segment of a typical temporal trace of the raw EEG signal in the region of stimulus presentation for a replicate at a particular channel. It can be seen that the signal is contaminated by very high magnitude spikes at the time the magnetic pulses are administered. This artefact has been controlled in Thut et al.

(2011a) by simply discarding the data in the region of the spike (20ms) and then interpolating to maintain the resolution of the signal as illustrated in Fig. 1.7(b).

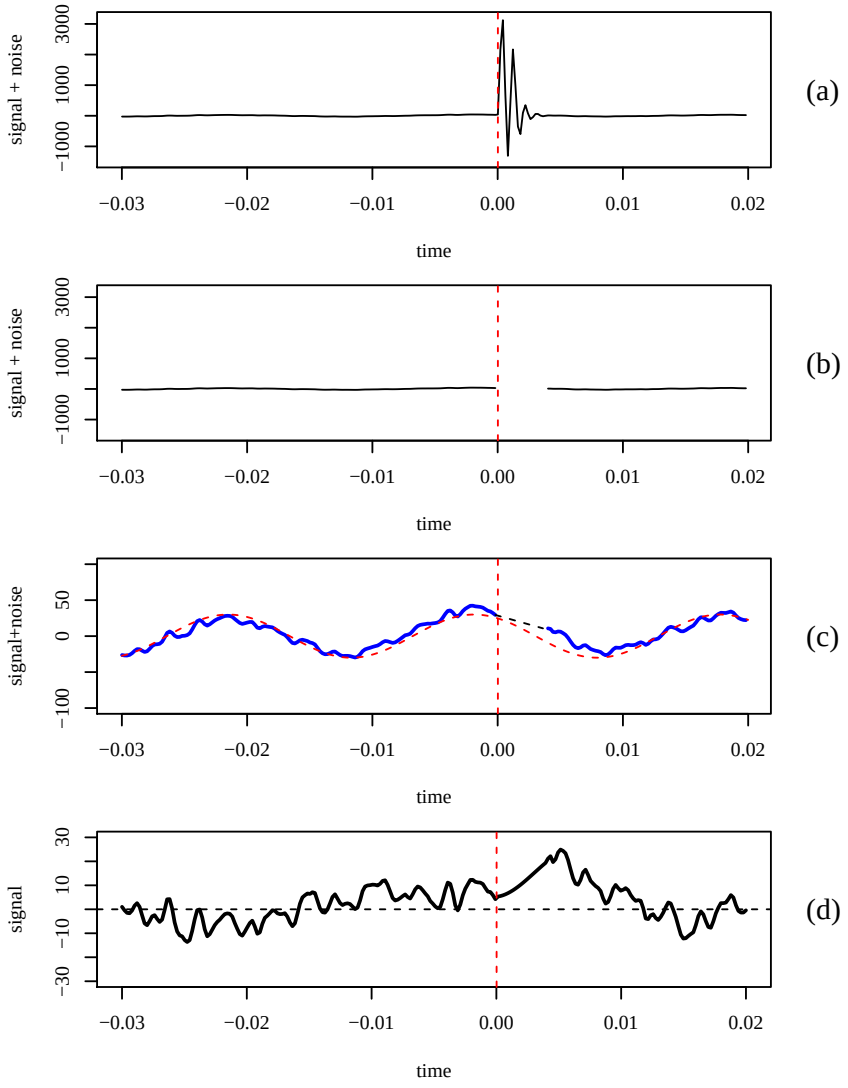

FIGURE 1.7: (a)Section of the time trace of raw EEG signal during stimulus presentation showing a spike and other artefacts (b)Artefact correction of spikes by discarding data (c) Spike corrected signal (in blue) with interpolation where spike data was discarded and overlay of a 50 Hz mains component (d) Signal corrected for spike (by deletion and interpolation) and 50 Hz mains (by subtracting an appropriate cosine function).

To extend this ad-hoc method in a modelling framework, an additive model (AM) described by Hastie and Tibshirani (1986) and later by Wood (2006) is proposed and applied for EEG signal responses in the TMS setting to decompose the signal into its main components. The additive model is applied to the data from the EEG experiment as a pre-processing *artefact correction* step. This class of flexible

models provides a method for data to be modelled simultaneously in space and time. It allows for the data to guide the model in estimating the functional dependence of the mean response on the predictors for a single replicate. Equation (1.2) can be re-written to include the smoothed spike, mains and trend components as artefacts along with the smoothed signal and overall mean. The additive models are fitted to estimate the signal and noise components of the TMS-EEG signals. The estimated signal of interest at each replicate after eliminating the noise components is then characterised temporally as the phase, frequency and amplitude curves. As stated earlier the MEG data are already pre-processed using the ICA techniques. These MEG signals are used to detect dipolar activity and then characterised spatially by location, orientation and size of the dominant dipole in each replicate, and temporally by average frequency and amplitude of the poles and a function for dipolar strength.

A simulation study is also designed to assess the validity of the additive model framework for preprocessing the TMS-EEG data. Data are simulated at a single channel for a time span of 1.1 s. The resolution is reduced by a factor of 10 such that a total of 550 time points are simulated per replicate iteration (in comparison to 5500 time points in the data) in order to gain in computational efficiency. This is equivalent to sampling 1 from every 10 data points available such that the sampled points are equidistant in time. Further, 4 categories of the phase angle of signal at onset of stimulus *phase-at-onset* are defined depending on where the TMS pulse 'catches' the 'brain' signal. Then a total of N iterations are computed for 4 groups of signals whose phase at onset of the stimulus (when the first TMS pulse is administered) correspond to the 4 categories of interest. The number of iterations per each group is then $N/4$. For this study, a total of 1000 iterations generate 250 iterations corresponding to each of the 4 *phase-at-onset* categories under each simulated scenario. An additive model is fitted to the simulated signal to eliminate noise and artefacts and estimate a signal component. This signal component is assumed to be the 'brain' signal of interest which is then analysed in later chapters to detect spatiotemporal patterns of interest.

The experimental TMS setup in the EEG experiment leads to investigating evidence of entrainment in the signals in a repeated measures mixed model framework. Further, characterisations are illustrated for the MEG data set based on earlier applications of similar techniques in (Ventrucci et al., 2014), results from which constitute the starting point for fitting functional mixed models to describe dipolar activity in the MEG data. The variability of the frequency, amplitude and dipolar strength is then modelled using the temporal characteristic functions in a functional mixed effects model setting.

Functional data analysis (FDA), a term first coined by Ramsay and Dalzell (1991), allows for such data to be modelled. FDA has gained increasing importance recently with numerous applications in analysis of spatial and temporal data. Chiou et al. (2003), James (2002), James et al. (2001), Müller and Stadtmüller (2005), Wang et al. (1998), Yao et al. (2005, 2006) are some of the key intensive methodological contributions to functional data analysis. A functional mixed effects model using a wavelet decomposition method to model the fixed and random effects is presented by Antoniadis and Sapatinas (2007). Bugli and Lambert (2006) describe a functional ANOVA application of EEG. A P-spline approach to modelling functional longitudinal data with random effects is described in Chen and Wang (2011). Yao et al. (2006) propose a P-spline based model for principal components analysis. Earlier developments in functional data analysis (Bosq, 2000, Ramsay and Dalzell, 1991, Ramsay and Silverman, 1997) methods focus primarily on temporal functions, i.e. functions dependent on time. Crainiceanu et al. (2007), Delicado et al. (2010), James et al. (2001) give an overview of functional data analysis methods for spatial data, realising the applicability of functional data analysis in two dimensional space. There is an increasing interest, however, in modelling spatial and temporal counterparts simultaneously, to adequately describe complex spatiotemporal data structures.

1.4 Research Aims

The main aim of this thesis is to develop suitable regression modelling strategies for analysis of noisy, complex and high dimensional functional neuroimaging data such as those described in the previous section, to explain neurological phenomena such as entrainment and dipolar activity. These modelling strategies have to be developed, after noise or artefact removal, taking into account the variability between subjects and replicates and across experimental conditions. The three specific research goals of this thesis are as follows:

1. **Signal Estimation:** The first goal is the retrieval of the 'brain' signals of interest after eliminating noise and artefacts. For the MEG application, standard approaches of artefact correction are applied, before the data is received, where signals of eye blinks, disturbances from the surroundings, etc. have already been removed. However, for the TMS-EEG case study, these standard approaches are not sufficient due to the nature of the experiment. So an additive model framework has been proposed to eliminate artefacts such as TMS induced spikes, trend and 50 Hz mains current signals and to estimate the 'brain' signal of interest.

2. **Data Reduction:** The second goal is to reduce the data size without losing much information, to make further modelling computationally efficient. Artefact corrected 'brain' signal estimates from EEG and MEG recordings consist of high dimensional spatiotemporal oscillatory brain signals which have particularly high resolution in time as demonstrated by the data described before. Follow up steps often involve modelling neurological phenomena such as entrainment and dipolar activity based on such data sets. However, the high dimensionality renders such models computationally intensive and expensive. It is therefore useful to reduce the volume of the data before model fitting is carried out. From the signal processing perspective, the problem to be addressed here is that of decimation, particularly in the time domain. Decimation is the reduction of the sampling rate by an integer

(or rational) factor that leads to down-sampling and hence a reduction in the data size. In this thesis, a novel and simple characterisation method for EEG and MEG brain signals based on Euler's formula (Eilers 2010) is proposed to decrease the size of the data by condensing the information to a small number of functional parameters based on zero-crossings - the time points where the signal crosses the the x axis ($y = 0$). This method does not employ a regular sampling rate, instead it simply extracts the information about the zero-crossings and reconstitutes the phase and frequency functions. The proposed method based on zero crossings is then used to estimate corresponding phase and frequency functions of the EEG and MEG signals. The amplitude of the signals is determined by the maximum amplitude between the zero-crossings and approximated as a smooth function joining the maximum amplitudes and the zeroes.

3. **Modelling Variation:** The third goal is to develop appropriate statistical models for analysing variability and patterns in the data, over space and time, across several subjects, replicates and experimental conditions. Specifically, entrainment of brain signals to α-band frequencies in the TMS-EEG setting and dipolar activity in the MEG experimental setting are modelled after accounting for variations between subjects and replicates within subjects. A repeated measures mixed model is developed for the TMS-EEG data results, which are used to successfully demonstrate entrainment of the signals. A mixed model is also developed to detect and explain dipolar activity in the MEG experiment, as a functional mixed model where the observations are the functions derived from the characterisation of the data as mentioned above.

Chapter 2 describes the proposed additive model for artefact rejection and signal estimation in TMS-EEG data. A novel characterisation method based on Euler's formula is proposed in Chapter 3 and then applied in both EEG and MEG data to estimate functional parameters. In this chapter, a summary of these functional

parameters for all replicates in selected subjects for each data set is reported. Corresponding mean functions and standard deviation curves for temporal functions such as frequency and phase for EEG and MEG as well as summary of magnitude of dipole strength and the time of occurence of dipoles in the MEG data are also reported. Once the functional curves are obtained for the TMS-EEG data in Section 3.3.1, linear mixed effects models for repeated measurements of phase/frequency and amplitude are fitted at a single channel across several replicates and conditions to estimate the coefficients associated with these parameters. These models are described and results from the model fitting are analysed in Chapter 4. Average frequency, phase and amplitude obtained from curve segments after each pulse serve as discrete repeated observations in these models. Multiple replicates within each subject, and subject are the two random effects that have been accounted for. When considering the mean signal for phase, frequency or amplitude, both random effects are of interest. In order to establish entrainment to an α band frequency, mixed effects models are fitted for frequency, phase and amplitude. Further, the variability around the mean frequency is expected to decrease over the repeated measurements in time especially in the case of the main condition as the signal entrains itself to the α frequency. In order to formally assess this, a mixed effects model for the standard deviation around the mean is fitted where the time indices of the average standard deviation at the repeated measurements and experimental conditions are the fixed factors and subject is a random factor in the model. Chapter 5 presents novel functional mixed effects models for MEG signals during the pre-stimulus period to account for the effects of random variation due to subjects and replicates within subjects. In order to study dipole signature profiles, smooth frequency, amplitude and dipole strength curves are estimated using penalised splines for the pre-stimulus period. The coefficients from these estimates are then used as responses to develop a mixed effects model for the pre-stimulus data. The three main contributions of the thesis and limitations of these models are discussed and future directions stemming from this research are also presented as concluding remarks. Examples from a smaller number of

subjects for the experimental data available from EEG and MEG are used as illustrations throughout the thesis. Summary results from the remaining subjects in the data set are provided in the supplementary Appendix A for completeness.

Chapter 2

Additive Models for Artefact Correction

2.1 Background

Single trial analysis of functional neuroimaging data is gaining importance since it provides additional information about trial to trial variation (Pernet et al., 2011). However, the main disadvantage of single trial analysis is low signal to noise ratio. This makes noise reduction and signal estimation particularly crucial in these studies. One of the three main objectives of this thesis, as outlined in the introductory Chapter 1, is the extraction of the brain signal of interest from each single replicate, sufficiently eliminating the noise and artefacts. The MEG data set has already been preprocessed using the conventional independent component analysis (ICA) based method of artefact rejection (Comon, 1994, Hyvärinen, 1999a,b, Hyvärinen and Oja, 1997, Jutten and Herault, 1991) before being provided for this research. The EEG data set on the other hand contains artefacts that need to be removed.

Although the additive model framework can be viewed as a reparametrisation of multiplicative ICA as demonstrated in Chapter 1, it distinguishes itself by using the information available about the sources and characteristics of the possible

artefact components of the signal to define each of the components. This seems particularly relevant in the case of the TMS-EEG data set where the sources, patterns of occurrence and shapes of the artefacts are known beforehand. In this chapter an additive model (AM) framework described by Hastie and Tibshirani (1986) and later by Wood (2006) is proposed and applied for EEG signal responses in the TMS setting to decompose the signal into its main components. This class of flexible models provides a method for data to guide the model in estimating the functional dependence of the mean response on the predictors for a single replicate.

The TMS-EEG application data set used to demonstrate the artefact rejection step by applying the additive model framework consist of EEG recordings from 8 subjects. These recordings are obtained from a TMS-EEG cognitive experiment that studies the effect of TMS pulses on entrainment of brain signals to α frequencies as recorded by EEG. The TMS pulses are administered within the α frequency band with the exact frequency determined previously for each subject. Initially a single replicate spatiotemporally for one subject is considered in order to fit the model. Further, the spatiotemporal variation across many different replicates, conditions and subjects are informally explored. An additive model is applied to the data from the EEG experiment as a pre-processing step. The EEG signals are assumed to be a sum of these different artefact components, a mean response, and the 'brain' signal of interest. Section 2.2 provides the theoretical details of the additive model framework. Section 2.3 describes the application of this method for the TMS-EEG data set. Three artefact components are identified in such EEG signals at each channel - spikes due to the transcranial magnetic stimulations, a cyclic mains current and a nonlinear trend component embedded in the recorded signal. The design and results from a simulation study to validate this method of artefact correction and signal estimation are reported in Section 2.4.

2.2 Additive Model

An additive model is a special case of linear models involving a sum of smooth functions of the covariates. In general, it can be represented as:

$$y = \mu + f_1(x_1) + f_2(x_2, x_3) + ... + \varepsilon,$$

where y is a response variable and f_i are smooth functions of the covariates x_k.

An additive model framework is proposed to estimate the artefact and signal components from the TMS-EEG data. Three artefact components are considered. A characteristic of the EEG signal is the presence of an underlying mains current of 50 Hz due to the electrical apparatus used. The magnitude of this 'cyclic' component varies depending on the position and orientation of the equipment, its distance from the electrodes, etc. This component may be estimated either (i) by approximating it with a 50 Hz cosine function or (ii) as one of the smoothed components with a periodicity of 0.02s in an additive model. An additional component estimating the effect of the spikes is added. This is initially designed to track the spike effect in the data for a fixed time duration (e.g. 10 or 20 milliseconds) after each TMS pulse. The magnitude of this component for the remainder of the time trace is set to 0, assuming that the spike effect lasts only for a short while after each pulse. Further a nonlinear long-term trend component is added. A smooth function estimates the remaining signal, which is referred to as the 'brain' signal of interest. The mains current, spikes and nonlinear trend components are assumed to be spatially uncorrelated, while the signal is smoothed spatially.

At each channel j the following model is proposed:

$$y_j(t) = \mu_j + m_{1j}(t) + m_{2j}(t) + m_{3j}(t) + m_4(s,t) + \varepsilon_j \quad \forall\, t = 1, ..., T; j = 1, ..., n; \quad (2.1)$$

where t is the time duration of the recordings, s is the spatial location of the EEG channels and n is the total number of channels (or electrodes). Here μ_j is the overall mean, m_{1j} represents the smooth trace of the TMS pulses, m_{2j} is a smooth

function defining the underlying cyclic 50 Hz. component, m_{3j} is a smooth long-term non-linear trend component and m_{4j} is the spatiotemporally smooth signal of interest. All these four terms are estimable because they operate on different timescales with different associated smoothing parameters. m_{1j} is active only over a 10ms or 20ms period after each pulse, m_{2j} is cyclical with period of 20 ms and m_{4j} is unrestricted. The smooth trend component m_{3j} is set up with a high smoothing parameter to estimate any long-term non-linear mean change in the data. The error ε_j is assumed to be independent and normally distributed.

2.2.1 Smoothing

Smoothing is employed to pick up specific characteristics of the temporal traces and spatial patterns in the data. A simple kernel smoothing approach called local linear smoothing (Cleveland, 1979, Fan, 1993, Fan and Gijbels, 1992) is applied to estimate the smooth functions which describe the spike, trend and signal of interest. This is done by fitting a local linear regression in the neighbourhood of the point y that is to be estimated, the width of neighbourhood determined by the corresponding smoothing parameter denoted by h_t and h_s for temporal and spatial smooths respectively. Kernel smoothing is the smoothing method of choice at this instance because of its simplicity. Basis spline (b-spline) and penalised b-spline (p-spline) basis functions, which are popular methods of smoothing, may also be employed. These more sophisticated methods are utilised as smoothing tools in later chapters and have been explained there.

The fitted values of the smooth function for a univariate smooth curve is given as $\hat{m}(t) = Sy$ where S is the 'smoothing matrix' of weights associated with each point at which the estimation is carried out (for computational details refer Bowman and Azzalini, 2003). For smoothing across the temporal trace at each channel then, a weight matrix S_t is computed as a local linear estimator. For a regression

model $y = m(t) + \varepsilon$, this is equivalent to a least square minimisation problem:

$$\min_{\alpha\beta} \sum_{i=1}^{n} \{y_i - \alpha - \beta(t_i - z)\}^2 w(t_i - z; h), \tag{2.2}$$

where the local linear estimator is the intercept $\hat{\alpha}$ of a linear regression, estimated at one particular point of time which is of interest z, w is the kernel density function of the points in the neighbourhood of z with weights decreasing as one moves away from z, y_i is the observed data, t_i are the points at which the smooth function is estimated and h is the *bandwidth* or *smoothing parameter* which determines the width or span of the neighbourhood in which the kernel density function lies (for theoretical and computational details refer to Bowman and Azzalini, 2003, Bowman and Azzalini, 1997).

In order to apply the additional spatial smoothing on the signal component m_{4j}, a corresponding weight matrix S_s along with S_t is computed as a solution to a minimisation problem in two covariates (s, t) (Bowman and Azzalini, 2003). The bivariate local linear estimation at the point (z_s, z_t) is then computed as the solution of the bivariate least squares minimisation problem:

$$\min_{\alpha\beta} \sum_{i=1}^{n} \{y_i - \alpha - \beta(s_i - z_s) - \gamma(t_i - z_t)\}^2 w(s_i - z_s; h_s) w(t_i - z_t; h_t). \tag{2.3}$$

The spatial and temporal weight matrices can then be used to estimate the smooth function:

$$\hat{m}_{4j}(s, t) = S_s Y S_t.$$

Here Y denotes the matrix containing the data with the number of rows corresponding to the number of channels/electrode (spatial locations at which the signal is observed) and the number of columns equal to the number of time points at which the observations are recorded at each channel. This computation is carried out under the assumptions that the signal recorded at each channel varies smoothly over time, and the magnitude of the signals recorded at the channels

at any particular time point is also spatially smooth. Pre-multiplying and post-multiplying the data with the weight matrices S_s and S_t respectively is then a bivariate smoothing method where S_s marginally smoothes the data spatially and S_t implements the marginal smoothing temporally.

For the estimation of the additive model with four components modelling the EEG recording, the components corresponding to the TMS pulses, mains current and trend (m_1, m_2 and m_3) are smoothed over time only, assuming that they are spatially unrelated between the channels. Local linear smoothers are employed for estimating the matrix of weights S_t in the time domain to estimate the temporally smoothed spike $m_1(t)$ and the trend $m_3(t)$ components as well as for spatiotemporal smoothing (corresponding weight matrices S_s and S_t) to estimate the signal of interest $m_4(s,t)$ using (2.1). A cyclic smoother is applied to estimate the temporally smoothed cyclic mains current with a frequency of 50 Hz $m_2(t)$. The basic matrix of weights for temporal smoothing of $m_1(t)$ is constructed to ensure that each spike is only estimated for a short window (10ms or 20 ms) in the data and is set to 0 elsewhere.

The temporal smoothing parameter h_t can be optimally adjusted to obtain estimates of the spikes and the trend for a single channel. A large smoothing parameter is applied to estimate any long-term effect. The neighbourhood of the kernel function is wide and this captures the behaviour of the data over the long span (less variable but highly biased). Similarly, a small smoothing parameter captures the detailed features of the data within a smaller 'bandwidth' or span and a very small h_t tracks the data almost completely (small bias and large variance). For the local linear estimation in one covariate, the bias and variance are given as:

$$\mathbb{E}\{\hat{m}(t)\} \approx m(t) + \frac{h_t^2}{2}\sigma_w^2 m''(t),$$

$$\text{var}\{\hat{m}(t)\} \approx \frac{\sigma^2}{nh_t}\frac{\alpha(w)}{f(t)},$$

where $\sigma_w^2 = \int z^2 w(z)$ and $\alpha(w) = \int w(z)^2 dz$.

Hence there is a tradeoff between bias and variance that needs to be taken into account in optimal selection of a smoothing parameter. It is desirable to set the temporal smoothing parameter for estimating the spike component to be very small, so that it tracks the spike effect within a small window almost completely. A large smoothing parameter is used to track any long-term trend effect present in the data.

Similarly, the spatial smoothing parameter h_s for estimating $m_4(s,t)$ can be adjusted to obtain a spatially smooth topology of the brain (by considering data from all channels simultaneously). The temporal smoothing parameter h_t for estimating the signal of interest must be able to identify signals between 8 to 12 Hz known as the α band frequencies, as occurrence of signals at these frequencies are of specific interest in the experiment.

2.2.2 Smoothing Parameter Selection Criteria

Smoothing parameters or bandwidths h are estimated as the first step in the model fitting. Many methods are available in the literature for selection of a smoothing parameter. There are primarily two types of bandwidth selection methods: the classic plug-in methods and the methods based on cross-validation. Details of the available methods are covered in (Jones et al., 1996, Park and Turlach, 1992). The plug-in methods utilise the simple idea that an estimator is substituted (or 'plugged in') in place of an unknown quantity (based on cross-validation, degrees of freedom, Akaike information criteria Hurvich et al. (1998), etc.). A simple estimator of the smoothing parameter h by a plug-in method is given by:

$$h_{opt} = \left\{ \frac{\gamma(w)\sigma^2}{\int [m''(x)]^2 f(x) dxn} \right\}^{1/5},$$

where $\gamma(w) = \alpha(w)/\sigma_w^4$. Here $m(x)$ is the unknown curve, the kernel function w is assumed to be standard normal and $f(x)$ is the density of the observed points. At any point of interest z, the local linear estimate is computed as the estimate of

the intercept term $\hat{\alpha}$ in the least square minimisation formulae given as equations (2.2) and (2.3) for the univariate and bivariate cases respectively.

Another very popular method is cross-validation (Stone, 1974) where the data point for which the curve is being estimated is eliminated and the remaining data is used for the estimation. So, for estimation at y_i, the estimate $\hat{m}_{-i}$ is computed, removing (x_i, y_i) from the training data. Thus the curve is estimated, and the smoothing parameter is optimised by minimising the mean squared error. The cross-validation function, which is an estimate of the mean squared error, may be written as:

$$CV(h) = \frac{1}{n}\sum_{i=1}^{n}\{y_i - \hat{m}_{-i}(x_i)\}^2.$$

Ordinary cross-validation method is computationally very expensive in case of additive models. To overcome this issue, a generalised cross-validation (Craven and Wahba, 1979, Golub et al., 1979) method may be used.

The methods of estimation of the smoothing parameters h provide closed form expressions of its estimation and makes computation straight-forward. However, they involve matrices of size n of the sample size making these computations very inefficient for large sample sizes. A number of fast smoothing algorithms are available in the literature (reviewed in Fan and Marron, 1994) as solutions, many of which employ grouping of the raw data as frequencies into fine grids or bins (Härdle, 1987, Härdle and Scott, 1992, Silverman, 1982, Wand and Jones, 1995). Bowman and Azzalini (2003) describe the binning of the data into smaller number of groups in the context of regression and smoothing parameter estimation. For the application in section 2.3 smoothing parameter h has been estimated using cross-validation methods, both with and without binning.

2.2.3 Backfitting for Model Estimation

Once the smoothing parameters are determined, the next step is to estimate the components of the additive model. This is accomplished using an iterative method to estimate the components. Let $\mu = \frac{1}{n}\sum_{j=1}^{n}\mu_j$ be the overall mean of the signals

for all channels, $y_j(t)$ be the observed signal at channel j and time t and $m_{jk}(t), j = 1, ...n; k = 1, 2, 3$ be the three smoothed artefact components to be estimated additively. The signal of interest is also smoothed spatially and is hence denoted as $m_4(s, t)$.

1. The overall spatiotemporal mean $\mu = \frac{1}{nT}\sum_{j=1}^{n}\sum_{t=1}^{T} y_j(t)$, is computed where $j = 1, ..., n$ represent the index for n channels and $t = 1, ..., T$ are the timepoints at which the data is observed.

2. The spatial and temporal weight matrices S_s and S_t are computed for each component, as outlined in Section 2.2. The components are then estimated using equations (2.2) - (2.4).

3. Each of the components is initialized as the difference between the observed data and the sum of the mean and other three components.

4. Sums of squares of errors are computed as $SS = \sum\{Y - \mu - \hat{m}_1 - \hat{m}_2 - \hat{m}_3 - \hat{m}_4\}^2$.

5. Steps 3 and 4 are repeated until absolute difference of the sums of squares from two adjacent iterations (say p and $p + 1$) are negligibly small:

$$\frac{\mid SS_p - SS_{p+1} \mid}{SS_p} < 0.0001.$$

6. Once the iteration stops, the $n \times T$ matrix $\hat{M}_k, k = 1, 2, 3, 4$ of smoothed estimates of the components are the final values of $\{\hat{m}_1(t)\}$, $\{\hat{m}_2(t)\}$, $\{\hat{m}_3(t)\}$ and $\{\hat{m}_4(s, t)\}$.

2.3 Application: TMS-EEG case

The smoothing and additive modelling methods described in the previous section are applied to a single replicate of a subject in the TMS-EEG experiment. A trial from the observed recordings of a subject labelled as S02 is used to demonstrate the methods discussed above. This consists of data from the 60 channels for 5500 points in time spanning over 1.1 seconds $(-0.1, 1)$.

2.3.1 Selection of Smoothing Parameter

To study the performance of automatically selected h_t, a simulation study is carried out. The data are designed as cosine curves of frequency 11 Hz (with added random normal noise) as this alpha frequency in the signals is of interest for a particular subject (illustrated in an application later). So $(x_i, y_i), 1 < i < 500$ are generated such that $y_i = f(x_i) + \varepsilon_i$, $\varepsilon_i \sim N(0, 0.5)$. The cosine curve $f(x)$ is given by:

$$f(x) = \alpha \cos\{(x - \beta)2\pi\phi\},$$

where, α denotes the amplitude, β denotes the location shift and ϕ is the period of the signal. The smoothing parameter is estimated using several methods (cross-validation with binning, degrees of freedom, AICC) as well as the cross-validation method (without binning) for 100 simulations. The mean estimated bandwidth obtained from both the plug-in methods as well as the cross-validation method are found to behave consistently well in estimating the underlying cosine function of the known frequency for a range of error variances (Fig. 2.1).

The values of h_t using the plug-in and the cross-validation methods, which correspondingly minimise the mean squared error curve for standard deviation of error $\sigma = 0.5$ are estimated to be 0.0077 and 0.0012 respectively. The smooth curves with the true cosine function are shown in Fig. 2.2. It is noted that although the bandwidth selected using cross-validation seems to estimate the true curve more accurately, the algorithm runs for much longer duration than the plug-in methods. The smoothed curve fitted by using the bandwidth estimated by the cross-validation method may perform better in picking up the features in the data but it is smaller and hence more 'wiggly'. The plug-in method estimates the bandwidth much faster for any given frequency (10 Hz in this example). However, it requires the estimation of the second derivative of the unknown curve $m''(x)$.

The smoothing parameters thus selected were then applied to the data from a single trial. Additive models with spatiotemporally smoothed estimates fitted to TMS-EEG data of a single trial over all channels separates out the TMS pulses,

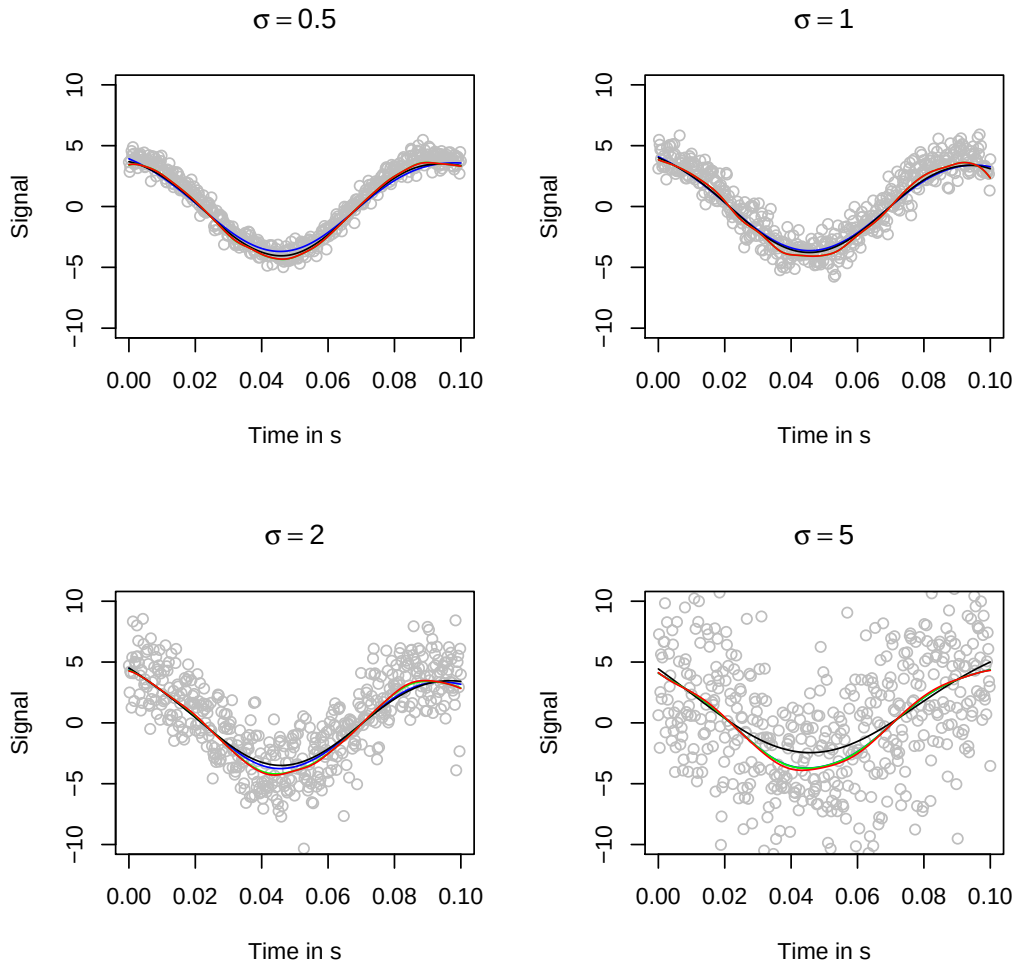

FIGURE 2.1: Estimated smooths using the cross-validation and plug-in methods to determine the bandwidth with the underlying 11 Hz true cosine curve for a range of standard deviations of error in the simulated datasets. Red line: cross-validation , Green line: plug-in cross-validation, Blue line: plug-in df, Black line: plug-in aicc; [Top left] $\sigma = 0.5$, [Top right] $\sigma = 1$, [Bottom left] $\sigma = 2.0$, [Bottom right] $\sigma = 5.0$

the mains current artefact, the long-term trend and signal of interest effectively (illustrated later).

2.3.2 Smoothed additive models

The TMS spikes are administered at intervals of approximately 0.9s starting at 0. This shows that the frequency at which TMS is applied is about 11 Hz, which is the intrinsic alpha frequency of subject S02's brain - determined from a separate

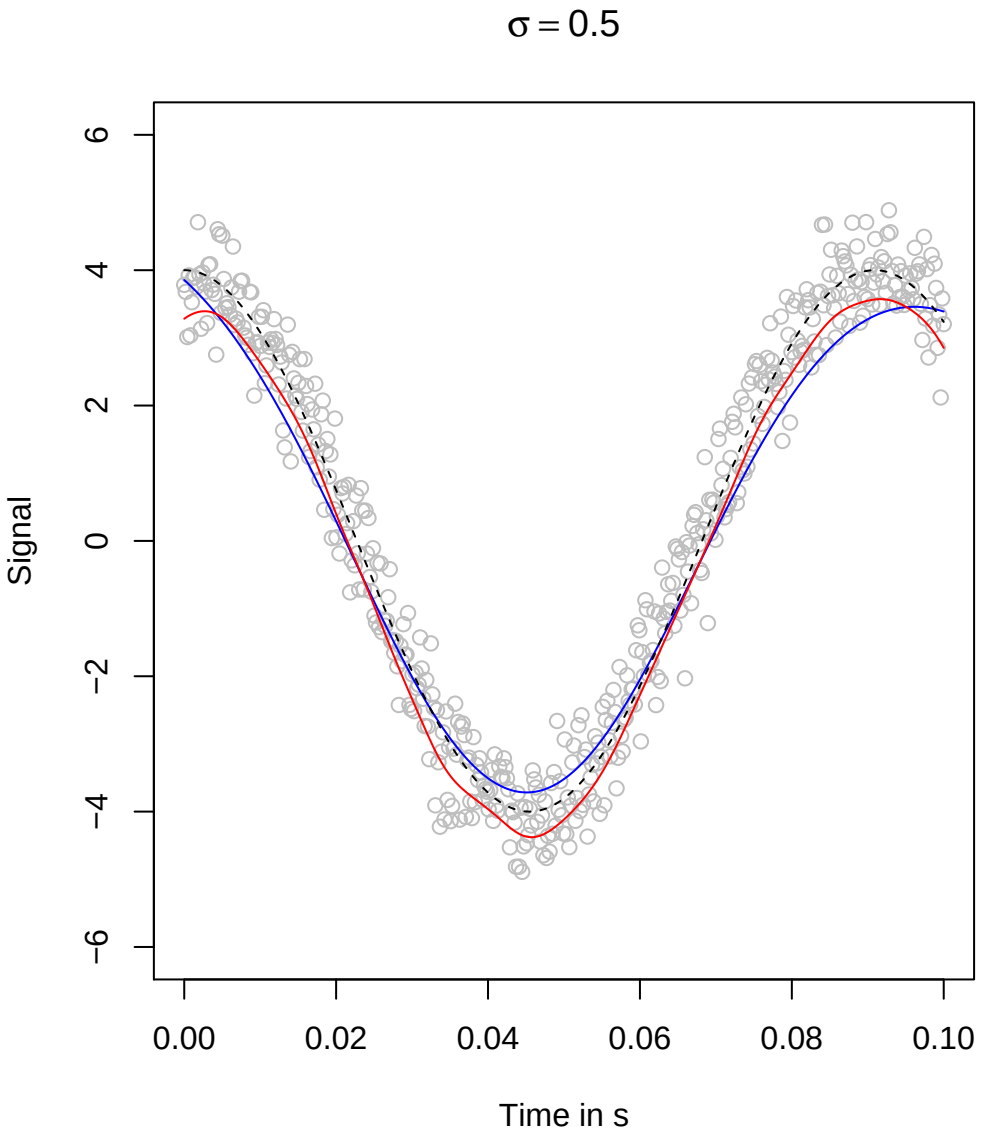

FIGURE 2.2: Estimated smooths using the cross-validation and plug-in (degrees of freedom) methods to determine the bandwidth with the underlying 11 Hz cosine curve, $\sigma = 0.5$. Red line: cross-validation, Blue solid line: plug-in df, Black dotted line: True signal

MEG recording obtained from the subject designed for this purpose. Thus we have prior knowledge of the frequency which needs to be picked up by the 'brain' signal of interest, and we use the plug-in method (in a simulation study, similar to that outlined before) to determine the temporal bandwidth for the signal component ($h_t = 0.008$). The window for which the spike is estimated is computed from the data itself. The spikes are estimated with a very small temporal bandwidth $h_{t(spike)} = 0.000007$. The mains current is estimated as a cyclic component and the corresponding smoothing parameter is $h_{t(mains)} = 0.005$ as used. A long-term trend component is estimated with a temporal bandwidth $h_{t(trend)} = 0.05$ providing a flexible non-linear estimate of the trend. The components effectively separate out using the additive model given in equation 2.1. The channels are assumed to record the artefact signals independent of each other. The normality assumption is also reasonable, since the residuals from the model fit do not show any systematic patterns in this example. A more formal assessment is not essential at this stage, since no inference is being performed. The four components are illustrated in Fig. 2.3. It is of interest to investigate the remaining estimated smooth signal once the effects of the TMS pulses, the mains current and the long-term trend have been eliminated. For each channel, particularly those that are in closest proximity to the TMS equipment (viz. P4, CP4 and P2), the signal of interest (Fig. 2.4) on visual inspection reveals subtle evidence of entrainment, possibly to the alpha band frequency (8-12 Hz), after the third TMS pulse.

2.3.3 Estimation of the duration of TMS pulse effect

One characteristic of the spike component is that it remains active for a very short period of time. On administering the TMS pulse, the signal rises very rapidly and then declines sharply to pre-spike levels almost instantaneously. Thut et al. (2011a) discard the data 20ms after each pulse and interpolate it to obtain a continuous signal trace. Initially in this thesis, the model is set up so that the spike component is active only over a 20ms period after each pulse over all channels in a replicate. For simplicity, this common window span is taken for

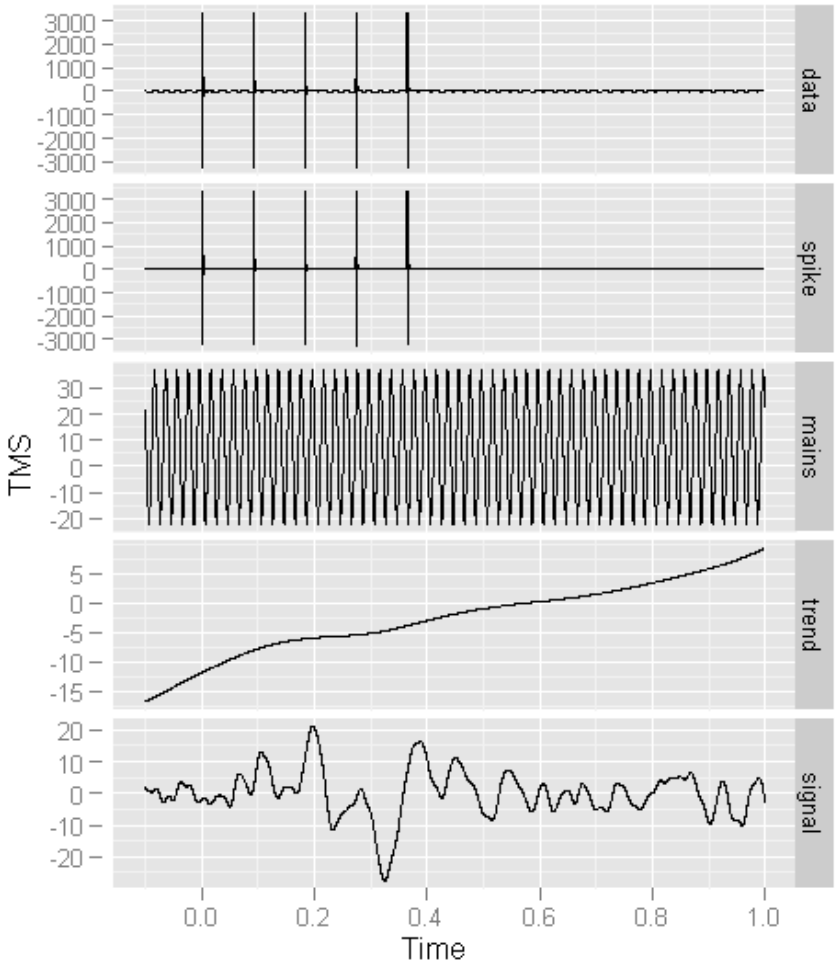

FIGURE 2.3: Additive components for channel CP4 in a single replicate of a subject: trace of data across the time span (topmost) and estimated spike, mains current, trend components and signal of interest estimated from the additive model.

the five pulses, across all channels in the replicate. Therefore, the component estimates are obtained allowing for estimation of spikes for 20ms after they are administered. The estimate is set to 0 at any other time. In the past analyses of this TMS data, signals from the time of TMS pulse to about 20ms after the pulse were deleted and the missing data were interpolated. As an improvement to this, the additive model allows us to model the spike effect along with the signal of interest and other components in a single modelling step.

However, the duration of spike effect varies across trials and subjects. Even within a single replicate, the duration of the spike varies from channel to channel. If the duration of the spike effect is fixed in the model (say to 20ms) for all the channels,

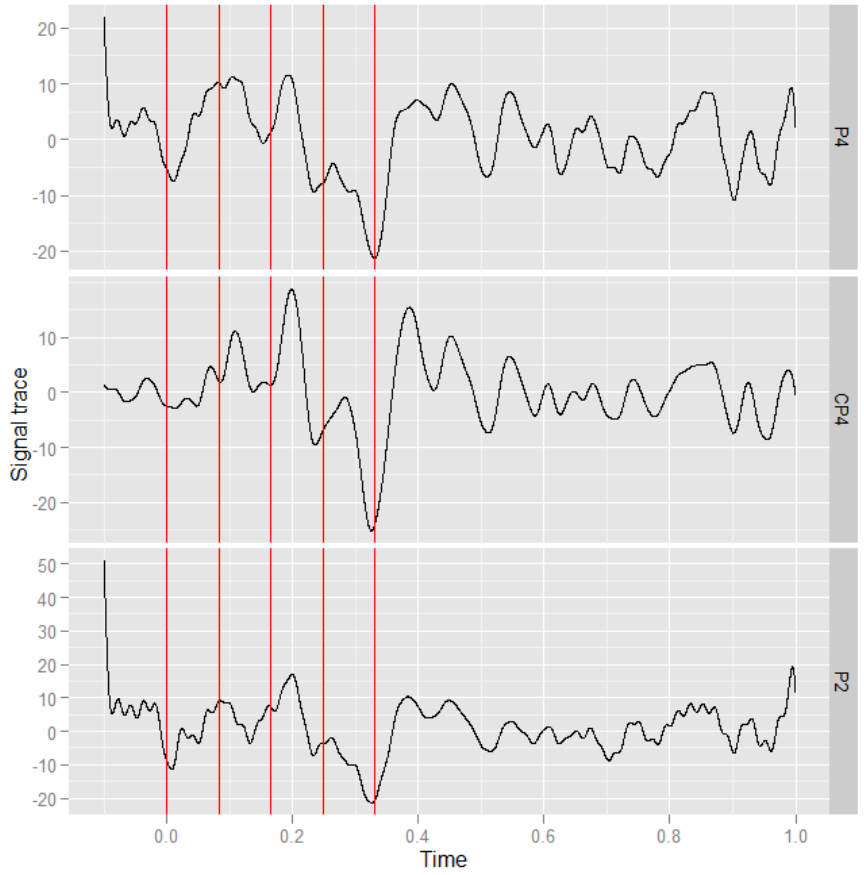

FIGURE 2.4: Signal of interest for channels P4, CP4 and P2 in a single replicate of a subject. The TMS pulses shown as vertical lines on the time axis are administered at intervals of approximately 0.09 s to this subject.

there may be signals from some channels in which the spike effect lasts for a much shorter duration (say 5ms). Here the spike component in the model will end up tracking most of the signal. This results in partial residuals for the signal component which are very close to the estimated signal when the actual duration of the spike effect is much shorter than that being tracked by the model, as shown in Fig. 2.5 (top). Moreover, there may also be some channels where the spike effect may last longer than this fixed time span. This is the other extreme case, where the spike will not be estimated fully - causing much of its effect to remain in the signal of interest, thus influencing any inference based on the 'brain' signal of interest component thus obtained, as illustrated in Fig. 2.5 (bottom).

This motivates determining a suitable spike window length for modelling a particular replicate, such that the spikes are not underestimated. Also, problems such

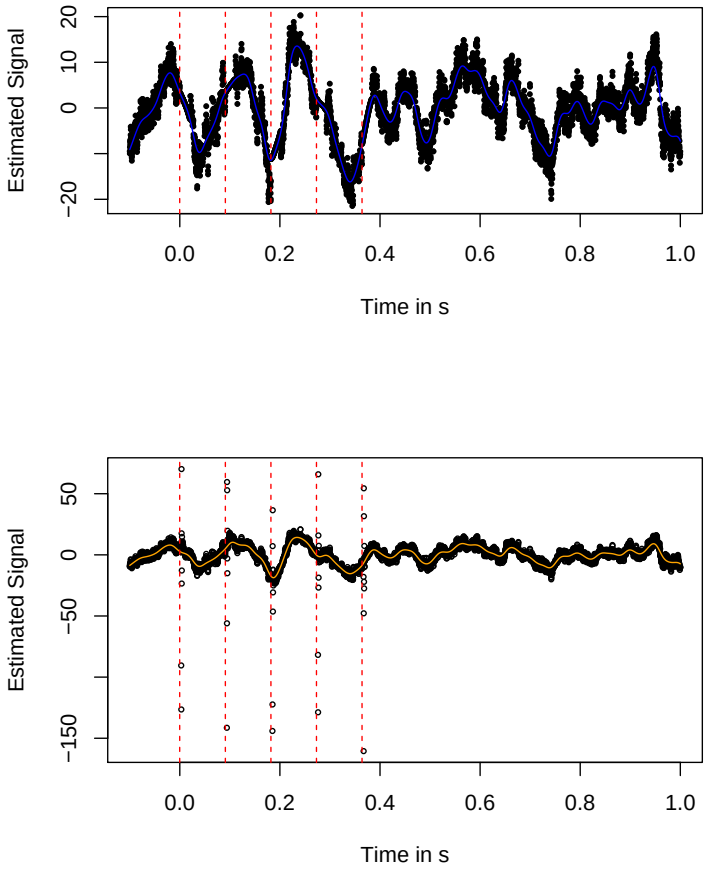

FIGURE 2.5: Signal of interest for a single channel with corresponding partial residuals as obtained from a spatiotemporal additive model at a single replicate level, with spike window fixed at 20ms (top) and 3ms (bottom).

as very close estimates of partial residuals to the signal of interest arise if the spike window length is overestimated. To track this effectively, before the additive model is applied to separate artefact components from the 'supposed' brain signal in each trial, the time span for which the spike effect remains in the signal must be estimated. We first investigate a variable length of spike window, for each channel in a single replicate depending upon the shape and nature of the spikes.

The following two algorithms were developed in this research to address the specific problem of estimating spike window length and are explored in order to determine a suitable spike window length, first at the channel level, and then applied to the replicate for fitting the spatiotemporal model:

2.3.3.1 Algorithm 1: Comparison of partial residual variation

Once a temporal additive model is fitted to data from a single channel j using equation (2.2), the partial residual for the estimated signal of interest $m_4(s,t)$ is computed as $\hat{\varepsilon}_{j,signal} = y_j - \mu_j - m_{1j}(t) - m_{2j}(t) - m_{3j}(t)$. The difference between the partial residuals and the estimated signal component in the region where the spike effect is not present but is still allowed for in the model is negligibly small. We use this to track the point in time where this change in the deviation of these residuals first occurs. We do this for a single channel only in the following steps:

1. Compute the deviation of the partial residuals from the estimated signal curve:

$$D = \mid \hat{m}_{4j} - \hat{\varepsilon}_{j,signal} \mid .$$

2. Estimate the standard deviations of the absolute differences in step 1, 5 ms after the first pulse (time indices 501 to 525) and for 1 ms after that (time indices 506 to 530).
   $SD1_{(1)} = sd(D \mid_{t=501}^{525})$ and $SD2_{(1)} = sd(D \mid_{t=506}^{530})$ where the subscripts (1) in $SD1_{(1)}$ and $SD2_{(1)}$ denote the iteration step 1.

3. Compute the absolute difference of the 2 standard deviations $\mid SD1_{(1)} - SD2_{(1)} \mid$. This value should be small when the deviation of the partial residuals from the estimated signal are similar.

4. In the next iteration, we slide the second window by 5 time indices (1ms) and recompute the standard deviations and absolute difference of the standard deviations as outlined in step 3. Thus, $SD1_{(2)} = SD1_{(1)} = sd(D \mid_{t=500}^{525})$ and $SD2_{(2)} = sd(D \mid_{t=511}^{535})$ and we compute $\mid SD1_{(2)} - SD2_{(2)} \mid$.

5. When this difference is more than 0.01 (say), the iterative process stops and decides the final cutoff point of the spike window as the starting point of the sliding window.

This is based on the assumption that when the standard deviation of the difference of the residuals from the estimated signal in the first window is equivalent to the standard deviation of the difference of the residuals from the estimated signal in the second window, the spike effect has ended. In the example above (Fig. 2.5), a model with spike window 20ms shows that the region after the TMS pulses have partial residuals close to the estimated signal, indicating that the spike effect may be much smaller. Estimated signal data from the same channel (subject 02, trial 03, channel 40) were taken to estimate what the spike window length should be. It was seen that for this channel, the location of the sliding window was moved by $50(5 \times 10)$ time indices in 10 iterations before the algorithm stops. Recalling that the sampling rate in this experiment is 5 time points per millisecond and the starting point (time index) of the second window at the last iteration is $505 + 50 = 555$, the approximate length of the spike window is estimated to be 11 ms after the TMS pulse is administered at $t = 501$. The spatiotemporal model is now refitted using the spike window length of 11 ms (Fig. 2.6).

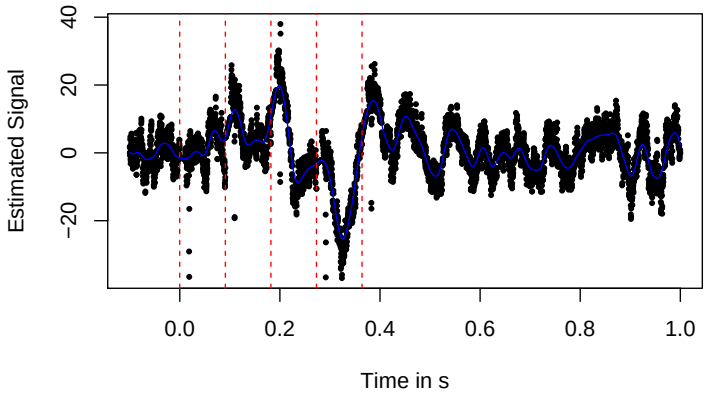

FIGURE 2.6: Signal of interest for a single channel with corresponding partial residuals as obtained from a spatiotemporal additive model at a single replicate level, with spike window fixed at 11 ms estimated from algorithm 1.

This method is time consuming, as the model requires to be fitted twice - once to compute the partial residuals, based on which the algorithm determines the optimum length of the window. However, it indicates that a variable window span should be considered to estimate the spikes while fitting the model. In order to

increase computational efficiency, the second algorithm considers estimating this span from the data itself, before fitting any additive models. Here we make use of the following data based technique:

2.3.3.2 Algorithm 2: Data based estimation of spike window length

The data for one replicate from subject 9, for channel 24 is considered as an illustrative example (Fig. 2.7). Zooming in on the first spike in this trial (Fig. 2.8), we can see that an approximate estimate of the spike window span should be about 4 ms.

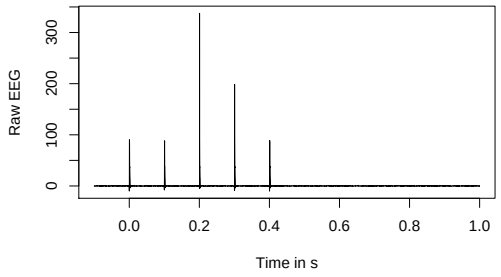

FIGURE 2.7: Time trace of EEG recording for subject S09, trial 9, channel 24

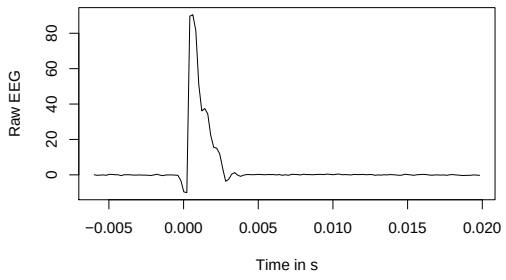

FIGURE 2.8: Time trace of first spike zoomed from the time trace above

In order to compute an approximate estimate of the window length l_1 for modelling the first spike effect, the following algorithm is implemented:

1. Obtain the maximum absolute value of the data in the pre-stimulus period $\mid \max(y_i)_{i=0}^{499} \mid$.

2. A time trace of the data from first pulse till just before second pulse $y_i \mid_{i=500}^{999}$ is considered. All the points in this trace where the absolute data values are less than the absolute maximum value of the prestimulus period can be regarded as largely signal. The indices of whenever $\mid (y_i)_{i=500}^{999} \mid < \mid \max(y_i)_{i=0}^{499} \mid$ are locations when the data is assumed to be largely signal and spike effect is not pronounced.

3. Probable spike positions are located wherever the condition in step 2 is violated. So,
$$\mid (y_i)_{i=500}^{999} \mid > \mid \max(y_i)_{i=0}^{499} \mid$$
at spike positions.

4. For all time indices less than $i = 600$ (spanning a duration of 20 ms after the first pulse so that the search is terminated much before the onset of the next TMS pulse at $i = 1000$), either the maximum of all time indices i where spike positions are located in step 3 (say i_{max}) or the cutoff $i = 600$ - whichever is smaller, marks the end of the spike effect for the first pulse.

5. Length of the first spike thus determined as
$$\hat{l}_1 = \frac{\min(i_{max}, 600) - 500}{5}$$
gives an approximate window span in milliseconds.

This estimated window length $\hat{l}_1$ computed using the data after the first TMS pulse is used as an approximate measure of spike window length for all 5 tms pulses. Note that:

(a) In the data based approach, we only use the data before model fitting, which makes this approach more efficient.

(b) When applied to the single channel, the estimated span from this is 19 (or about 4 ms). Comparing it to 4 ms of the above estimate, this method gives a reasonable estimate.

(c) It may also be noted here that the approach based on standard deviation of the difference of partial residuals and estimated signal from the model (algorithm 1) gives very similar estimate (5 ms) for this data.

For channel 40, the data based method estimates a spike window span of 19 units ($\approx$ 4ms). This seems suitable from the figure (Fig. 2.9, top). For channel 34 it is estimated as 49 units (50units = 10ms) based on the data (Fig. 2.9, centre). For channel 8, the estimate is $\approx$ 7ms. Data based method gives spike window length as 43 ($\approx$ 9ms) (Fig. 2.9 bottom). Partial residuals are randomly distributed for all the three channels.

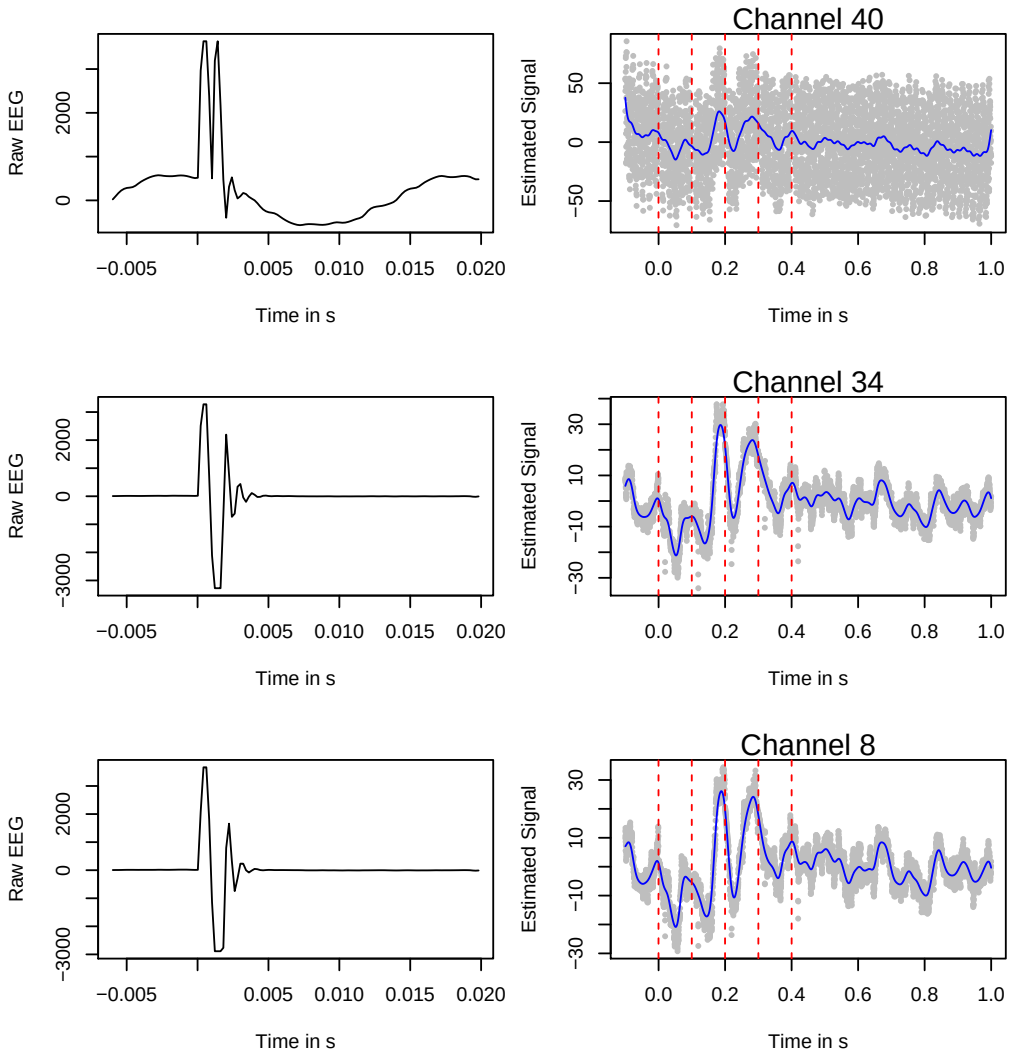

FIGURE 2.9: Model fits for channels 40, 34 and 8 with partial residuals

The method based on assessing the length of the spike window from the data works well in determining the varying window spike. It traces the spike for the full length of time in which the raw signal is greater than some threshold. This is desirable because in order to estimate brain activity, we want to do our best to remove any spike component, for the whole duration the spike effect may be occurring. However it is limited because the different channels may have different spike window length in the replicate and so the model has to be fitted separately for each channel in order to compute the partial residuals and fits. So we select the 4 channels of interest in this case and choose the maximum length of the spike window in these four channels based on the raw data. This is then fixed as the spike window length for a particular additive model (for each trial, condition and subject) which is then fitted simultaneously for all channels in a spatiotemporal additive model. [Note that this may underestimate spikes in some channels, but those are not of importance to this particular experiment.]

For example in replicate 4 of subject 9, condition 2, the maximum spike length of the four channels 8, 24, 34 and 40 is estimated as 23 units (4 to 5 ms) and this is taken as the fixed window span for this replicate. We note that channel 2 has the maximum spike length of 10 ms in this replicate, which is underestimated by the fixed window span. However on fitting the spatiotemporal model, the partial residuals from channel 2 look reasonable (Fig. 2.10).

The four channels of interest (8, 24, 34 and 40) also look reasonable (Fig. 2.11).

2.3.4 Variation within and between subjects in TMS-EEG experiments

Once the 'brain' signal of interest is extracted after discarding the artefact estimates, we plot the spatiotemporal signal as a topological map of the brain over time to investigate the spatiotemporal patterns. These plots highlight the change in intensity (amplitude) over time. Considerable variability is detected across several time instances between channels in a single replicate as well as between

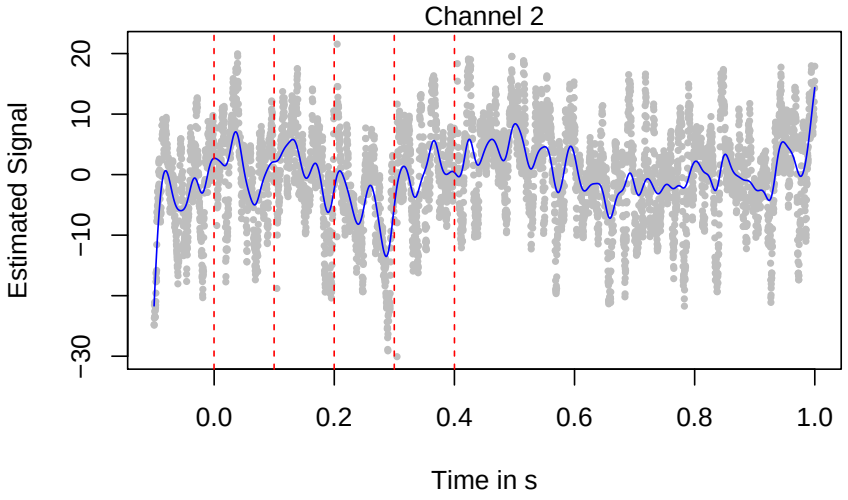

FIGURE 2.10: Fitted signal and partial residual from channel 2 using fixed length span of spike window as maximum length of 4 channels of interest (8, 24, 34 and 40)

replicates within a subject. Fig. 2.12 shows the spatial variation of the signal of interest in three replicates of the same subject. Further, the range of amplitude of the signal also varies from replicate to replicate (as seen in Fig. 2.12) and between subjects. The TMS pulses are administered at different alpha frequencies for different subjects, as the intrinsic alpha frequency of a human brain varies from subject to subject. Some of the channels are reported to 'entrain' to the alpha frequency after the third pulse (Thut et al., 2011a) and its intensity is thought to be related to the phase angle at which the signal is at the first pulse. Hence the alpha frequency of the stimulus and phase angle of the signal may be further sources of variation.

2.4 Validation of Models

A simulation study is designed to assess the validity of the additive model framework for preprocessing raw neuroimaging data. As described before, an additive model is fitted to eliminate noise and artefacts and estimate a signal component. This signal component is assumed to be the 'brain' signal of interest which is

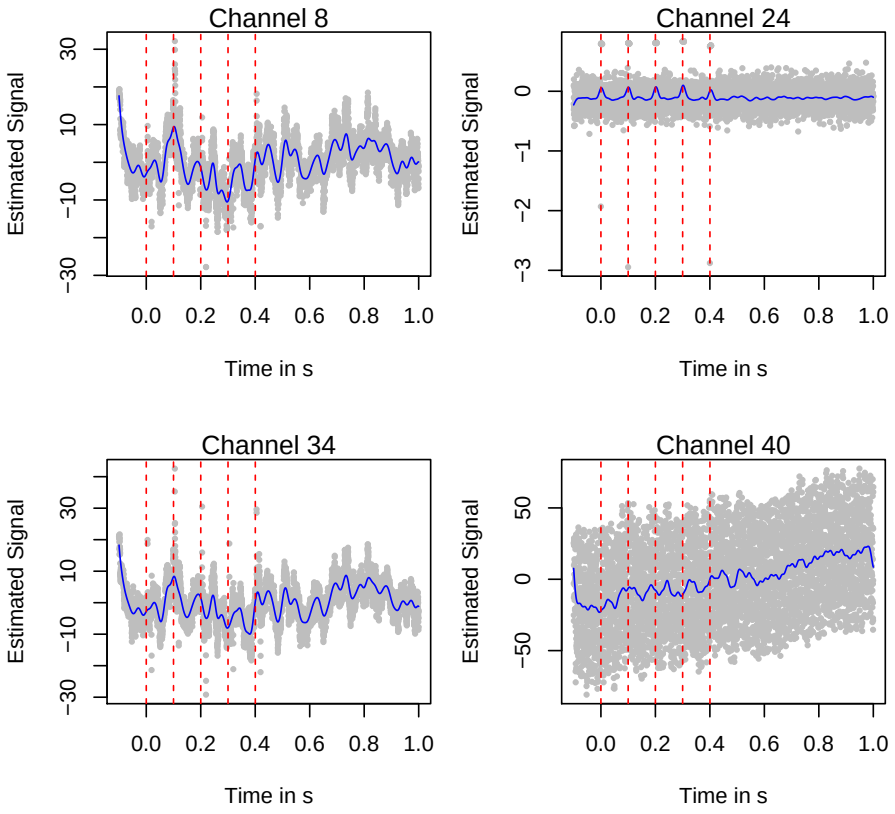

FIGURE 2.11: Fitted signal and partial residual from channels 8, 24, 34 and 40 using fixed length span of spike window as maximum length of these four channels of interest

then analysed to detect spatiotemporal patterns of interest. Bias or error in these estimates can then be of mainly two types: (i) differences in estimated and true amplitude (error along the y axis) and (ii) differences in the position of the zero-crossings (where the signal crosses the $y = 0$ line) of the true and estimated signals (error along the x or time axis). The simulation study investigates the accuracy and precision of the signal estimates in terms of these two types of biases, under certain scenarios. It is noted here that zero-crossings are described in further detail in Chapter 3.

First, a simulated signal is generated as a sum of an overall mean ν, four components denoted as $g_i, i = 1, ..., 4$ (spike, mains, trend and signal) plus an overall

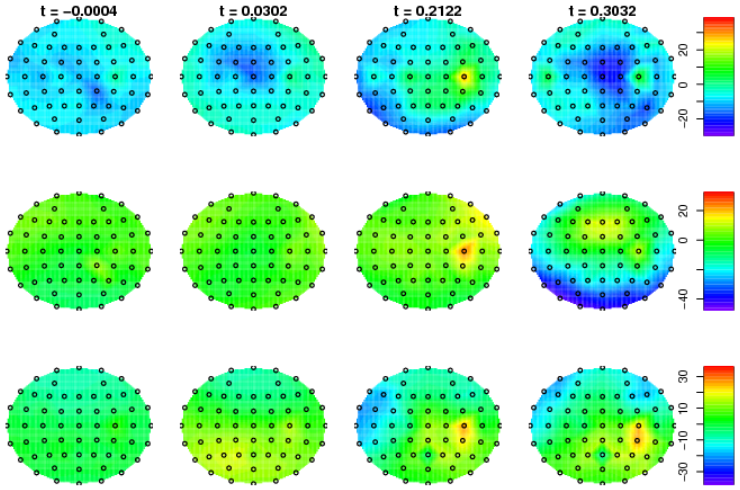

FIGURE 2.12: The spatial distribution of the signal of interest for three replicates of the same subject. Rows 1-3 show spatial brain maps for time $t = -0.0004$ (at an instant before the first TMS pulse), $t = 0.0302$ (30 milliseconds after the first pulse), $t = 0.2122$ (30 milliseconds after the third pulse) and $t = 0.3032$ (30 milliseconds after the fourth pulse) for three replicates of the same subject.

random error $\epsilon \sim N(0, \sigma_\epsilon^2)$. The simulated data is generated as:

$$y = \nu + g_1(\lambda) + g_2(t, \alpha_2, \phi_2, \beta_2) + g_3(m, c) + g_4(t, \alpha_4, \phi_4, \beta_4, f) + \varepsilon. \tag{2.4}$$

Here $g_i(), i = 1, 2, 3, 4$ define unique functions describing each component with their parameters in the parentheses. Each of the components in (2.4) is then defined as follows:

- ν denotes an overall mean.
- The spike component (g_1) is simulated using the following equation where λ determines the shape of the spikes.

$$n_1 = \begin{cases} g_1(\lambda), & \text{for 20ms at 5 pulse locations} \\ 0, & \text{otherwise.} \end{cases}$$

- The mains component $g_2(t, \alpha_2, \phi_2, \beta_2) = \alpha_2 \cos(\phi_2 t - \beta_2)$ is a cosine function of frequency 50 Hz mimicking the mains current component in the real data. Here t denotes the entire timescale, α_2 is the amplitude of the mains function fixed at 5 units, ϕ is the phase angle, β_2 is offset of the phase.

- A linear trend is denoted as a straight line $g_3(m, c) = mx + c$ where m is the slope and c is the intercept.

- The signal component $g_4(t, \alpha_4, \phi_4, \beta_4, f) = \alpha_4 \cos(\phi_4 t(1 + f) - \beta_4$ is a cosine function with a variable frequency. The signal frequency varies within the α band frequencies, with about 8 to 9 Hz pre- and post-stimulus (for the first 0.1s and the last 0.6s) and 10 Hz during the stimulus period (0.4s in between). Here t denotes the entire timescale, α_4 is the amplitude of the signal function fixed at 25 units, ϕ is the phase angle, β_4 is offset of the phase. f is a function which contributes how the frequency of the signal changes.

- ε is the error term $\sim N(0, \sigma^2)$ where σ^2 is a known variance of the error.

When the signal has constant frequency during the whole time trace, $f = c$ it implies that the signal is periodic with a periodicity $\frac{1}{f}$. To simulate an aperiodic function, f should be a changing function. In order to mimic entrainment patterns in brain-like signals, it has to change continuously from an initial frequency f_0 to a final frequency f_k. Here, we use an exponential function (like the normal pdf). We multiply by a factor $(f_k + \delta - f_0)$ to make the median roughly constant over replicates. Here δ is a random jitter $\sim N(0, 0.2)$

$$f = f_0 + \exp\left[\frac{-0.5}{\pi}\frac{(t - 0.45)^2}{0.1^2}(f_k + \delta - f_0)\right]. \tag{2.5}$$

Further, the phase of the signal at the onset of the first TMS pulse varies from replicate to replicate. In the set of 1000 simulations, 250 iterations each of the four varying phase angles at onset ($\frac{\pi}{2}, \pi, \frac{3\pi}{2}, 2\pi$ plus a small deflection ζ) are generated where $\zeta \sim U(-1, 1)$.

For the additive model framework to work well, the signal component needs to be estimated accurately. It should correctly detect (i) the amplitude of the signal and (ii) the positions of the zero-crossings of the signal. This will ensure that the amplitude, phase and frequency functions are accurate. This should be achieved irrespective of the shape of the spike (denoted as a function $f(\lambda, t)$ of the decay constant λ and the resolution of the signal $\frac{1}{t}$), variability associated with the model (σ^2), the frequency of the spike component (f_1), the presence of linear or nonlinear trend or a combination of these.

2.4.1 Design

For each scenario and the specific case within each scenario, N signals $y_i (i = 1, ...N)$ are simulated where $N = 1000$ denotes the total number of iterations for each scenario. A time span of 1.1s is considered as in the data. The resolution is reduced by a factor of 10 with respect to the experimental data such that a total of 550 time points are simulated per replicate iteration (in comparison to 5500 time points in the data). This is equivalent to sampling 1 from every 10 data points available such that the sampled points are equidistant in time. Let 4 categories of the phase angle of signal at onset of stimulus *phase_at_onset* be defined depending on where the TMS pulse 'catches' the 'brain' signal. Then a total of N iterations are computed for 4 groups of signals whose phase at onset of the signal correspond to the 4 categories of interest, number of iterations per each group then being $N/4$. For this study, a total of 1000 iterations will generate 250 iterations corresponding to each of the 4 *phase_at_onset* categories. Fig. 2.13 shows the simulated signal components in four distinct phases at the onset of the stimuli ($\frac{\pi}{2}$ radians apart).

Generation of signals of variable frequency was achieved by using a bell shaped frequency function as defined in equation (2.5). This is illustrated in Fig. 2.14. It was noted earlier that the decaying parameter λ in $g_1(\lambda)$ determines the shape of the spike component. Fig. 2.15 illustrates how the shape of the spike varies with variable $\lambda = (5, 25, 50, 100)$.

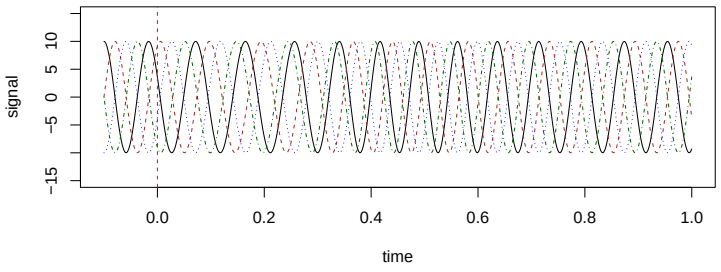

FIGURE 2.13: Simulated signal components at four distinct phases at onset (red dotted line)

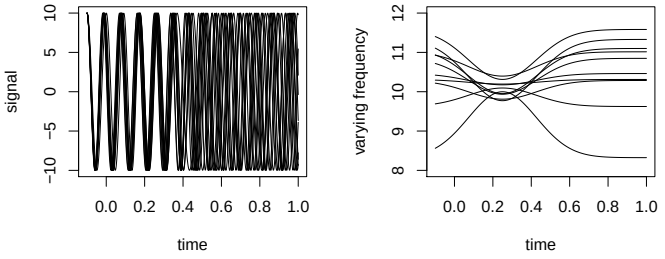

FIGURE 2.14: 10 simulated signal components (left) at varying frequency f denoted by curves (right)

To illustrate the generated simulation, plots of the 4 components in a single iteration with $\sigma^2 = 1$ and $\lambda = 25$ are shown in Fig. 2.16. The top plot shows the simulated signal. The estimates of these components from the additive model are shown in the four figures below.

2.4.2 Scenarios

We examine the component denoting the 'brain' signal of interest obtained from simulated data, under various scenarios to study the effects of these factors on the signal estimates that have been computed using the additive model framework via the backfitting algorithm. The variance of the error σ^2, the parameter that determines the shape of the spike λ and the slope of the linear trend are varied, one at a time keeping the other parameters constant. Error associated with the signal σ^2 takes values $1, 4, 9, 16$ and λ the decay constant of the spike varies as

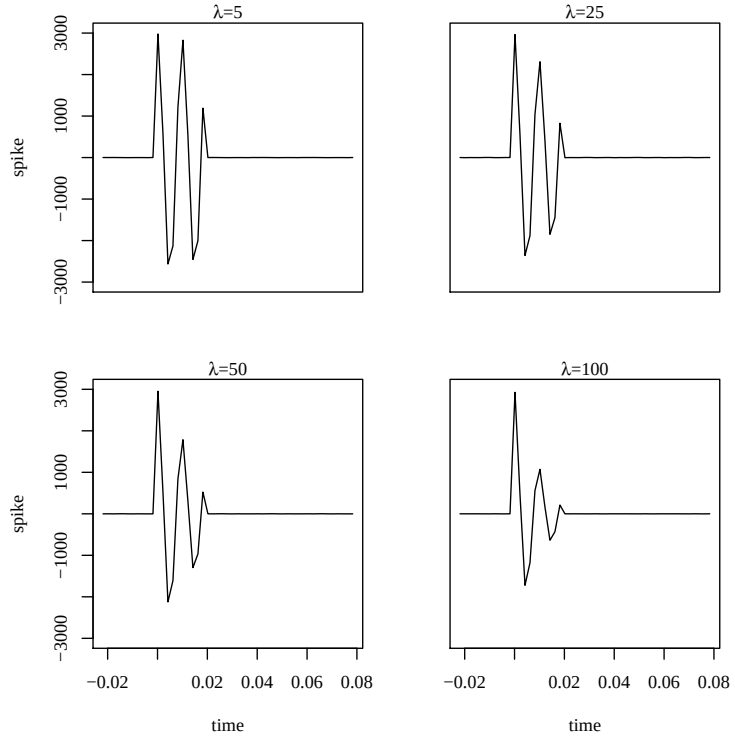

FIGURE 2.15: Simulated spike components at varying decay constants $\lambda = (5, 25, 50, 100)$

$5, 25, 50, 100$, all other parameters remaining fixed as before. A small trend is also introduced in the data, to be modelled by the additive model algorithm. Once the signals are simulated, the additive model framework is applied to all the raw simulations to estimate the various components. The signal estimates are then compared with their simulated counterparts for (i) mean squared differences in the amplitude and (ii) position of zero-crossings. Two mean squared error statistics are computed as follows:

$$MSE_1 = \frac{1}{550}\sum_{t=1}^{550}(g_4[t] - \hat{g_4}[t])^2,$$

where the index $[t]$ denotes the t^{th} time point.

$$MSE_2 = \frac{1}{n}\sum_{n}(c_0 - \hat{c_0})^2,$$

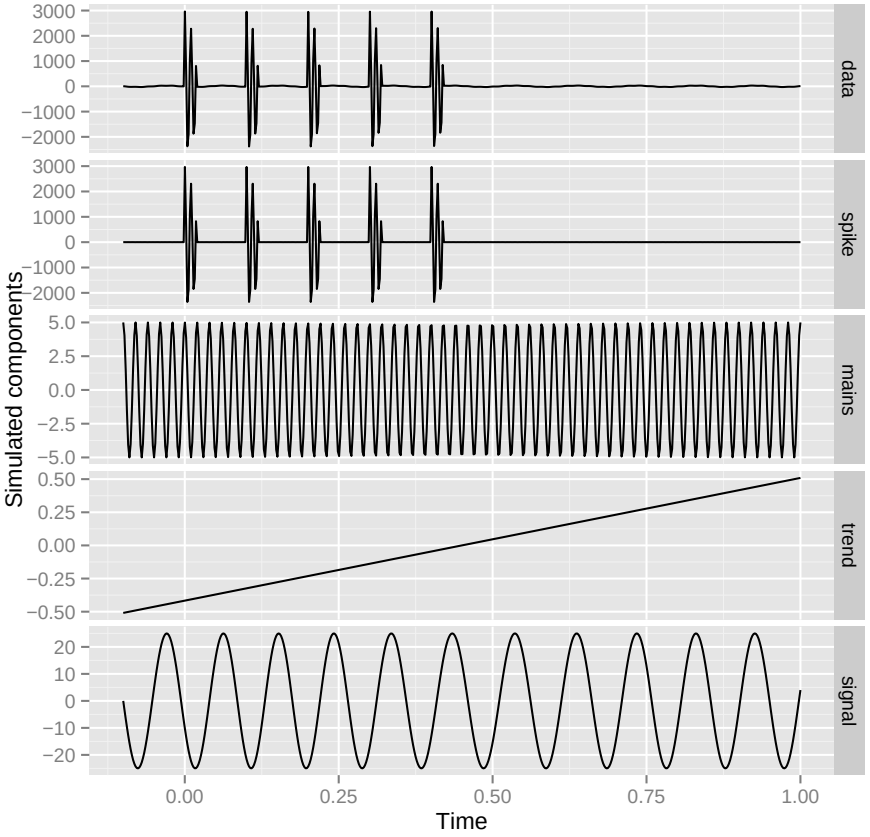

FIGURE 2.16: Simulated data (top) for an example scenario $\lambda = 25, \sigma_4^2 = 1$, a linear trend and estimates of the 4 simulated components (bottom)

where c_0 and $\hat{c_0}$ indicate the positions of zero-crossings in the simulated and estimated signals respectively, while $n = \min(n_{c_0}, \hat{n}_{c_0})$ denotes the number of zero-crossings in the simulated or estimated signals, whichever is lower.

2.4.3 Results

Fig. 2.17 and Fig. 2.18 show the distribution MSE_1 and MSE_2 for varying values of λ and σ^2. The two mean squared errors are plotted against each other in Fig. 2.19 to look for the values of these two varying parameters that minimize both the errors.

The comparatively tighter variances and low magnitudes of mean squared errors associated with both amplitude (MSE_1) and zero-crossing positions (MSE_2) for

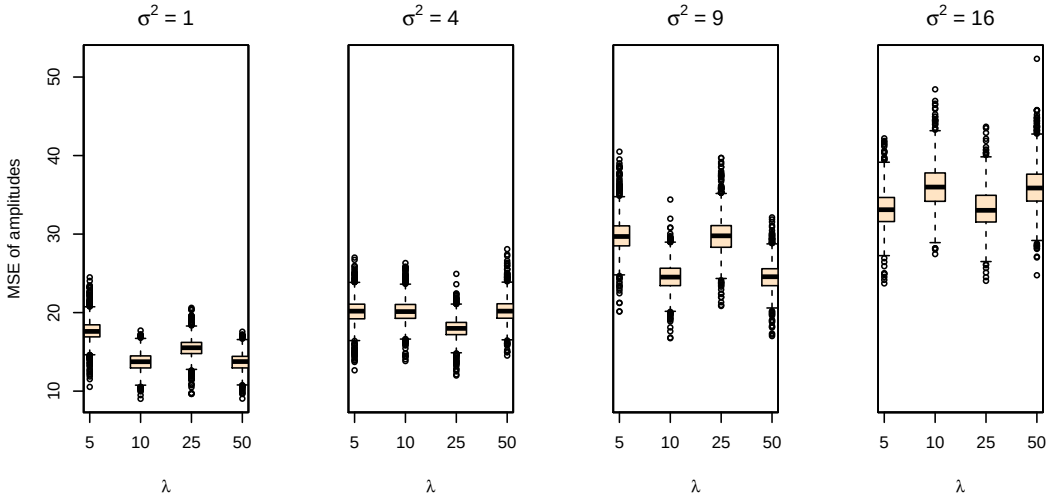

FIGURE 2.17: Distribution of the mean squared errors of amplitude in 1000 simulated and estimated signals (MSE_1) for varying $\lambda = (5, 25, 50, 100)$ and $\sigma^2 = (1, 4, 9, 16)$

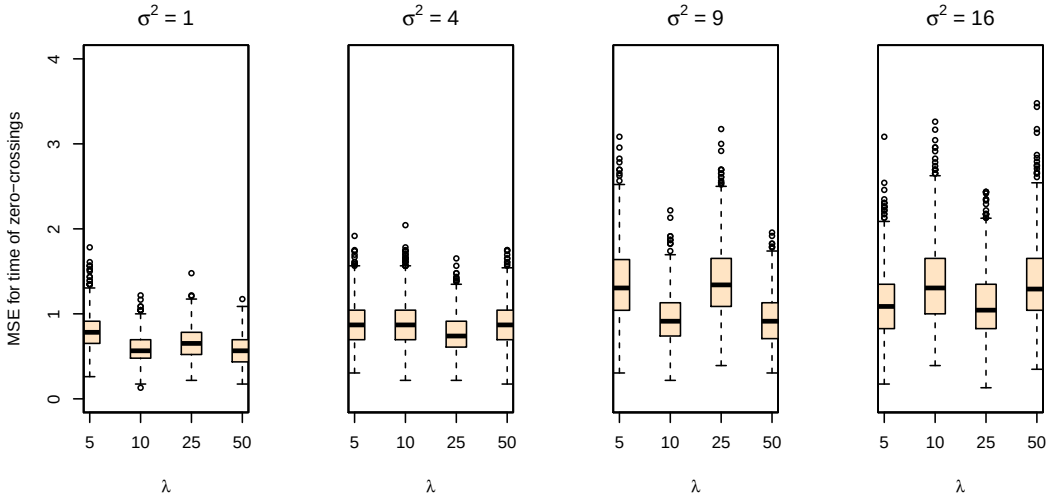

FIGURE 2.18: Distribution of the mean squared error of time differences at occurrence of zero-crossings in 1000 simulated and estimated signals (MSE_2) for varying $\lambda = (5, 25, 50, 100)$ and $\sigma^2 = (1, 4, 9, 16)$

lower values of σ_4^2 (Fig. 2.17 and Fig. 2.18) indicate that the additive model estimates are better when the variability associated with the signal is low. However, as the decay constant of the spike component λ changes, the magnitude as well as the variability in the mean squared errors of amplitude (MSE_1) and of zero-crossing positions (MSE_2) do not show any consistent change for a fixed value of σ_4^2 , high or low. The range and spread of both the MSEs are fairly low especially for the signals with less variation σ_4^2 (Fig. 2.19) making the additive model more

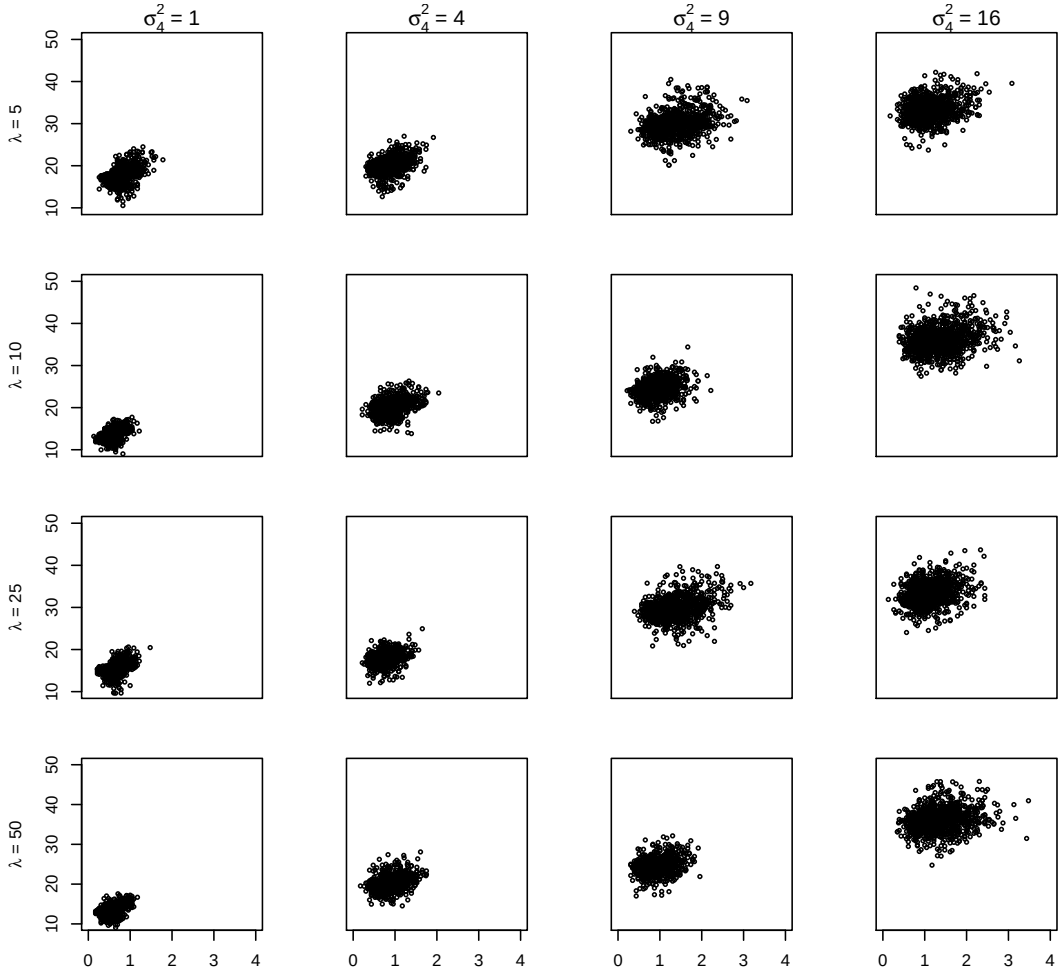

FIGURE 2.19: Mean squared errors of signal amplitudes vs mean squared errors of occurrence of zero-crossings in 1000 simulated and estimated signals

robust when the variance in the signal component is low. The mean squared errors for amplitude range between 10 and 50 and the mean squared errors for the zero crossing positions are < 4 indicating that additive models estimate the signal and artefact components well. The algorithms perform better when the variability associated with the signal is low σ_4^2.

In general, reparametrisation of the TMS-EEG data from the traditional ICA framework to an additive model and consequent application of this additive modelling strategy to decompose the data into signal and noise components provides a new framework for estimating the predominant spikes and other artefacts from such data. Since the shapes of the artefacts are all different and known to a certain degree, it becomes quite straightforward to identify these unique sources of artefacts by including this information during model fitting. The simulation study

validates the method by showing that the deviations in amplitude and location and number of zero-crossings, can be minimised with the correct choice of the decay parameters and depending upon the error variance in the data. This pre-processing step thus eliminates unwanted artefacts, and significantly improves the signal to noise ratio. This method is applied to all replicates in all the subjects for noise reduction to obtain subject-replicate level 'brain' signal of interest with a frequency within the α band of interest.

The signal estimates thus obtained, although artefact corrected and smooth, are of the same high spatiotemporal resolution (5500 time points in a span of 1.1 s for 60 channels over the scalp) as the raw signals. The next focus of this thesis is to develop dimension reduction methods for this data in order to down-sample these signals efficiently without much loss of information. This will lead to development of computationally more efficient modelling strategies for describing the neurological phenomenon of entrainment. The MEG data set on the other hand, has been received after the pre-processing step. Similar dimension reduction methods will be applied to the MEG data set as well, before the models to investigate dipolar activity are developed.

Instead of direct sampling and decimation methods, where a sample of time points and channels are selected, the signals are characterised in terms of parametric curves that describe the signals. For the TMS-EEG data temporal characterisations into frequency, phase and amplitude, adequately summarise the data features required to explain entrainment. For the MEG data further functions of these will be required to describe dipolar activity. Development of this characterisation method with applications to both TMS-EEG and MEG data sets forms the content of the next chapter.

Chapter 3

Characterisation of Signals

3.1 Introduction

Artefact corrected 'brain' signal estimates from MEG and EEG as described in Chapters 1 and 2 now consist of high dimensional oscillatory brain signals for a number of channels or sensors which have particularly high resolution in time. High resolution of the data results in computationally intensive and expensive statistical models. It is therefore imperative to reduce the dimensions of the data sets before model fitting is carried out. Moreover, in order to model temporal phenomena such as 'entrainment' of the signals over time and spatiotemporal features such as 'dipoles' as captured by a group of sensors over time, the information embedded in the signals can be transformed into characteristic temporal curves such as frequency, phase and amplitude and spatial features such as out-of-phase activity at the poles of a dipole.

From the signal processing perspective, the first problem to be addressed here is that of down-sampling to reduce the number of sensors and time-points at which the signal measurements are recorded. Filters applied to the signals allow for signal components of certain frequency to pass through and others to be attenuated. Decimation is the reduction of the sampling rate by an integer (or rational) factor that leads to downsampling and hence a reduction in the data size. It can

simply be viewed as a projection or mapping from a vector of size D to a vector of size L, where $D > L$ (Carreira-Perpiñán, 1997). This amounts to passing the signal through a low-pass filter - where low frequency signals (less than a threshold frequency) pass through and high frequency signals are attenuated. There are several methods for down-sampling and transforming to the time-frequency domain in neuroimaging, some popular techniques being based on discrete or short term Fourier transforms (Salehin and Abhayapala, 2010, Zhang et al., 2005), discrete wavelet transforms, polynomial and spline based detrending (Tanabe et al., 2002), spatial spectral decomposition (Nikulin et al., 2011) and principal components (Haufe et al., 2014, Naeem et al., 2009). A low-pass filter is limited by a disadvantage that it tends to introduce correlation into the signal (Catherine E. Davey, 2013, Friston et al., 2000).

In this chapter, a simple and novel characterisation method for EEG and MEG brain signals based on Euler's formula (Eilers, 2010, Moskowitz, 2002) is proposed which performs both the functions simultaneously. This method condenses the information to a few functional parameters based on temporal functions such as phase/instantaneous frequency and amplitude of the signals and spatial functions such as location, orientation and size of dipolar activity in the brain and their functions thereof. In the process, the dimensionality of the data is automatically reduced quite drastically without compromising on the information required to explain the neurological phenomena. In situations where the brain is stimulated by externally controlled Transcranial Magnetic Stimuli (TMS) while being simultaneously recorded by EEG, statistical evidence of entrainment of the brain signal as tracked by the EEG signals to the specific α band frequency (8-12 Hz) is of interest. In MEG experiments, dipolar behaviour, where adjacent regions in the brain oscillate at similar α frequency and amplitude in an out-of-phase manner, is often under investigation. Hence the characterisation of the signals must be carried out in such a manner that the transformed data retain the information required to describe these spatiotemporal patterns.

It should be noted that the signals vary between channels or sensors, replicates and subjects. These signals are not periodic as they do not adhere to a fixed time

period or frequency. Further, the amplitude may also vary over time. These characteristics of the 'brain' signals suggest that they are quasi-periodic in nature. The objectives of this chapter are then firstly, to characterise these signals in terms of temporal and spatial parameters and secondly, to summarise the variation in these functions across experimental conditions, and check for variability at the subject and replicate levels. Temporal and spatiotemporal patterns in these functions for assessing statistical evidence in support of the two neurological phenomena - entrainment and dipolar behaviour respectively - are dealt with in subsequent chapters.

Section 3.2 outlines the theoretical concepts used to characterise the 'brain' signals of interest for each of the EEG and MEG applications. The time traces of the estimated signals from the spatiotemporally smoothed additive model (estimated 'brain' signal of interest) for a particular EEG channel CP4 (which is of primary interest) for three selected subjects are summarised in terms of characteristic functions of phase, frequency and amplitude in Section 3.3. Only temporal characteristics are considered in case of the EEG data since the phenomenon being described is temporal in nature. For the MEG data set in Section 3.3, temporal as well as spatial characteristic functions are illustrated for three individuals. To provide a complete treatment of the data sets, a summary of the characterisation for the remaining subjects are reported as supplementary material in Appendix I. A detailed discussion of the illustrative results in Section 3.3 is carried out in Section 3.4. This section also explains how the results obtained from the characterisation is further utilised for statistical modelling to describe the neurological phenomena under investigation.

3.2 Characterisation of 'brain' signals of interest

As mentioned earlier, functional neuroimaging signals are high dimensional in space and time having particularly high resolution in time. In the TMS-EEG data set, signals are simultaneously recorded from 60 channels at very fine temporal

resolution of 5 time-points per millisecond. The MEG data set has a finer spatial resolution (256 sensors) and has high resolution in time (1 time-point per millisecond). In order to gain efficiency during model fitting to such large data sets, it is therefore useful to reduce its dimensionality. Further both 'entrainment' and 'dipolar activity' can be explained as a combination of features of their temporal and spatiotemporal characteristic functions respectively. Entrainment, for example, occurs when the frequency of the signal changes to the desired α band for a considerable period of time, and is often associated to an enhancement in amplitude. Dipolar activity, on the other hand, constitutes adjacent groups of sensors showing oscillations in the α band - with the two poles being out-of-phase. Temporal characteristics such as frequency, phase and amplitude plays a significant role in describing these phenomena adequately. Further, spatial characteristics such as location or size of the dipole may be of relevance.

3.2.1 Complex Logarithm model

In order to compute the phase and amplitude curves from the signal, zero-crossings from the complex logarithm model paradigm discussed in (Eilers, 2010) are used. This model is not directly fitted to the data - only some of its features are made use of in computing the phase and frequency using the zero-crossings. A complex logarithm model for quasi-periodic signals is based on Euler's formula (Moskowitz, 2002) from complex analysis given as:

$$\exp(\alpha + i\phi) = e^{\alpha}(\cos\phi + i\sin\phi),$$

The 'brain' signals of interest, obtained after estimating and subtracting the artefacts, present themselves with variable frequency and amplitude within and between replicates and subjects as well as across experimental conditions. In this particular application of the complex logarithm model, the real part of the equation is used to estimate the variable frequency and amplitude as functions of time, given by the functions $\phi'(t) = \frac{1}{2\pi}\frac{d\phi(t)}{dt}$ and $e^{\alpha(t)}$ respectively. The model for the brain signal of interest obtained at the i^{th} channel in the j^{th} replicate of the k^{th}

subject can then be written as:

$$\exp(\alpha(t)) = e^{\alpha_{ijk}(t)}(\cos\phi_{ijk}(t))), \tag{3.1}$$

where α is the amplitude and ϕ is the phase of the signal.

Zero-Crossings

A simple idea that is used in order to estimate the functional forms of the phase, frequency and amplitude is that of the zero-crossing. A zero-crossing is the point in time at which the signal has a zero value. A vector of zero-crossings is defined by a vector ($\mathbf{z}$) of p positive integers which mark the time indices $t_z, z = 1, ..., p$ where the signal crosses the zero line (Fig. 3.1) along the entire time trace. Thus p denotes the total number of zero-crossings in the trace. It follows that:

1. the phase angle moves by π radians between two consecutive zero-crossings t_z and t_{z+1},

2. the difference between the z^{th} zero-crossing and the $(z+2)^{th}$ zero-crossing illustrate a complete oscillation or cycle (Fig. 3.1) which is also equivalent to the angular distance travelled by the signal in one cycle (2π radians or $360°$) and

3. the zero-crossings $[0, \pi, 2\pi, ..., (p-1)\pi]$ (in the y axis) plotted against the corresponding time indices (in the x axis) and smoothed give the phase function (Fig. 3.2(b)).

An underlying assumption here is that the phase, and hence the frequency changes smoothly over time.

3.2.2 Functional Parameters

The zero-crossings of a signal trace determine the cumulative phase in multiples of 2π. These zero-crossings are plotted against their corresponding time indices,

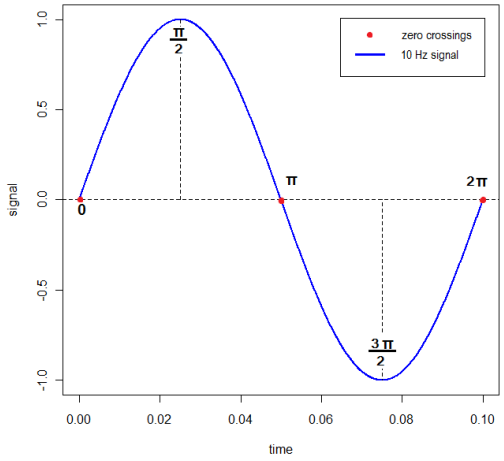

FIGURE 3.1: Graphical representation of zero-crossings (red dots) and phase angle (in radians) for a single oscillatory cycle in a sinusoidal function of 10 Hz frequency.

to obtain a phase function. Instantaneous frequency (Boashash, 1992) is obtained by differentiating the smooth phase function. The variable amplitude function is estimated by obtaining a smooth function and subsequent exponentiation of $\alpha_{ijk}(t)$.

Absolute signal values sampled at regular intervals in time and subsequently smoothed, give an approximate curve describing the amplitude. The number of sample points selected depend upon the frequency of interest and the degree of variation of the frequency in time. Capturing higher frequencies requires a finer timescale and vice versa. Alternatively the points of inflection and the time indices where they occur, provide a good description of the varying amplitude. The frequency (first derivative of phase) function and the amplitude function together provide the information to reconstruct the signal approximately. Before, the signals are characterised, the parameters are discussed in some detail.

Phase of a signal at a channel at a specific time point refers to the fraction of a complete oscillation elapsed as measured from a specified reference point, illustrated in Fig. 3.2(b). Here the reference point is taken to be the first zero-crossing, and its value is assigned as 0 or π depending on whether the signal at that point is increasing or decreasing. The phase at the reference point is 0

or π radian(s) and at each successive zero-crossing it increments by $180° = \pi$ radians. An entire oscillatory cycle lasts for $360° = 2\pi$ radians (Fig. 3.1). Once the zero-crossings are determined (Fig. 3.2(a)), the phase function is determined by smoothing over the phases at these zero-crossings (Fig. 3.2(b)).

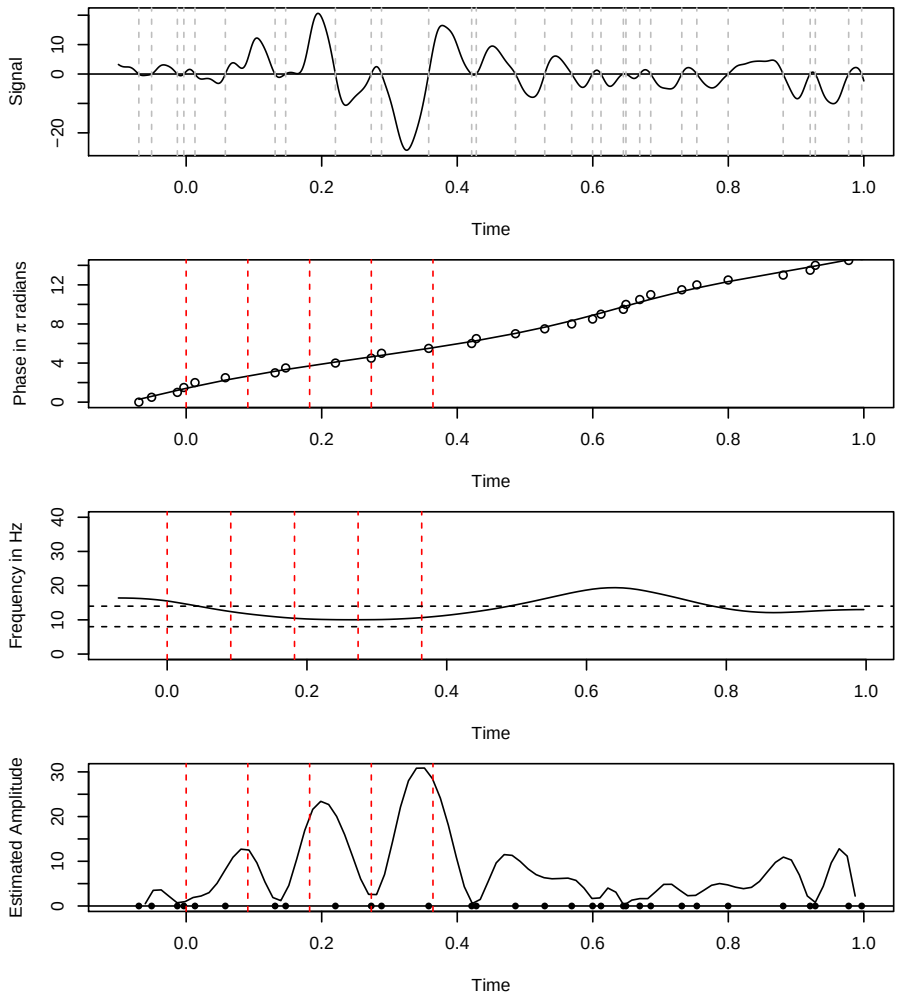

FIGURE 3.2: (a) Signal trace of a single channel with zero-crossings, (b) estimated phase and smooth phase function, (c) estimated frequency function, (d) estimated amplitude function.

Instantaneous frequency is given by:

$$\phi'_{ijk}(t) = \frac{1}{2\pi}\frac{d\phi_{ijk}}{dt}.$$

Using this equation, the first derivative of the phase function $\phi_{ijk}(t)$ denotes a frequency function $\phi'_{ijk}(t)$. The estimated frequency function is shown in Fig. 3.2(c).

Amplitude at any time point may be thought of as the deviation of the signal from the zero line at that time point. Thus, it is the absolute value of the signal. In the complex logarithm Eqn. 3.1, the amplitude is given by $e^{\alpha_{ijk}(t)}$. Another method to estimate an approximate amplitude curve directly from the zero-crossings is to compute the maximum absolute signal between two consecutive zero-crossings. This value when plotted at the mid point between the zero-crossings and smoothed provides an approximate amplitude curve. An example of this is illustrated in Fig. 3.2(d).

Since dipoles occur when the two adjacent regions are out-of-phase, it involves two poles. A function of the difference of phase in two adjacent poles of a dipole is defined as **Dipolar Strength**. A dipole is detected when two conditions are satisfied: poles oscillate at the same frequency and the pole signals are out-of-phase, so a function showing the difference in phase - which takes the value $[0, \pi]$ is of interest in order to locate when the the phase of the two signals are out-of-phase. This difference function $\beta(t)$ is denoted as:

$$\beta(t) = \min(\Delta(t), 2\pi - \Delta(t)); \qquad \Delta(t) = |\hat{\phi}_1(t) - \hat{\phi}_2(t)| \mod 2\pi,$$

where the closeness of $\beta(t)$ to π indicates the presence of dipolar activity when the frequency at the two poles are similar (A simple rule used by Ventrucci et al. (2014) is $|\hat{f}_1(t) - \hat{f}_2(t)| < 2$ or the pole frequencies lie within 2 Hz of each other at the time when the dipolar strength is maximum). A more appealing function of the dipole strength is the continuous temporal weight function given as:

$$\omega(t) = \exp\{-0.5(\hat{f}_1(t) - \hat{f}_2(t))^2/1^2\} \exp\{-0.5(\pi - \beta(t))^2/0.5^2\}, \tag{3.2}$$

which decreases from 1 in a smooth fashion as $\hat{f}_1(t)$ and $\hat{f}_2(t)$ move away from each other and as $\beta(t)$ moves away from π. So the function $\omega(t)$ given by (3.2) consolidates information about the similarity of frequencies between the poles as well as their out-of-phaseness.

Further, since occurrence of a dipole has a spatial component, three spatial characteristics, namely the **location**, **size** and **orientation** of the dipole are of interest. A search algorithm developed by Ventrucci et al. (2014) establishes a simple technique to assess the presence of a dipole and model it. A brief description of the techniques from their paper and used for this research is presented below.

As already pointed out, neuronal activity in the brain is detected by MEG sensors and assumed to be spatiotemporally smooth, following a dipolar pattern, with random noise. The spatially smooth component of this dipolar pattern consists of two adjacent regions in the scalp oscillating with similar frequency (and amplitude) in an out-of-phase manner. They may vary in location, size and orientation of one pole relative to the other. Assuming that the location and orientation of the dipole is fixed for a particular replicate, the model can be given as:

$$m(x, y, t) = \varphi_1(x, y).\gamma_1(t) + \varphi_2(x, y).\gamma_2(t) \quad ,$$

where the spatially smooth functions $\varphi_i(x, y), i = 1, 2$ describe the spatial characteristics of the two poles and the temporally smooth $\gamma_i(x, y), i = 1, 2$ describe their temporal characteristics. (Ventrucci et al., 2014) proposed a simple but effective model for this dipole topography where the shape of each pole is modelled using a bivariate normal density function. The temporal trace each pole is modelled using a quasi-periodic model described above.

Bivariate model for spatial topography:

In order to model the spatial topography of the dominant dipole during the prestimulus period, a scaled bivariate density function is used (Ventrucci et al., 2014) and applied to all replicates in multiple subjects, for this thesis:

$$\varphi_i(x, y) = \exp\left[-\frac{1}{2h^2}\{(x - \mu_{x,i})^2 + (y - \mu_{x,i})^2\}\right]; \quad i = 1, 2 \quad ,$$

where h is the radial size, $(\mu_{x,i}, \mu_{y,i})$ gives the location in cartesian coordinates and $i = 1, 2$ denote the indices for the two poles. Further, expressed as polar

co-ordinates, the location for each pole can be denoted as:

$$\mu_{x,1} = \mu_x + r\cos\theta, \qquad \mu_{y,1} = \mu_y + r\sin\theta \quad ,$$

$$\mu_{x,2} = \mu_x - r\cos\theta, \qquad \mu_{y,1} = \mu_y - r\sin\theta \quad ,$$

where (μ_x, μ_y) is the centre of the poles, θ denotes the angle of orientation, and r is the distance between the two poles. The sizes of both the poles are assumed to be fixed and equal to h.

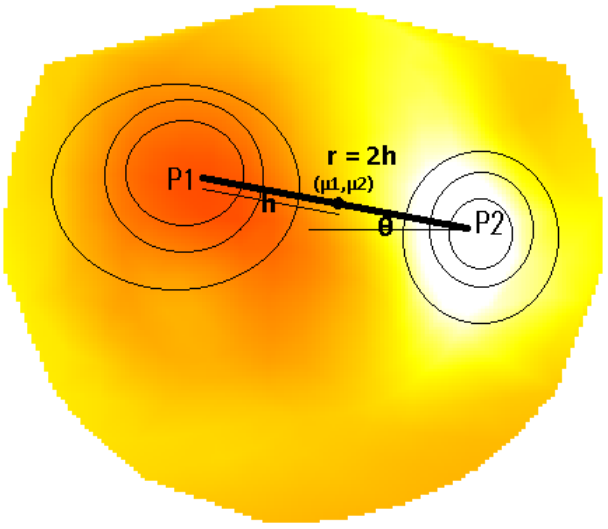

FIGURE 3.3: Diagramatic representation of a dipole, where (μ_1, μ_2) denote the location; $r = 2h$ the distance between the poles and h the size of one pole together quantify the size of the dipole, and θ denotes the angle of orientation in radians

Fig. 3.3 depicts the location, size and orientation of a fitted dipole. After the signals are characterised in terms of the temporal parameters - phase, frequency and amplitude for the EEG case and frequency, amplitude, dipolar strength and spatial parameters of location, orientation and size of dipoles for the MEG case - the corresponding functional curves are summarised for all subjects across all

replicates and experimental conditions. Summary results from 3 subjects are presented in this chapter and similar summary from the remaining 12 subjects are reported in the Appendix A for completeness of data. These summaries are further investigated to study the entrainment and dipole patterns in the 'brain' signals in later chapters.

3.3 Summary of Experimental Data

3.3.1 Case Study I: EEG

The phase, frequency and amplitude curve of the estimated 'brain' signals, capture functional data at each channel of the TMS-EEG setup. Functional data is a representation of data observations as a functions, which in practise may be represented as a set of discrete data points tracing the functions for computational ease. For each channel at each replicate of a subject, the phase is determined by an increment of π at each successive discrete zero-crossing and smoothed using a `smooth.spline` function `R package` in order to obtain the phase function over time $\phi(t)$. The frequency function is predicted as a first derivative of the phase curve $\phi'(t)$ using `predict()`. The mean and variance functions of the phase and frequency are evaluated by computing the mean and variance as $\bar{x}(t) = N^{-1}\sum_{i=1}^{N} x_i(t)$ and $var_X(t) = (N-1)^{-1}\sum_{i=1}^{N}[x_i(t) - \bar{x}(t)]^2$ for N replicates (usually 54 replicates for each subject and condition) at $t = 1, ...100$ equidistant points using the smoothed parameter functions and then interpolated as a smooth curve. The standard deviation σ is the square root of the variance.

The distribution of frequency/phase functions, amplitudes and phase angles at pulse locations is then studied across several subjects for the main condition and the three controls. The artefact corrected 'brain' signals of interest for subject S02 corresponding to all the four conditions is illustrated in (Fig. 3.4). The zero-crossing method is applied to these signals to obtain their phases (Fig. 3.5), frequencies (Fig. 3.6) and amplitudes (Fig. 3.7). The curves for phase and frequency,

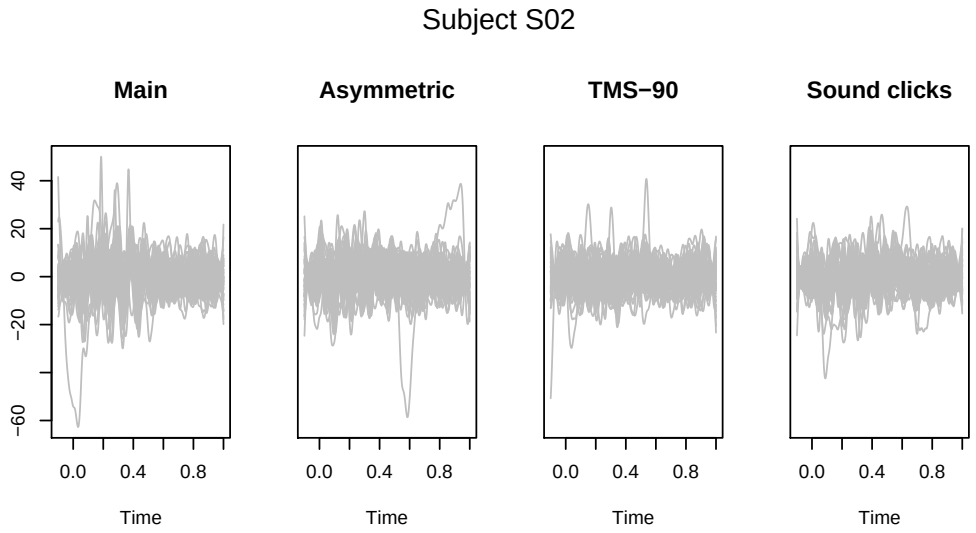

FIGURE 3.4: Estimated signals for all replicates of subject S02 across all four conditions with the estimated functional mean curve of the signals shown by a red solid line and estimated functional standard deviation curves around the mean curve by blue dotted lines. Vertical red dotted lines represent the positions of the TMS pulses in time.

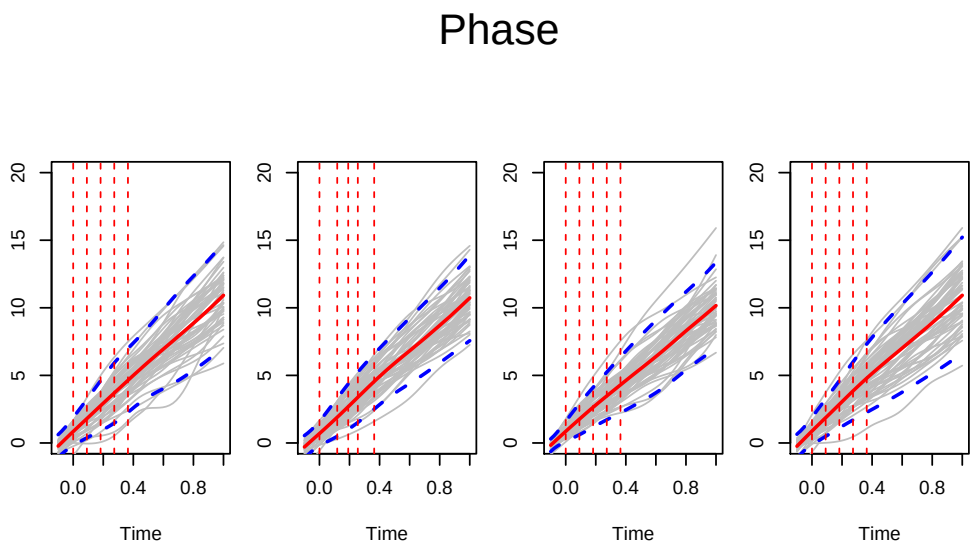

FIGURE 3.5: Estimated phases for all replicates of subject S02 across all four conditions. Vertical red dotted lines represent the positions of the TMS pulses in time.

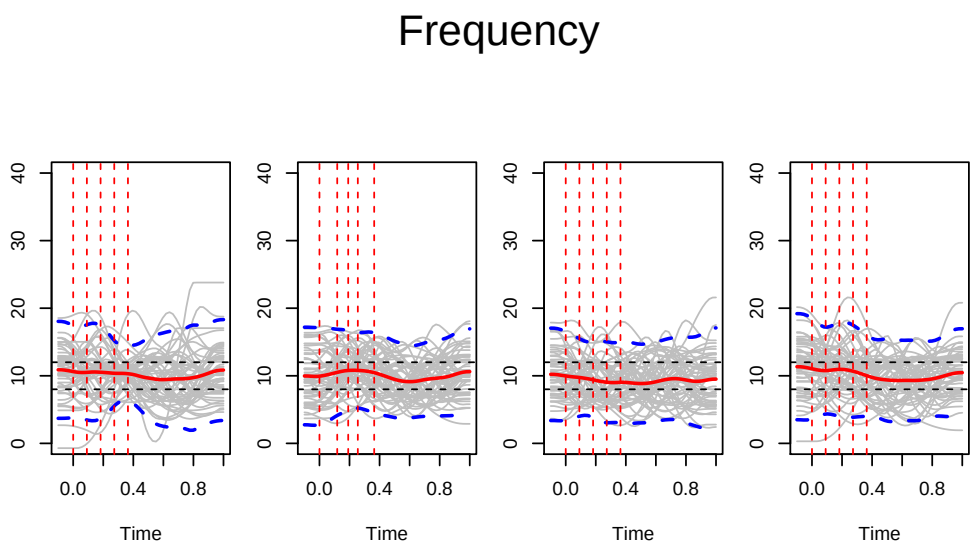

FIGURE 3.6: Estimated frequencies for all replicates of subject S02 across all four conditions. Vertical red dotted lines represent the positions of the TMS pulses in time. Black dotted lines denote the α band of frequencies.

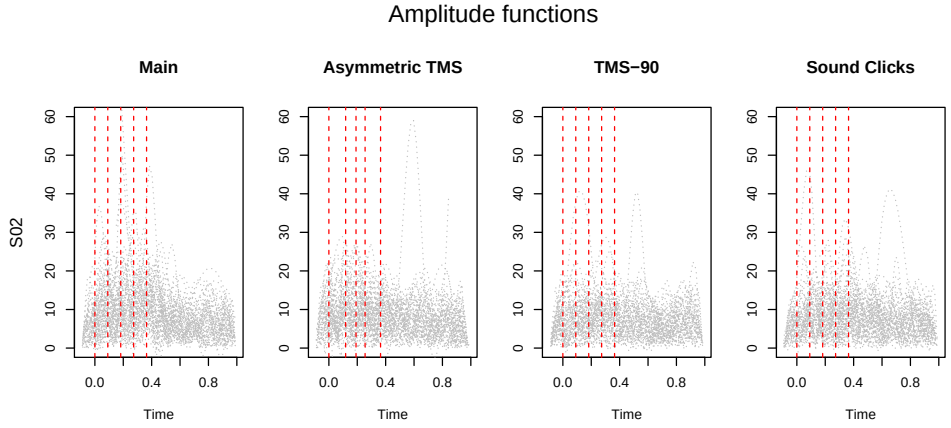

FIGURE 3.7: Estimated amplitudes for all replicates of subject S02 across all four conditions. Vertical red dotted lines represent the positions of the TMS pulses in time.

are summarised as a functional mean curve (red solid) and functional 2σ confidence bands (blue dotted) around the mean curve in these plots.

Fig. 3.8 shows the three temporal characteristics for 3 subjects when the main condition of TMS pulses at regular intervals is administered. These plots start to show a difference in patterns of variation over replicates for each subject and also between the different subjects. The frequency curves tend to lie in the α band of interest indicating that the signals show evidence of entrainment. Amplitude

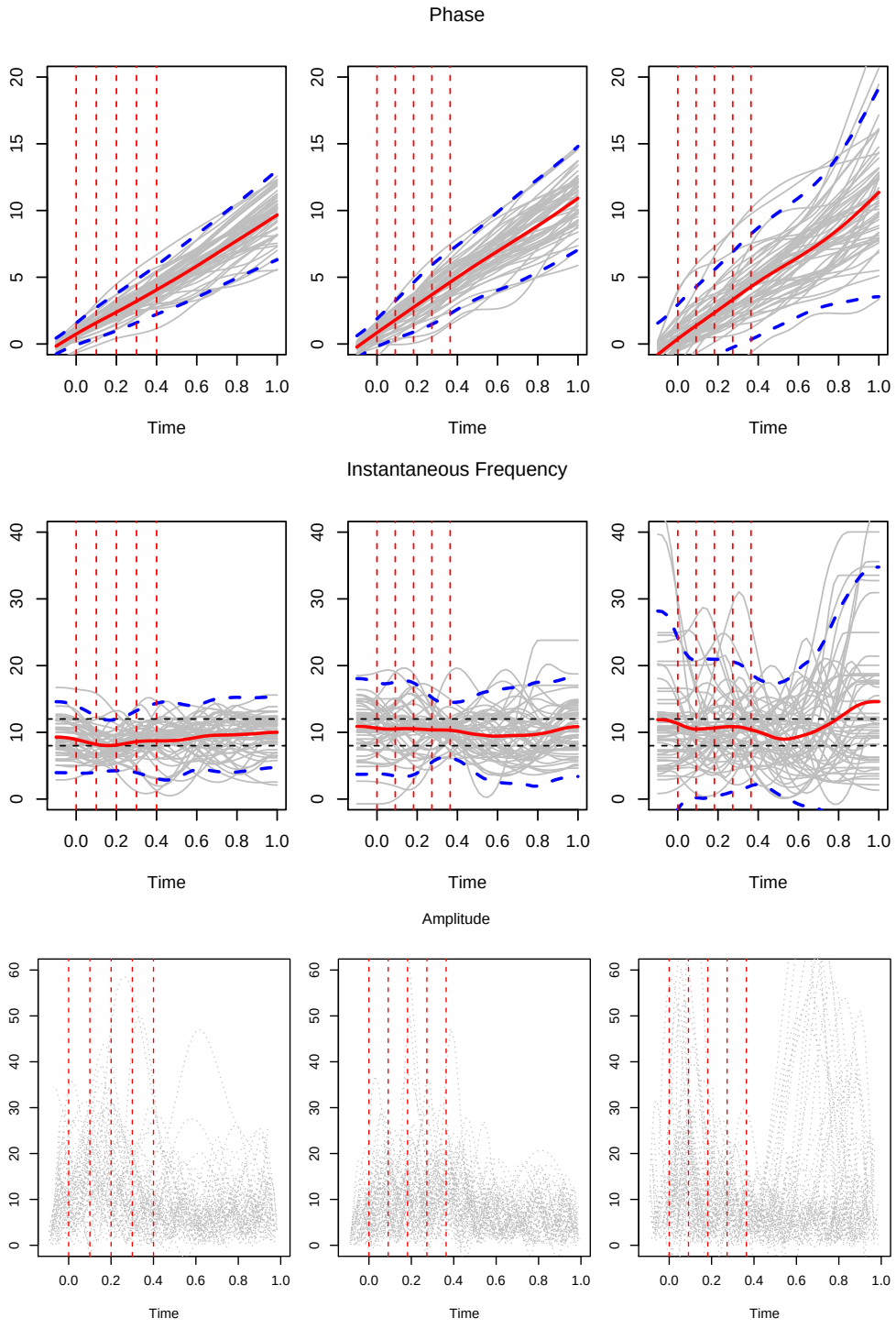

FIGURE 3.8: Estimated phase, frequency and amplitude curves for all replicates in the main condition for 3 different subjects with smoothed functional mean curves (red) and 2× smoothed functional standard deviations (blue dotted) around the mean curve.

curves do not demonstrate a marked enhancement in time duration of following the first TMS pulse being administered, although some replicates show increase in amplitudes for all these three subjects

3.3.2 Case Study II: MEG

Activation in MEG signals is thought to be a dipole pattern where typically two adjacent regions of the brain have positive and negative electromagnetic fields which oscillate smoothly over time in an out-of-phase manner. Dipole modelling for resting states in single trials using a quasi periodic spatiotemporal model is shown in (Ventrucci et al., 2014). Here similar approaches are applied to characterise and summarise dipolar behaviour in the pre-stimulus resting state for all replicates of 3 selected subjects in an experiment for illustration.

Estimated MEG signals are considered for all replicates of 15 individual subjects for a period of 1s. At 0.5s one of four predetermined visual stimuli is administered and the subject is asked for a motor response. Data considered here is from the first 0.5s resting state before any visual stimulus is presented to 3 of these subjects. Dipolar activity during this period is modelled using a quasi-periodic search algorithm (due to Ventrucci et al., 2014) which characterises each trial as a set of spatial parameters - orientation, spatial location and size; and temporal functions - mean frequency, amplitude and dipole strength.

Quasi-periodic model for temporal trace

Based on the theory outlined in Section 3.2 and equation (3.1), the temporal trace in the general form of the dipole model in (3.3) is a smooth function in time at each pole $\gamma_i(t), i = 1, 2$. Since these functions vary over time, they characterise the oscillation of the pole over the time duration of the chosen pre-stimulus period. The MEG dipoles temporally exhibit quasi-periodic behaviour. A smooth complex logarithm model (Eilers, 2010) is hence used to describe the temporal oscillatory signature of the signal.

The model is given as:

$$\gamma_i(t) = \exp(\alpha_i(t)) \cos \phi_i(t); \quad i = 1, 2$$

where, $\alpha(t)$ denotes the amplitude function on the log scale and $\phi(t)$ denotes the phase function. Further, a smooth intercept function $\delta_i, i = 1, 2$ is included in the model to track the shifts in the mean level of the signal:

$$\gamma_i(t) = \delta_i(t) + \exp(\alpha_i(t)) \cos \phi_i(t); \quad i = 1, 2 \tag{3.3}$$

The spatial functions - location, size and orientation of the poles and temporal functions - frequency and amplitude are estimated using the models described above (and methods described in detail in Ventrucci et al., 2014) for all replicates of each experimental condition for each of the 15 subjects. In a single replicate, the spatial information identifies the location size and orientation of the most dominant dipole in the pre-stimulus period. Spatial topography of a dipole at a specific time point for a single replicate is displayed in figure 1.6.

The smooth pole signals at each pole of the detected dominant dipole is computed by the functions derived from $\gamma_1(t)$ and $\gamma_2(t)$ after subtracting the mean shift. The phase $\phi_i(t), i = 1, 2$, frequency $\hat{f}_i(t) = \frac{\hat{\phi}'(t)}{2\pi}$ and amplitude $\alpha_i(t), i = 1, 2$ curves are derived using the zero-crossings method described in section 2 of Chapter 3 for EEG and the quasi-periodic model (3.1). These functional curves from a single trial in subject AHE08 are provided in Fig. 3.9.

Fig. 3.9 (b) shows that the frequency of the signals is in the α band as expected, and dipolar activity is detected 0.1 s into the pre-stimulus period (t = -0.4). This is also picked up in the curve for dipolar strength (d). The pole signals depict out-of-phase behaviour at 0.1 s into the pre-stimulus period (t = -0.4). The amplitude functions (c) show that the amplitudes are similar, and an average amplitude curve (red dotted line) is derived for each pair of pole signals in order to capture a mean amplitude behaviour of the dipole.

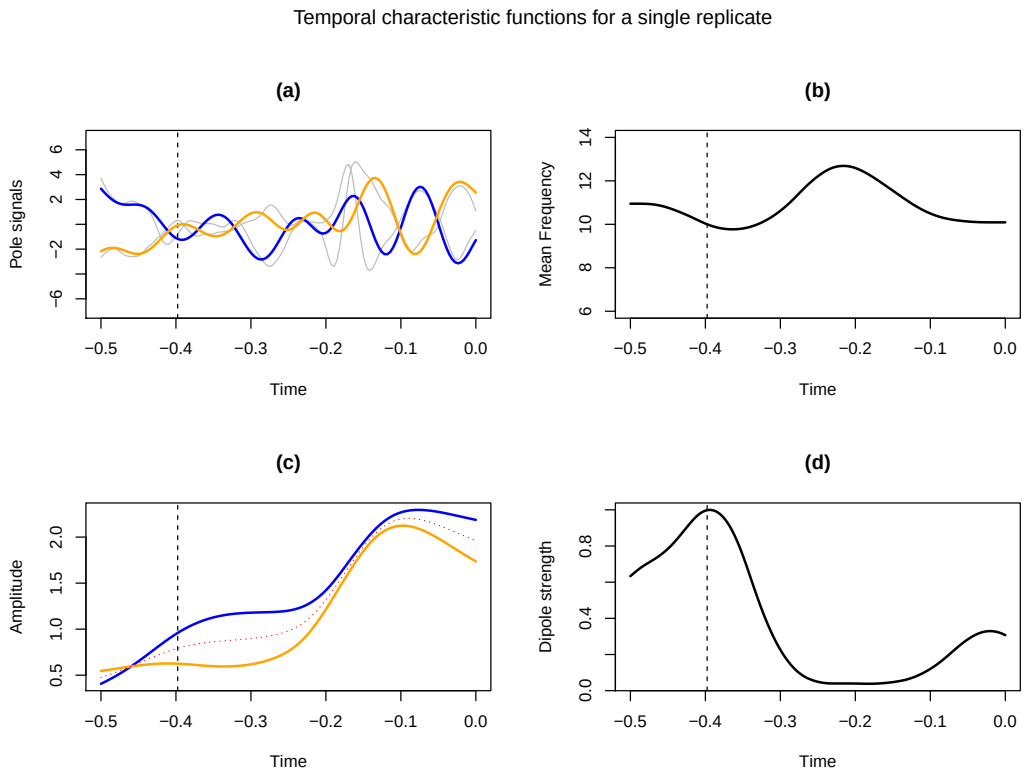

FIGURE 3.9: Temporal characteristics of a single replicate: (a) Smooth pole signals (orange and blue) with actual time trace of the signals in grey, (b) Mean frequency of the poles, (c) Amplitude curves of the poles (orange and blue) with mean amplitude in red dotted line, (d) Dipole strength

Temporal functions

The temporal curves of mean frequency and amplitude averaged over the two poles are derived for all replicates in 3 subjects and are displayed in Fig. 3.10 and Fig. 3.11. The functional mean curves for all replicates in each subject are denoted by the red dotted curves and the functional 2× standard deviations are denoted by the blue dotted curves. It can be seen that the functional means of frequency (Fig. 3.10) lie in or close to the α band of frequencies which are of interest in the study. Further, they are flat in nature without much fluctuations in the values, although the frequencies of individual replicates vary with time. This is because averaging the means cancels out the variations within subjects. Between subject variation is evident in the differences of the functional mean functions and variability of the first two subjects (AHE08 and MME25) and the third (TMR04). Similar variation patterns between subjects and replicates within subjects are seen in Fig. 3.11. Also TMR04 has a much broader band of magnitude within the

2× standard deviations around the functional mean amplitude in comparison to AHE08 and MME25.

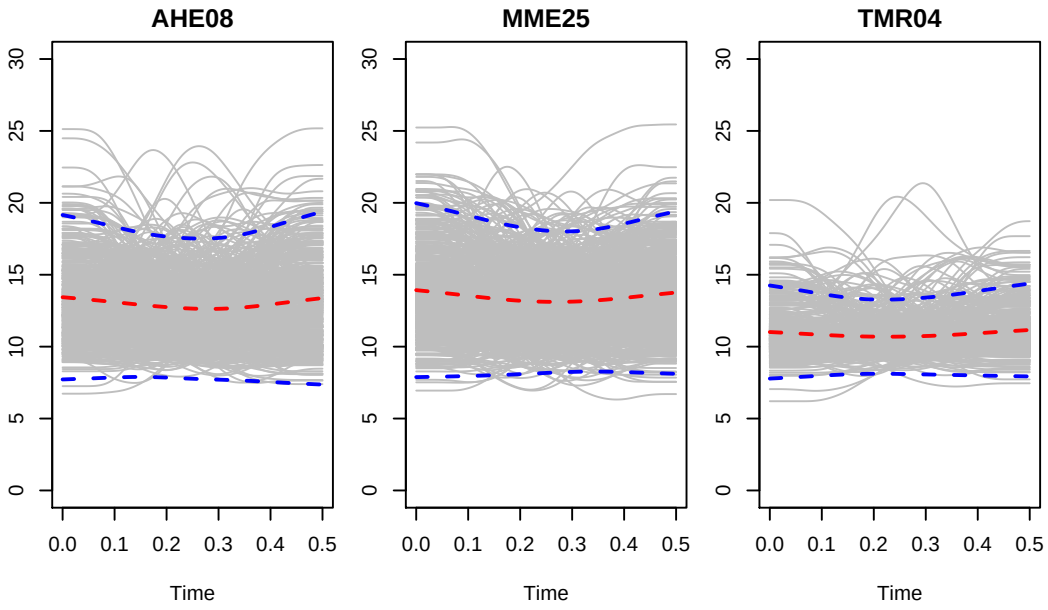

FIGURE 3.10: Mean frequencies across all replicates for 3 subjects with subject specific functional mean (red dotted line) and 2 standard deviations (blue dotted line) around the mean frequencies.

Fig. 3.12(top) shows the distribution of the strength of the dominant dipole across the entire pre-stimulus time interval. Further, Fig. 3.12(bottom) displays the distribution of dipole strength of the dominant for all replicates, across 3 subjects showing variability across subjects. Here the dotted red curve is the functional mean of the dipolar strength. TMR04 has a consistently higher distribution of the dipole strengths for the dominant dipole. This means that the dipoles in the replicates of this subject are more strongly detected than the other two subjects in this illustrative example. This variation in the strengths is randomly distributed between 0 and 1 for subjects such as MME25 and more skewed towards 1 for TMR04.

Spatial functions

Fig. 3.13 shows the topological map of the dominant dipoles in the pre-stimulus period in terms of their location, size and orientation. The centre point of each line

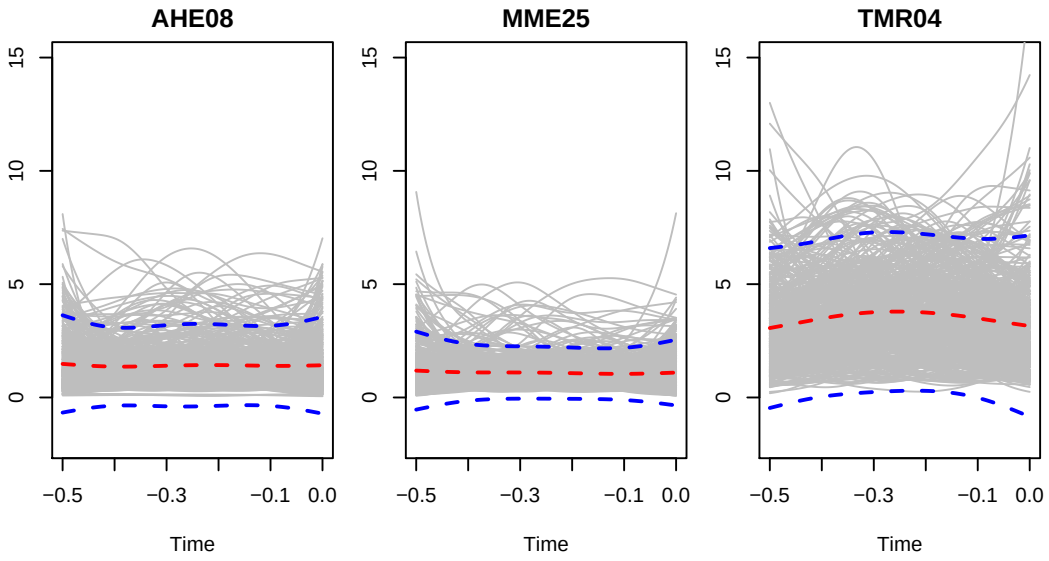

FIGURE 3.11: Amplitudes (averaged for two poles) across all replicates for 3 subjects

represents the centre of the distance between the two poles of the dominant dipole detected during the pre-stimulus for each replicate in the 3 selected subjects. The length of the lines correspond to the size and the colour of the lines represent the strength of the corresponding dipole.

3.4 Discussion

In this chapter, the relationship of the temporal and spatial characteristics with the phenomena of interest is assessed. For EEG, entrainment of 'brain' signals of interest as estimated by the additive models in the previous chapter is computed for all the replicates of the 4 experimental conditions in 6 subjects. Temporal functions of a specific subject S02 over all replicates for the different experimental conditions, start to show that the main condition tends to demonstrate more pronounced evidence of entrainment. For instance, the frequency of the signals tend to become closer to the α range of frequencies between the third and the fifth TMS pulse with a tighter confidence band in the main condition (Fig. 3.6), where a clear indication of change in frequency during the third to fifth pulse is ascertained on

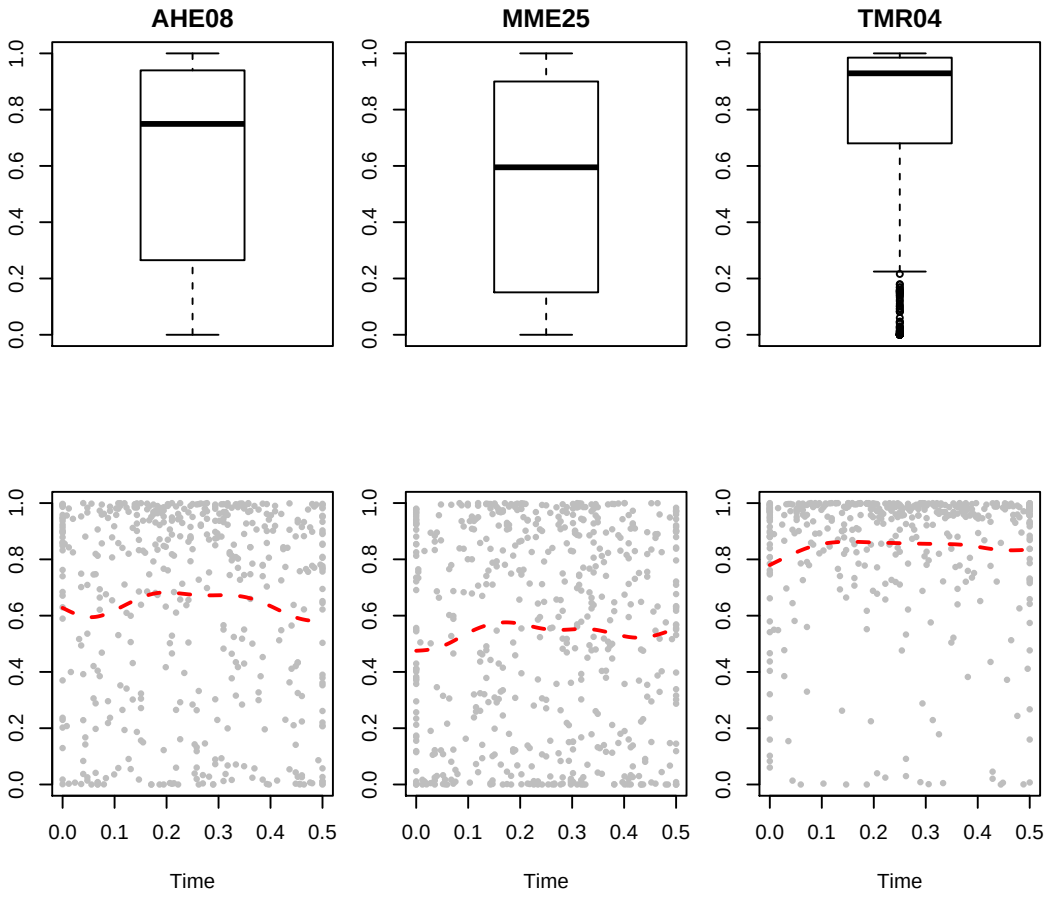

FIGURE 3.12: (above) Spread of the maximum dipolar strength over time across all replicates for 3 subjects; (below) Distribution of maximum dipolar strength across all replicates for 3 subjects

visual inspection of these curves. Amplitude functions of the replicates associated with the main condition show significant enhancement (Fig. 3.7). Further, when comparing curves associated with the main condition for 3 subjects, it is found that the frequency and amplitude of the signals vary across the replicates and between subjects. This is demonstrated by Fig. 3.8 and indicates that it may be feasible to account for these random effects of subjects and replicates within subjects in the modelling step. This leads to a mixed model framework for describing 'entrainment' based on these temporal functions which is expounded in detail in the next chapter.

The mean frequencies of the MEG dipoles (Fig. 3.10) lie mostly in the α band as expected. They show random variability between replicates as well as between

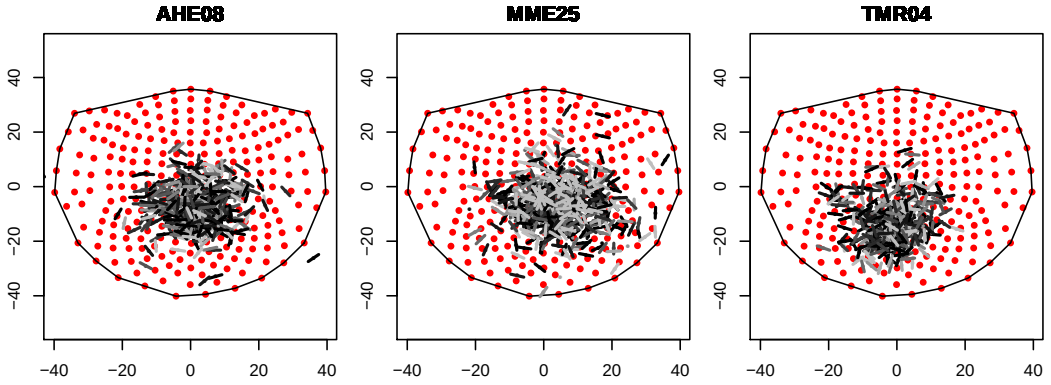

FIGURE 3.13: Spatial distribution of dipoles in all replicates for 3 subjects with greyscale indicating strength of the dipoles, length indicating the size of the dipoles and the tilt indicating the orientation of one pole relative to the other.

subjects. Amplitudes averaged over the two poles (Fig. 3.11) vary between subjects as well as between replicates within each subject. For some of the subjects, there seems to be an increased dipolar activity between 0.2 to 0.4s as displayed in Fig. 3.12(above). However, there is a lot of variability in the time at which the dipole occurs during the pre-stimulus resting state. For example, referring to Fig. 3.10 subject MME25 shows a symmetric distribution across the whole spectrum of dipole strength ranging between 0 and 1 among its replicates. In comparison, subject TMR04 has more pronounced dipolar activity as the average dipolar strength values tend to be closer to 1. The spatial distribution of the dipoles (Fig. 3.13) show further variation in the location, size and orientation across the three subjects and between replicates.

Chapter 4

Repeated Measures Mixed Effects Models

4.1 Background

The TMS-EEG data have been pre-processed using additive models to decompose the data into artefacts and 'brain' signals of interest in Chapter 2. The signals of interest from all the channels can be characterised into temporal functions - phase, frequency and amplitude - for all replicates in each subject. This is discussed in Chapter 3. The aim of the experiment is to find evidence of entrainment of brain signals to the frequency at which the stimulus is applied. So the next step in analysis is to model the features of the EEG signal to establish statistical evidence of entrainment, which is the focus of this chapter. The design of the experiment from which the EEG recordings are obtained produces data at multiple channels over a duration of time and are collected for a number of replicates within each subject. This introduces variation in the signals between replicates within the subject as well as between subjects.

Here, the stimulus comprises of 5 TMS pulses at a certain pre-determined frequency which is the inherent α frequency of the subject. Then the curve segments 0.1s immediately after each pulse can be treated as repeated measurements of

the functional curve. The four sections of the temporal curves (phase, frequency and amplitude) between two consecutive pulses are treated as four repeated observations. In order to model the temporal characteristics, a linear mixed effects model framework for these repeated measurements is proposed with subjects and replicates as random effects accounting for the variation between subjects as well as replicates within subjects. The differences in the degree of variation in the phase/frequency and amplitude functions are investigated and models are developed to find evidence of entrainment in the 'brain' signals.

Linear mixed effects models are a class of linear models that account for fixed and random effects. This model class is an extensive topic in statistics with rapid growth in various applications in the recent decades. Overview of theory, advancements in literature and in depth discussions about various topics pertaining to mixed models are covered in McLean et al. (1991), Searle et al. (2006) (variance components), Pinheiro and Bates (2000) and McCulloch and Searle (2005). Vonesh and Chinchilli (1997) discuss mixed models specifically in context of repeated measurements. Ruppert and Carroll (2003) explain mixed model in the non-parametric framework in the book Semiparametric Regression. Applications of mixed models in the analysis of longitudinal data are described by Laird and Ware (1982) and more recently by Diggle et al. (2002).

Section 4.2 outlines the descriptive statistics methods and linear mixed effects model theory. The methods and models introduced in this section are applied to a particular channel 'CP4'. This channel is selected, owing to its close proximity to the TMS equipment, as the maximum effect of the stimulus is recorded by this channel. Artefact corrected time traces for this particular channel are summarised in terms of the repeated measurements (segments) of its characteristic temporal functions - phase, frequency and amplitude curves. For constructing the model, the mean of the curve segments are computed and used as an observed measurement. These measurements are then modelled in the repeated measures mixed model framework. The summary results and model output from this application are reported in Section 4.3. Section 4.4 presents a discussion of the results and summarises the key findings.

4.2 Repeated Measures and Mixed Models

Repeated Measurements: Derivation and Summary

The functional curves are summarized as repeated measures of phase, mean frequency and amplitude for epochs between two successive TMS pulses. Additionally, the phase angle of the signal at the onset of the first pulse is estimated, in order to assess whether the entrainment signature is dependent on where the stimulus catches the ongoing oscillation of the signal. Mean phase/frequency and amplitude curves for each channel, and intervals based on standard deviations of the frequency curves at each channel are produced to assess the behaviour of the signals in terms of their average frequency and amplitude. Then, various measures of location and spread are computed for discrete time epochs from these curves. A natural epoch to consider would be the time interval between two successive TMS pulses. This provides four repeated observations for any characteristic or summary measure between pulses 1 and 2, 2 and 3, 3 and 4 and 4 and 5. This is illustrated in Fig. 4.1

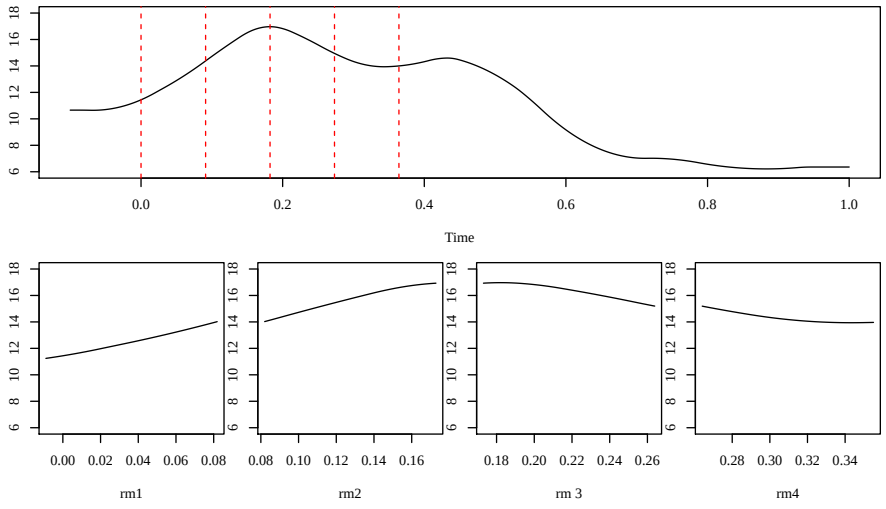

FIGURE 4.1: Frequency function for 1 replicate in subject S02, condition 2 with 4 repeated functional measurements illustrated.

The phase angle of the 'brain' signals of interest where the first TMS pulse 'catches' the signal may also influence the entrainment pattern. Intuitively, when the stimulus 'catches' the 'brain' signal of interest in the same phase, clearer entrainment

patterns should emerge. With an aim to investigate the influence of this covariate (henceforth referred to as 'phase angle at stimulus onset') on the changes in frequency and amplitude patterns, four categories of this covariate are determined depending on the magnitude and direction of the phase angle at stimulus onset. These 4 groups based on the position of the phase angle at stimulus onset are described in the following table:

Group	Description	Range of values of phase angle
1	in-phase near zero-crossings	between $0° - 45°$ or between $315° - 360°$
2	near the signal's peak	between 45°-135°
3	out-of-phase near zero-crossings	between 135°-225°
4	near the signal's troughs	between 225°-315°

TABLE 4.1: Classification of signals based on phase angle at stimulus onset

In order to simplify the functional repeated measurements further, average magnitude of the phase, frequency and amplitude of each repeated observation in each group classified by the phase at stimulus onset is computed. Let f_{ijk}, $i = 1...t$; $j = 1...r$, $k = 1, 2, 3, 4$ be the magnitude of a temporal function at i^{th} time point and j^{th} replicate for the k^{th} group at a particular experimental condition. A simple mean $f_{.jk} = \frac{1}{t}\sum_{i=1}^{t} f_{ijk}$ gives the estimate of the function at each repeated time for the j^{th} replicate and k^{th} group. These values are then averaged for all replicates to give the subject-wise mean for the group and condition $f_{..k}$ to assess the changes in patterns over time corresponding to the groups and conditions.

Linear Mixed Effects (LME) Models for Repeated Measurements

Linear models for repeated measurements of phase/frequency and amplitude are considered to estimate these parameters. Multiple replicates within each subject as a random effect and subject itself as a random effect are the two random effects to be accounted for. When considering the mean signal for phase, frequency or amplitude, both random effects are of interest. Further, the variability around

the mean frequency tends to decrease over the repeated measurements in time especially in case of the main condition. In order to formally assess this, standard deviations for each segment of the frequency for all replicates are computed. A mixed effects model is fitted to repeated measurements of the standard deviation after accounting for subject as a random effect. In the matrix notation, the model fitted to observed values for all replicates in each subject is represented by:

$$\mathbf{Y_i} = \mathbf{X_i}\beta + \mathbf{Z_i}\gamma_\mathbf{i} + \epsilon_i, \tag{4.1}$$

where $\mathbf{Y_i}$ is the $n_i \times 1$ vector of response observations (phase, frequency or amplitude) of n_i replicates in the i^{th} subject, $\mathbf{X_i}$ is the $n_i \times p$ model matrix for p fixed effects (which include the main effects as well as any two-way significant interaction) in the i^{th} subject, β is a $p \times 1$ vector of fixed effect coefficients, $\mathbf{Z_i}$ denotes the $n_i \times q$ model matrix of q random effects of observations in the i^{th} subject and γ_i is the $q \times 1$ vector of coefficients of random effects for the i^{th} subject where $\gamma_i \sim \mathbf{N_q}(\mathbf{0}, \mathbf{\Psi})$. $\mathbf{\Psi}$ denotes the $q \times q$ covariance matrix for the random effects. $\epsilon_i \sim \mathbf{N_{n_i}}(\mathbf{0}, \sigma^\mathbf{2}\mathbf{\Lambda_i})$ is the error term where $\mathbf{\Lambda_i}$ is the $n_i \times n_i$ covariance matrix for errors in the i^{th} subject.

More generally and equivalently, the *Laird-Ware form* (Laird and Ware, 1982) of model 4.1 is expressed as:

$$\begin{aligned} y_{ij} &= \beta_0 x_{int} + \beta_1 x_{1ij} + \beta_2 x_{2ij} + ... + \beta_p x_{pij} \\ &+ b_{1ij} + b_{2ij} + ... + b_{qij} + \epsilon_{ij}, \\ b_{kij} &\sim N(0, \psi_k^2), \mathrm{Cov}(b_{kij}, b_{k'ij}) = \psi_{kk'}, \\ \epsilon_{ij} &\sim N(0, \sigma^2\lambda_{ijj}), \mathrm{Cov}(\epsilon_{ij}, \epsilon_{ij'}) = \sigma^2\lambda_{ijj'}, \end{aligned} \tag{4.2}$$

where, y_{ij} is the value of the j^{th} observed repeated measurement from total n_i observations in the i^{th} subject and $x_{1ij}, ..., x_{pij}$ are the fixed effects regressors for the j^{th} observation in the i^{th} subject, the first regressor being the intercept $x_{int} = 1$.

Further when considering the model for the standard deviation of the frequency

and the corresponding interval, only the random effect of subjects is relevant. The model is then denoted as:

$$\mathbf{Y} = \mathbf{X}\beta + \mathbf{Z}\gamma + \epsilon, \tag{4.3}$$

where $\mathbf{Y}$ is the $n \times 1$ vector of n response observations, $\mathbf{X}$ is the $n \times p$ model matrix for p fixed effects, β is a $p \times 1$ vector of fixed effect coefficients, $\mathbf{Z}$ denotes the $n \times q$ model matrix of q random effects and γ is the $q \times 1$ vector of coefficients of random effects where $\gamma \sim \mathbf{N_q}(\mathbf{0}, \mathbf{\Psi})$. $\mathbf{\Psi}$ denotes the $q \times q$ covariance matrix for the random effects. $\epsilon \sim \mathbf{N_n}(\mathbf{0}, \sigma^2\mathbf{\Lambda})$ is the error term where $\mathbf{\Lambda}$ is the $n \times n$ covariance matrix for errors.

4.2.1 Model for Mean Frequency

In order to test if the estimated mean frequency varies significantly over time in each condition, a repeated measures model (4.4) was fitted to the mean frequency where the time indices of the mean frequency (`Rtime-freq` as a time factor with 4 levels corresponding to the 4 time segments where frequency was averaged) was computed between two consecutive pulses in each replicate of each subject at each condition (`cond`). Subjects (`subj`)and replicates (`repl`) were treated as random effects to allow for differences between and within subjects. These model also accounts for the 4 categories based phase angles at stimulus onset `phsonset`, to model any differences with respect to the groups where the TMS pulse α frequency 'catches' the brain signal. Further two interactions were considered. Interaction of conditions with the repeated measures of the time indices of the mean frequency (`Rtime-freq`*`cond`) was included in the model, to see if the pattern of variation in the mean frequency over time, differed significantly between conditions. Interaction of the phase at onset with the repeated time indices of the mean frequency (`Rtime-freq`*`phsonset`) accounted for difference in patterns of the repeated frequency over time depending upon when the stimulus 'catches' the signal. Only the statistically significant interaction terms were considered in the final models. (Please note that the models outlined here are based only on the terms that have

been included in the final analysis of the application data discussed in the next section.)

The model for the i^{th} subject and $j = 1, 2, ..., n_i$ replicates can then be specified as:

$$\begin{aligned} y_{ijt} &= \beta_0 + \beta_t + \beta_{k(i,j)} + \beta_{l(i,j)} + \beta_{t*l} \\ &+ \mathbf{b_{ij}} + \mathbf{b_i} + \epsilon_{ijt}. \end{aligned} \tag{4.4}$$

Here, β_0 is the constant or intercept for the model associated with the model for i^{th} subject having j replicates and $t = 1, 2, 3, 4$ (4 repeated measurements), β_t denotes coefficient associated with the time index t of the repeated frequency measurements ($t = 1, 2, 3, 4$) corresponding to the fixed repeated time index factor $\texttt{Rtime-freq}_{ij}$. Similarly, $\beta_{k(i,j)}$ represents the coefficient associated with each of the four levels ($k = 1, 2, 3, 4$) of the fixed factor conditions (`cond`) for the i^{th} subject and j^{th} replicate, $\beta_{l(i,j)}$ represents the coefficient associated with the four levels ($l = 1, 2, 3, 4$) of the fixed factor phase-at-onset (`phsonset`), β_{t*l} represents the coefficients associated with the interaction term `Rtime-freq`*`phsonset`, $\mathbf{b_{ij}}$ represents the coefficients associated with the levels of the random factor replicate within subject ($\texttt{repl}_{ij}$) and $\mathbf{b_i}$ denote the coefficients of the levels of the random factor subject ($\texttt{subj}_i$).

4.2.2 Model for Standard Deviation of the Mean Frequency

With the aim of assessing statistical evidence of entrainment of the brain signal to α-band frequency (8-12 Hz), repeated measures ANOVA is applied on the width of the interval 2 standard deviations on either side of the mean frequency for each of the 6 subjects across all conditions. The two fixed effects for this model are (i) the repeated measures of the average width of the interval over replicates within a subject, and (ii) the experimental conditions. $\mathbf{b_i}$ denotes the random effect of subjects. When considering the standard deviation of the frequency and

the corresponding interval, only the random effect of subjects is relevant and is denoted by the model 4.5.

The model equation for the i^{th} subject can be rewritten as:

$$\begin{aligned} y_{it} &= \beta_0 + \beta_t + \beta_{k(i)} + \beta_{t*k} \\ &+ b_i + \epsilon_{it}. \end{aligned} \tag{4.5}$$

The vectors β_t, $\beta_{k(i)}$ and β_{t*k} represent coefficients associated with the levels ($t = 1, 2, 3, 4$) of the time indices of the repeated SD measurement `Rtime-SDfreq`, the levels ($k = 1, 2, 3, 4$) of the fixed factor conditions (`cond`) in the i^{th} subject and the levels of the interaction term `Rtime-SDfreq`*`cond` respectively and for the i^{th} subject. b_i denotes the coefficient corresponding to the random subject effect (`subj`).

4.2.3 Model for Coefficient of Phase

The phase of a signal increments by π radians at every zero-crossing. So in order to establish that the oscillation carries on for a complete cycle instead of being another artefact at the pulses, it will be shown that the coefficient of 2π `Rtime-coefp` is significantly close to 1 in condition 2 (as well as other conditions). To test the coefficient of phase between pulses as a measure of the angular distance that a signal travels, a linear mixed effect model is fitted to the time indices of the repeated measurement of the multiplier of 2π that the signal travels between consecutive pulses. The fixed effect of conditions `cond` and phase at onset `phsonset` were taken into account. An interaction term of `Rtime-coefp`*`phsonset` was also included. Subjects (`subj`) and replicates (`repl`) were treated as random effects to allow for differences between and within subjects. The model for coefficient of phase is given by:

The model for the i^{th} subject and $j = 1, 2, ..., n_i$ replicates can then be specified as:

$$\begin{aligned} y_{ijt} &= \beta_0 + \gamma_t + \beta_{k(i,j)} + \beta_{l(i,j)} + \beta_{t*l} \\ &+ \mathbf{b_{ij}} + \mathbf{b_i} + \epsilon_{ijt}. \end{aligned} \tag{4.6}$$

β_0 is the constant or intercept associated with the phase coefficient model for i^{th} subject having j replicates, γ_t now represents the coefficient associated with the t^{th} element of $\texttt{Rtime-coefp}_{ij}$, the time index of the fixed main effect phase coefficient. The representations of the other fixed and random coefficients are similar to the model for mean frequency. Hence, $\beta_{k(i,j)}$ represents the coefficient associated with each of the four levels ($k = 1, 2, 3, 4$) of the fixed factor conditions (`cond`) for the i^{th} subject and j^{th} replicate, $\beta_{l(i,j)}$ represents the coefficient associated with the four levels ($l = 1, 2, 3, 4$) of the fixed factor phase-at-onset (`phsonset`), β_{t*l} represents the coefficients associated with the interaction term `Rtime-coefp`*`phsonset`, $\mathbf{b_{ij}}$ represents the coefficients associated with the levels of the random factor replicate within subject ($\texttt{repl}_{ij}$) and $\mathbf{b_i}$ denote the coefficients of the levels of the random factor subject ($\texttt{subj}_i$).

4.2.4 Model for Amplitude

Amplitude is computed as the maximum value the signal reaches between two successive zero-crossings. These points are then smoothed giving the amplitude at any point over time. Amplitude between two successive pulses are then the maximum value that the amplitude curve reaches between the pulses. Using a linear mixed model setting, the amplitude over time was tested by modelling the effect of time indices of repeated measure between successive pulses (`Rtime-ampl`). The main effects of condition (`cond`) and phase-at-onset (`phsonset`) and the interactions of the time indices of the repeated measures (`Rtime-ampl`*`cond`) as well as phase-at-onset (`Rtime-ampl`*`phsonset`) were considered. Only (`Rtime-ampl`*`phsonset`)

was found significant and retained in the model. Subjects (`subj`) and replicates (`repl`) were treated as random effects.

The model for the i^{th} subject and $j = 1, 2, ..., n_i$ replicates can then be specified as:

$$\begin{aligned} y_{ijt} &= \beta_0 + \alpha_t + \beta_{k(i,j)} + \beta_{l(i,j)} + \beta_{t*l} \\ &+ \mathbf{b_{ij}} + \mathbf{b_i} + \epsilon_{ijt}. \end{aligned} \tag{4.7}$$

Here, β_0 is the constant or intercept associated with the amplitude model for i^{th} subject having j replicates and α_t now represents the coefficients associated with each element of $\texttt{Rtime-ampl}_{ij}$ corresponding to the coefficient of the time indices ($t = 1, 2, 3, 4$) of the repeated measurements of the amplitudes. Once again, $\beta_{k(i,j)}$ gives the coefficient associated with each of the four levels ($k = 1, 2, 3, 4$) of the fixed factor conditions (`cond`) for the i^{th} subject and j^{th} replicate, $\beta_{l(i,j)}$ represents the coefficient associated with the four levels ($l = 1, 2, 3, 4$) of the fixed factor phase-at-onset (`phsonset`), β_{t*l} represents the coefficients associated with the interaction term `Rtime-coefp`*`phsonset`, $\mathbf{b_{ij}}$ represents the coefficients associated with the levels of the random factor replicate within subject ($\texttt{repl}_{ij}$) and $\mathbf{b_i}$ denote the coefficients of the levels of the random factor subject ($\texttt{subj}_i$).

4.3 Results

As stated earlier, the temporal curves of the channel CP4 are of particular interest, because it lies in the head region in the vicinity of which the TMS equipment is held. So this channel is expected to pick up and demonstrate maximum effect of the TMS pulses, if present. Mean and standard deviation of the average frequency between successive pulses for subject S02 at the main condition are illustrated in Fig. 4.2. It can be seen here that although the mean frequency estimates across the four conditions remain comparatively constant, there is pattern of variation of the confidence intervals at successive measurements. This indicates that as the

stimulation progresses, the brain signals follow α-band frequency with a much tighter confidence interval, in the main condition. In the three control conditions, no such effects can be seen.

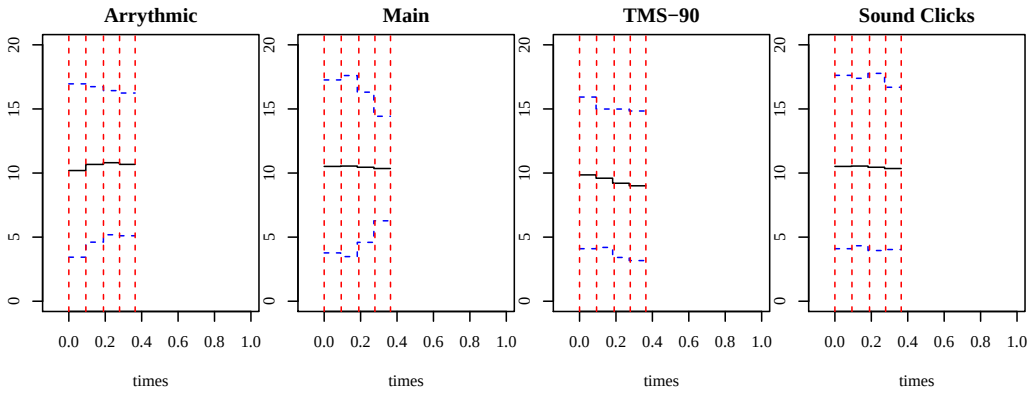

FIGURE 4.2: Estimated frequency between successive TMS pulses with corresponding mean and 2σ confidence bands for all replicates of subject S02 across 4 experimental conditions.

The overall mean frequency in all subjects, by group of phase angle at stimulus onset and by condition is plotted in Fig. 4.3. Mean frequency lies within the α-band of frequencies between $9-11$ Hz. A pronounced feature of the main condition is that the frequency stabilises to a constant magnitude for all the groups between pulse $3-5$. This may be due to the fact that the signals are entrained to the frequency of the stimulus. This is further supported by the tighter confidence bands around the mean frequency in the main condition (Fig. 4.3).

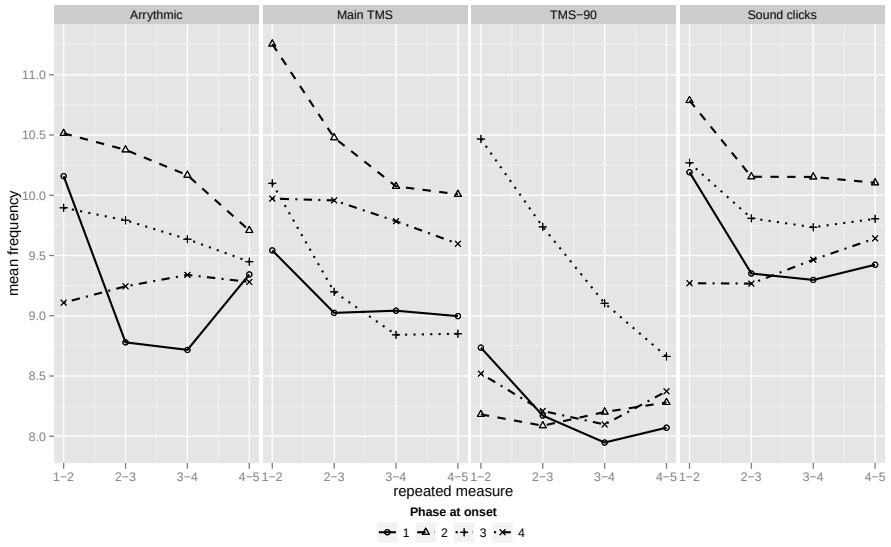

FIGURE 4.3: Mean frequency between successive TMS pulses for all subjects for each condition and 4 categories of phase at onset (where the first TMS pulse 'catches' the signal) - 1: phase at onset near zero-crossing at 0, 360° etc., 2: phase angle at onset between 45° and 135° (Peaks), 3: phase angle at onset between 135° and 225°, 4: phase angle at onset between 225° and 315° (Troughs).

Fig. 4.4 shows the overall mean amplitudes for all subjects at times of each repeated measurement by their grouping of phase angle at the stimulus onset and condition. The mean amplitudes do not show an enhancement(increment) over time. These mean amplitude by groups of phase angle at the stimulus onset for each individual subject are plotted in Fig. 4.5. In some cases, it can be informally ascertained that the variability around the mean amplitude tends to decrease over the repeated measurements in time. This behaviour seems more prominent in the main experimental condition (amplitude plots corresponding to subject S02 in Fig. 4.5 illustrates this point).

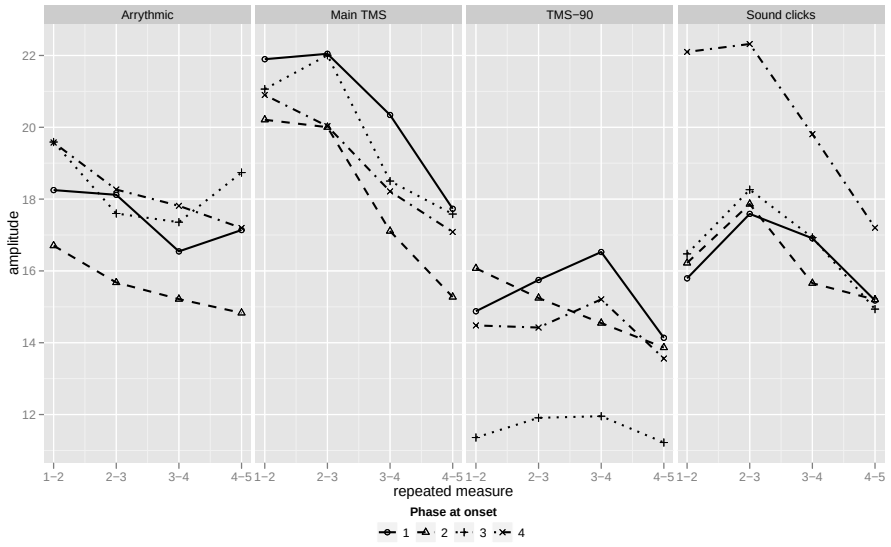

FIGURE 4.4: Mean amplitude between successive TMS pulses for all subjects for each condition and 4 categories of phase at onset (where the first TMS pulse 'catches' the signal) - 1: phase at onset near zero-crossing at 0, 360° etc., 2: phase angle at onset between 45° and 135° (Peaks), 3: phase angle at onset between 135° and 225°, 4: phase angle at onset between 225° and 315° (Troughs).

Mean frequencies and amplitudes over the repeated measurements for subject S02 are shown in Fig. 4.6 and Fig. 4.7. For this subject, in the main condition - both the frequency and amplitude tend to a similar magnitude between the pulse 4 and 5 for all the groups. These values indicate that there is some degree of entrainment in terms of frequency, although there is little evidence of enhancement of the amplitudes. However, there is random variation between subjects between replicates within subjects that have to be accounted for.

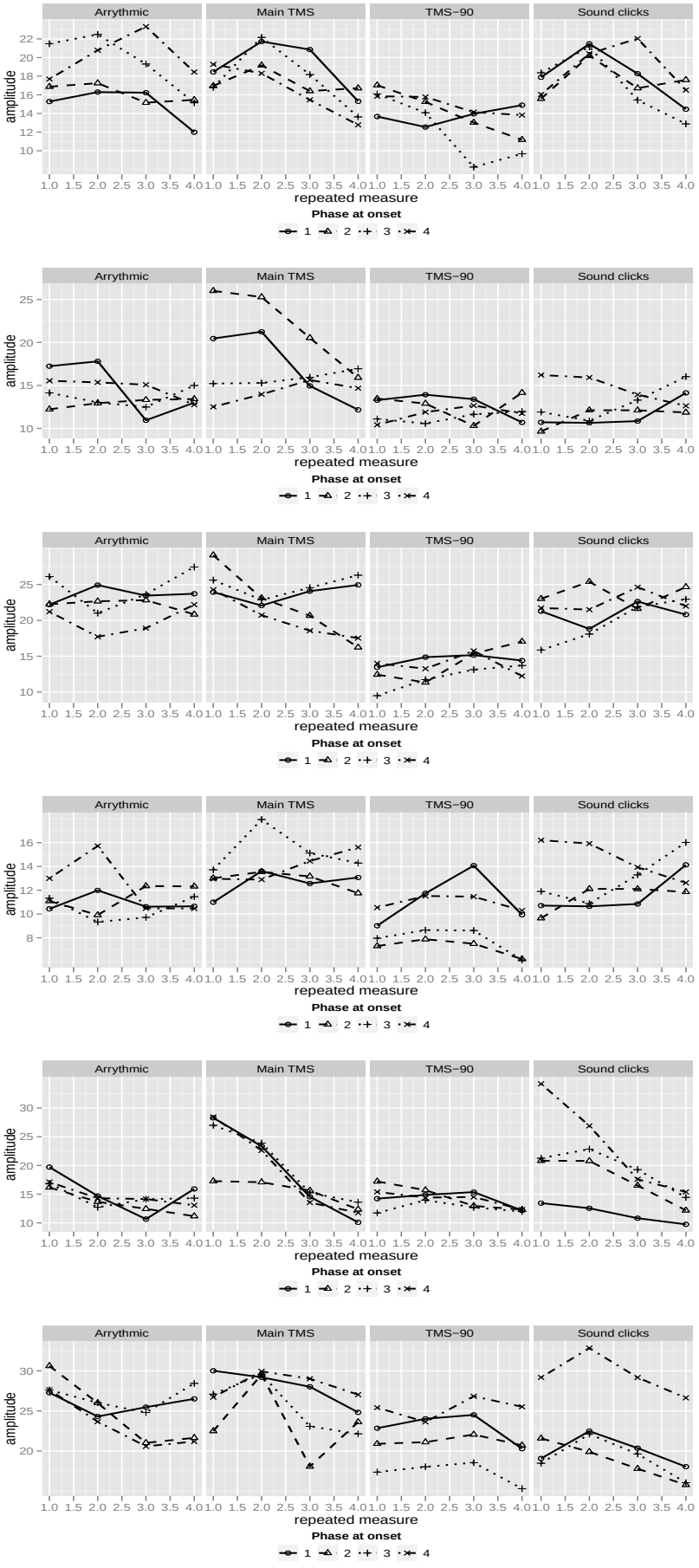

FIGURE 4.5: Mean amplitudes for 6 subjects across 4 conditions, by phase at onset.

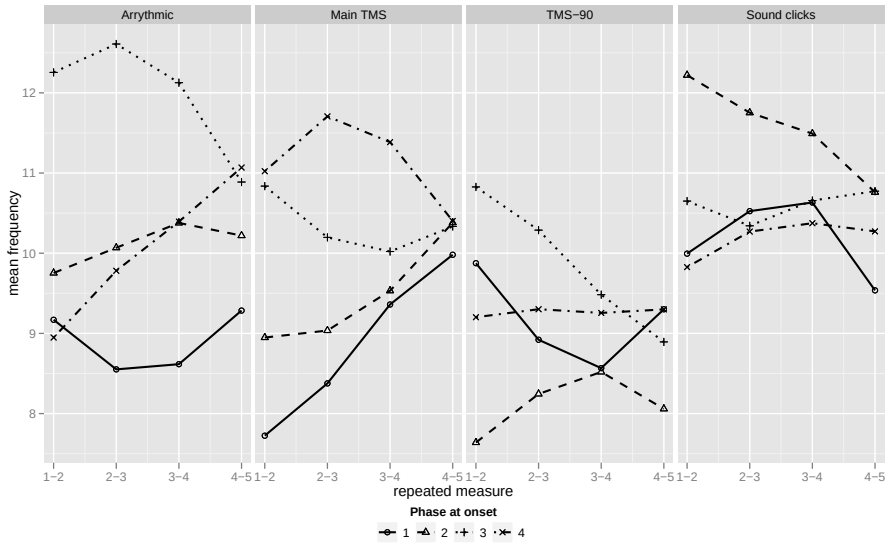

FIGURE 4.6: Mean frequency between successive TMS pulses for subject S02 for each condition and 4 categories of phase at onset (where the first TMS pulse 'catches' the signal) - 1: phase at onset near zero-crossing at 0, 360° etc., 2: phase angle at onset between 45° and 135° (Peaks), 3: phase angle at onset between 135° and 225°, 4: phase angle at onset between 225° and 315° (Troughs).

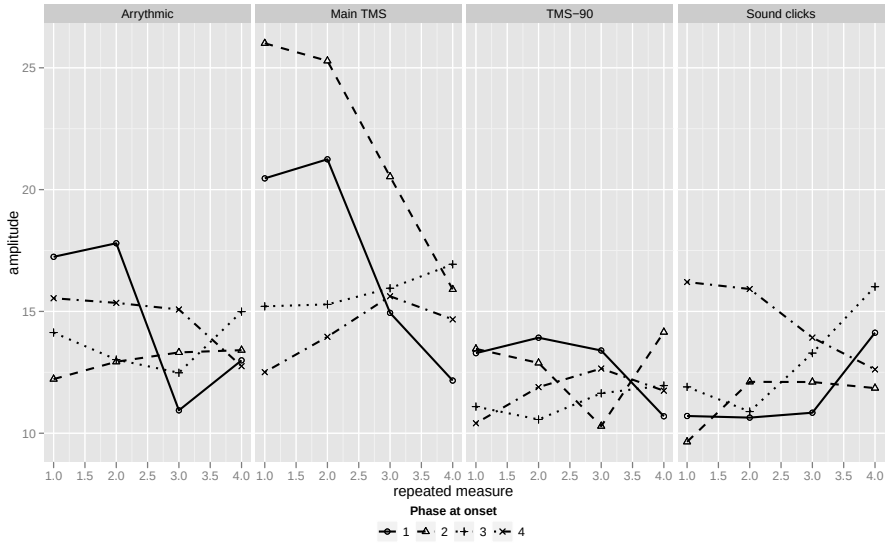

FIGURE 4.7: Mean amplitude between successive TMS pulses for subject S02 for each condition and 4 categories of phase at onset (where the first TMS pulse 'catches' the signal) - 1: phase at onset near zero-crossing at 0, 360° etc., 2: phase angle at onset between 45° and 135° (Peaks), 3: phase angle at onset between 135° and 225°, 4: phase angle at onset between 225° and 315° (Troughs).

The four linear mixed effects models are applied to the mean frequency (model 4.4), standard deviation of the frequency (model 4.5), phase coefficient between two successive pulses (model 4.6) and mean amplitude (model 4.7). Mean frequency and amplitudes are modelled with their corresponding repeated measurements as the predictor, and experimental conditions and phase angle at stimulus onset as covariates. Further two-way interactions between the repeated measure of the corresponding summary variable and condition as well as between repeated measure of the summary variable and phase angle at onset are considered and retained if found significant in the model. The repeated standard deviations of the frequency (or equivalently the width of the confidence interval around the mean frequency) are estimated for each combination of subject and condition for the standard deviation model. The specific models are described in details below:

4.3.1 To test if the mean frequency varies over time in each condition:

The model (4.4) is fitted to the average frequencies corresponding to the time factors. The interaction term of time indices of the repeated frequency measurements with conditions (`Rtime-freq*cond`) in this model was not found to be statistically significant (marginal ANOVA F statistic = 0.357, p value = 0.955) and was dropped. The two-way interaction of the time indices of the repeated frequency measure with phase angle at onset (`Rtime-freq*phsonset`) was also found to be non-significant (marginal ANOVA F statistic = 1.749, p value = 0.073) at 5% level of significance. However, since this may be considered a significant interaction at 10% level of significance, we retain it, while investigating the dependency of entrainment pattern on phase at onset later.

Fig. 4.8 illustrates the estimated repeated mean frequencies obtained from this model for each condition and corresponding to each category of phase angle at onset for all subjects (top) and for subject S02 (bottom). Since the interaction of the time indices of mean frequency with conditions was dropped, the mean frequency values over time for each group have the same slope. The interaction

of the time indices of mean frequency with the factor phase at stimulus onset estimates variable slopes and intercepts for the mean frequency over time for each group. For the group of signal in phase with the TMS pulses (`phsonset` level 1) the mean frequency between the 4^{th} and 5^{th} pulse is the lowest among the groups in the main condition.

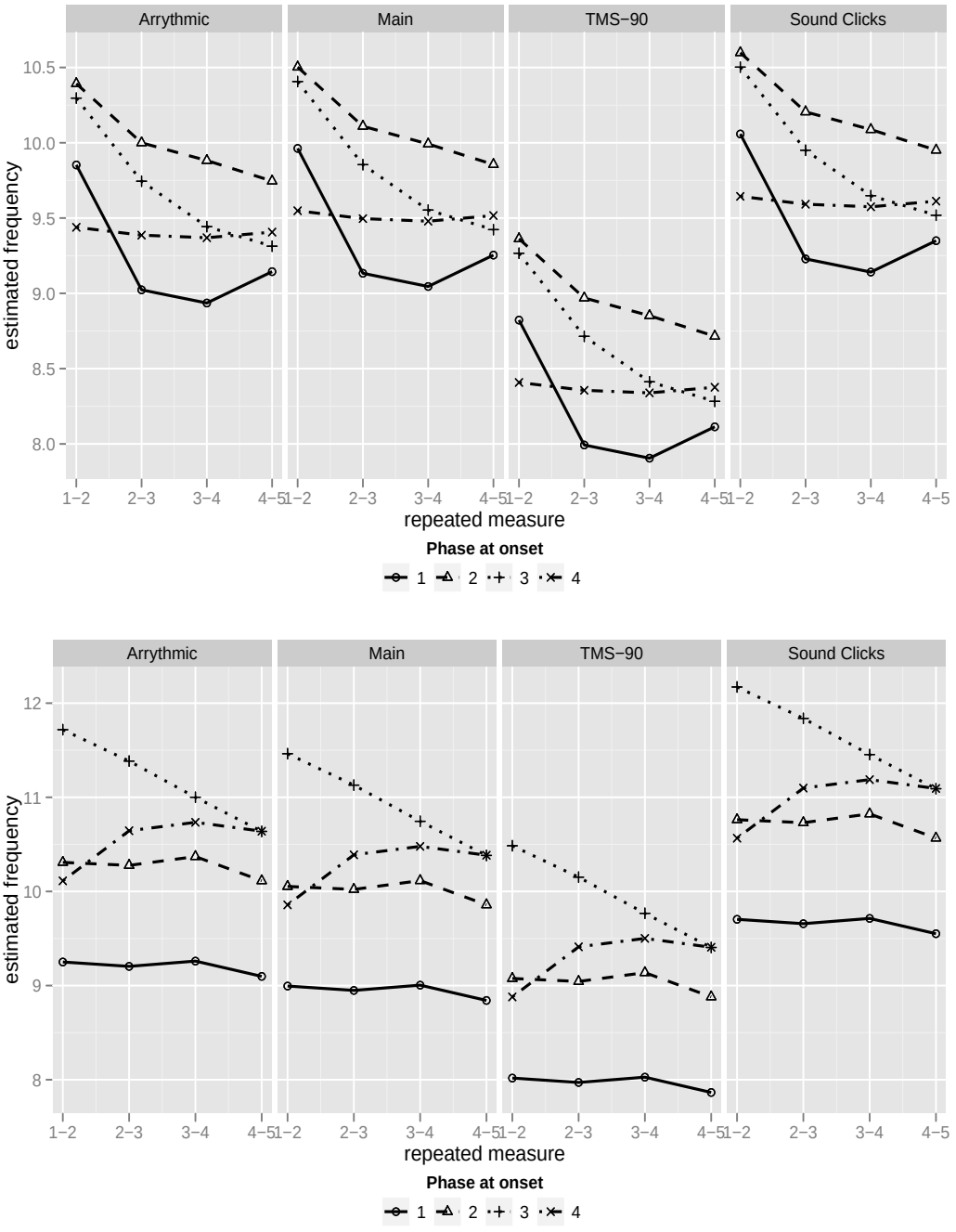

FIGURE 4.8: Estimates of mean of frequency between successive TMS pulses from repeated measures linear mixed effects model for all subject (above) and subject S02 only (below) at each condition and phase at onset - 1: phase at onset near zero-crossing at $0° - 45°$ or $315° - 360°$2: phase angle at onset between 45° and 135° (Peaks), 3: phase angle at onset between 135° and 225°, 4: phase angle at onset between 225° and 315° (Troughs) from a model with interactions of repeated measures and phase angle at onset

4.3.2 To test if the standard deviation of the mean frequency varies over time in each condition:

Model (4.5) with a main effect time indices of the repeated measure of standard deviation (`Rtime-SDfreq`), condition (`cond`) and an interaction (`Rtime-SDfreq*cond`) for the 6 subjects gives significant main effects of `Rtime-SDfreq` (marginal F statistic = 5.540, p-value = 0.001) and `cond` (marginal F statistic = 4.710, p-value = 0.003). The interaction of these two main effects is not significant (marginal F statistic = 1.634,p-value = 0.104). However since it is close to 10% level of significance, we retain it in the model to see if the standard deviation shows different patterns across conditions.

Fig. 4.9 illustrates the estimates of the standard deviation from the model (4.5). This gives a clear indication that the variation of estimates of the mean frequency decrease over time in the main condition, once the random effects between and within subjects are accounted for. The fluctuations in the frequency reduce and the frequency stabilises to an α frequency of between $9 - 11.5$ Hz.

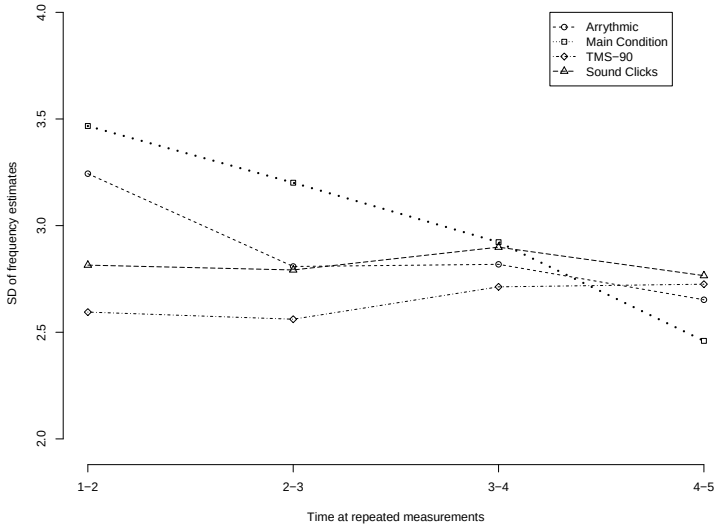

FIGURE 4.9: Estimates of standard deviation of frequency between successive TMS pulses from repeated measures linear mixed effects model over replicates for all subjects (with subject as random effect) for each condition, and interaction of the repeated measures with condition

4.3.3 To test for coefficient of phase:

The results are shown in Fig. 4.10 for the main condition in 6 subjects (top) and subject S02 below. It can be seen that the phase coefficient converges to 1 for all the groups and this is particularly indicative for S02. This implies that for the main condition, the signals complete one full oscillation on average between pulses 4 and 5, of their frequencies at the onset of stimulus giving further evidence that the signals have picked up the α frequency.

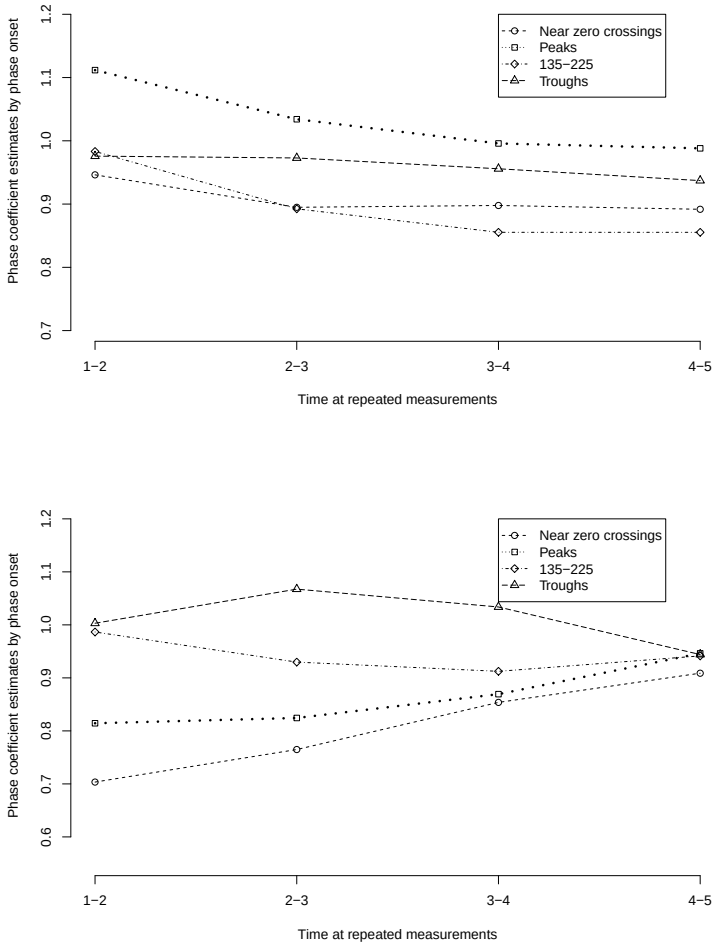

FIGURE 4.10: Estimates of phase traveled (oscillation completed) between successive TMS pulses for the main condition only - by phase at onset and interaction of the repeated measures with the phase at onset for (above) all conditions and (below) subject S02.

4.3.4 To test enhancement of amplitude over time:

Model (4.7) is fitted to the maximum amplitude attained in a particular time segment at each replicate for 6 subjects. Fig. 4.11 shows that there is no evident enhancement for the main condition when the average amplitudes for 6 subjects are considered. However, when focussing on the estimates of average amplitude for subject S02, there is a degree of increase in the amplitude between pulses $1-3$.

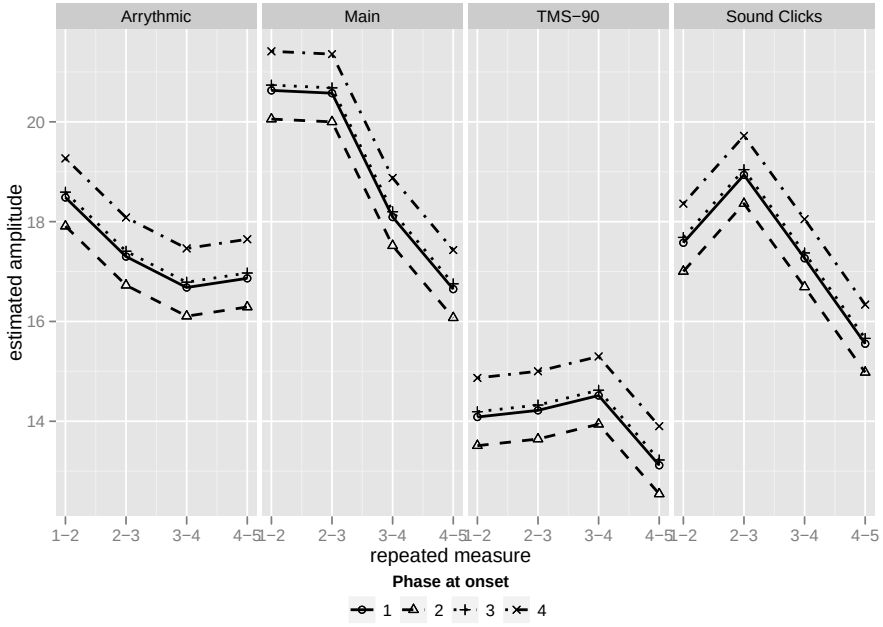

FIGURE 4.11: Estimates of amplitude between successive TMS pulses for each condition and phase at onset, and interaction of the repeated measures with conditions for all subjects.

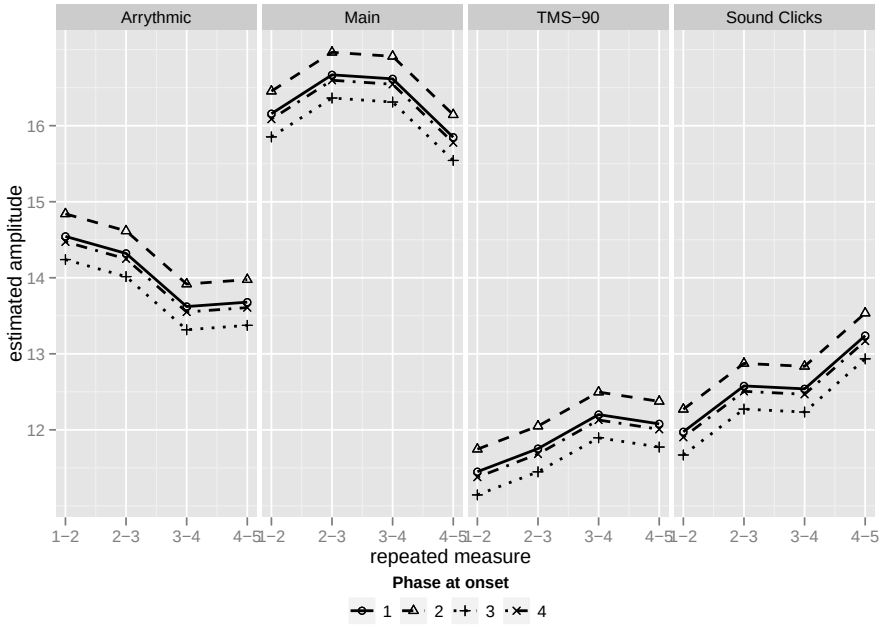

FIGURE 4.12: Estimates of amplitude between successive TMS pulses for each condition and phase at onset, and interaction of the repeated measures with conditions for subject S02.

Further, the dependence of the amplitude on the phase angle at TMS onset is illustrated by subject S02, where the replicates whose first TMS pulse coincided with the peak of the signal's own oscillation, have a higher amplitude than that of the replicates whose first TMS pulse coincided with a zero-crossing of the signal. Signals picked at the troughs, had the least amplitude (Fig. 4.11).

4.4 Discussion

Mixed models for repeated measures of the functional curves provide a flexible framework for testing neurological phenomena. For the TMS-EEG data considered here, the mean frequency is estimated using the repeated measures model 4.4 to be in the α-band of frequencies (Fig. 4.8). This compares with the means computed as averages from the data itself (Fig. 4.3). It can be seen from Fig. 4.9 that the standard deviation of the estimated frequencies tend to become smaller at each successive repeated measurement for the main condition, particularly in subject

S02. The model 4.5 for the standard deviations of frequency over all subjects indicates that the standard deviation around a mean frequency of 10 Hz (in the α band) decreases over time for the main condition over all subjects (Fig. 4.9) indicating tighter confidence bands and more stable α frequency . Estimates of phase coefficients from model 4.6 are approximately equal to 1 and without any fluctuations, indicating that complete oscillations occur in the main condition (Fig. 4.10).

The mixed effect models for frequency and standard deviation of frequency show that the brain signals tend to entrain to an α-band frequency during the TMS stimulus. This is further corroborated by the fact that the signals complete a full oscillation between the pulses 4 and 5. The model on amplitude does not show any enhancement of amplitude in the signal, although it is expected to increase over time as evident from the previous study. However, this could be due to the fact that the error variance associated with the model for amplitude is not constant. Once the heteroscedasticity is properly accounted for, an enhancement of the amplitude may emerge. The phase coefficient model also shows that the signals are oscillatory in nature.

Enhancement (increase in the magnitude) of the amplitude over time is not evident from the model estimates using the amplitude based model 4.7. However, the main condition seems to have the highest amplitude on average as compared to the other conditions for all levels of the phase at stimulus onset group (Fig. 4.11). This is particularly evident in subject S02 (Fig. 4.12).

The results discussed above indicate an entrainment of 'brain' signals to the α band of frequencies, particularly in the main condition of interest, as confirmed by the decreasing pattern of standard deviations. This further supports a similar finding in Thut et al. (2011b). The phase coefficients are devoid of fluctuations as desirable, indicating that the estimated signals are consistent with the expectation that complete oscillations are present.

Chapter 5

Functional Mixed Effects Models

5.1 Introduction

In the previous chapter, mixed effects models are developed for an application in EEG. The repeated measurements in the models are computed from segments of characteristic curves by calculating their averages over the corresponding segments of time. This is possible due to the repeated nature of the TMS stimulus in the EEG experiment. However, in many neurological studies, the stimulus is applied at one instant, giving rise to two groups of curves: pre-stimulus and post-stimulus. One of the broader goals of such experiments is then to model neurological phenomena such as dipolar activity in the brain for the pre-stimulus and post-stimulus period to compare the two groups.

MEG recordings can be represented spatially as maps of the brain topology at several discrete time points as well temporally as time traces at specific channels or sensors. This generates a large volume of data that can be smoothed over time and space to obtain the temporal traces and spatial maps as demonstrated in Chapter 3. This step does two things: (i) it converts discrete data to continuous smooth functions giving rise to functional data; (ii) since the data are now represented as functions instead of discrete observations, it drastically reduced

the data dimensionality, while preserving the data features by evaluating the corresponding functions. When such functions are considered for several replicates of many different subjects, random variability due to the subjects and replicates within subjects are also present in the data. The MEG data have already been characterised as temporal functions (frequency, amplitude and dipolar strength) and spatial characteristics (location, size and orientation of the dipole) for each subject and replicates within subjects to reduce dimensions (Chapter 3). In this chapter, the temporal functions for all replicates in 15 subjects for the pre-stimulus period are considered as units of observation leading to functional data, and the objective is to explain random variation from subject and replicate within subject effects in the functional data framework based on their temporal characteristics only.

A particular example in neuroimaging where FDA may be employed is for modelling spatiotemporal neurological phenomenon such as dipolar activity in the human brain. Ventrucci et al. (2014) describe a search and optimisation algorithm over space and time to locate dipolar activity. Once the group of sensors and time frames are located as dipoles, average temporal data at each pole can be transformed into the frequency domain for a time frequency type analysis. Further, features such as amplitude and phase of the signal at the poles over time may be studied. This chapter focuses on using a combination of such characteristic curves (functional data) as observations to model and estimate mean behaviour of the dipoles in the population based on 15 individual subjects on whom data are available for several replicates.

In order to understand how a dipole behaves in general, first the dipolar behaviour is characterised based on temporal signature profiles such as average polar frequency, amplitude and dipolar strength. In the remainder of this chapter, an average frequency curve obtained from the frequency curves at the 2 poles in a dipole is simply referred to as a (dipolar) frequency curve. Similarly, average curve of the polar amplitudes is referred to as a (dipolar) amplitude curve. The strength of a dipole occurring over time is derived as a function of phase and frequency curves of a group of adjacent sensors showing dipolar activity (Ventrucci et al.,

2014) and is referred to as dipolar strength. In order to study these signature profiles, smooth frequency, amplitude and dipole strength curves are fitted using penalised basis splines or P-splines. The coefficients from these estimates are then used to fit functional mixed effects models to the data.

Section 5.2 outlines the spline methods of curve estimation used to generate the coefficients as well as the theory of functional mixed effects models developed for MEG studies. Section 5.3 describes the proposed functional mixed model setting to characterise the dipoles in the pre-stimulus period in order to establish their characteristic features. Pre-stimulus observations are considered as an application to demonstrate the mixed model development in such data sets. A similar model framework may be applied to compare between pre-stimulus and post-stimulus recordings and investigate differences between experimental conditions. The model fitting and results are reported in Section 5.4 and further discussed in Section 5.5.

5.2 Methods

Spline based smoothing is a well established technique to compute an approximate function that captures important long-term features of time traces without the noise and other high frequency changes. A B-spline or basis spline (De Boor, 1978) of order p is a piecewise polynomial function consisting of $p+1$ polynomial curves joined using a vector of m inner knots. At any given x, $p+1$ B-splines are non-zero. For any function $f(x)$, the B-splines can be written as:

$$f(x) = \mathbf{B}\theta,$$

where $\mathbf{B}$ is the matrix of bases derived from x such that $\mathbf{B} = \mathbf{B}(x)$ and θ is the vector of spline coefficients. The estimates of θ are obtained by minimising the error sum of squares $(y-\mathbf{B}\theta)'(y-\mathbf{B}\theta)$ which leads to the standard solution of θ as $\hat{\theta} = (\mathbf{B}'\mathbf{B})^{-1}\mathbf{B}'\mathbf{y}$. To find a solution of θ to a specified degree of smoothness, the number of knots or basis functions and their locations are required to be selected.

Considering a regression of p data points (x_i, y_i), $i = 1, ..., m$ on n B-splines $\mathbf{B_j}(.)$, the least square solution using the B-splines can be written as

$$S = \sum_{i=1}^{m} \{y_i - \sum_{j=1}^{n} \theta_j \mathbf{B_j}(x_i)\}^2. \tag{5.1}$$

If a large number of spline functions are selected, B-splines method tends to overfit the data and smooth estimates appear *wiggly*. P-splines, originally proposed in O'Sullivan (1986) and popularised by Eilers and Marx (1996), are B-splines with a penalty term to control the degree of fit. Eilers and Marx (1996) proposed the use of a simplified penalty term based on k^{th} order finite differences of adjacent B-splines thus controlling the smoothness of the estimated fit. Equation (5.1) can then be written with the penalty term as:

$$S = \sum_{i=1}^{m} \{y_i - \sum_{j=1}^{n} \theta_j \mathbf{B_j}(x_i)\}^2 + \lambda \sum_{k+1}^{n} (\Delta^k \theta_j)^2. \tag{5.2}$$

Here, λ denotes a continuous penalty parameter to smoothly control the fit of the data.

Selection of appropriate bases for the P-splines is of much interest. Conventionally, selecting equidistant knots are proposed in the literature to avoid complexity in the algorithms and is adhered to in this application. Ruppert (2002) provides a detailed description of selection of the number of knots for P-splines based smoothing. In order to select the optimum number of knots for this application, a sensitivity analysis was carried out. The differences of the estimated curves and their corresponding curves from the dipole model for each replicate were summed over all replicates in the subjects and averaged over the total number of replicates to obtain a Mean Squared Error (MSE) measurement. If the curves from the dipole model are denoted as $f_{ij}(.)$ and the refitted curves using one of the spline based methods as $g_{ij}(.)$ where t is the time index $t = 1, ...T$, and $\hat{f}_{ij}(t)$ and $\hat{g}_{ij}(t)$ are realisations of the functions at the T time points for the i^{th} replicate of the j^{th} subject, then for this i^{th} replicate of the j^{th} subject, the MSE for any curve is

denoted as:

$$MSE_{ij} = \frac{1}{T}\sum_{t=1}^{T}(\hat{f}_{ij}(t) - \hat{g}_{ij}(t))^2.$$

Once the number of spline coefficients to be used to model the functional curves is fixed, a functional model is applied to these curves in order to estimate the mean frequency, dipole strength and amplitude. When doing so, it is important to adjust for random variation due to subjects and replicates within subjects in the models. So a flexible mixed effects framework is proposed to estimate these means while simultaneously accounting for the random effects between subjects and between replicates within each subject.

In the matrix notation, the model fitted to these observed functions for all replicates in each subject is represented by:

$$\mathbf{Y(t)} = \mathbf{X}\beta(\mathbf{t}) + \mathbf{Z}\gamma(\mathbf{t}) + \epsilon, \tag{5.3}$$

where

- $\mathbf{Y(t)}$ are N observed responses for s subjects, r_i, $i = 1, ...s$ replicates within each subject and $p + 1$ spline coefficients.
- $\mathbf{X}$ is the $N \times m$ model matrix for m fixed effects (which include main effects as well as any significant interactions).
- $\beta(t)$ is a $m \times 1$ vector of fixed effects coefficients.
- $\mathbf{Z}$ denotes $N \times q$ model matrix of q random effects.
- $\gamma(t)$ is the $q \times 1$ vector of coefficients of random effects where $\gamma \sim \mathbf{N_q}(\mathbf{0}, \mathbf{\Psi})$. Here $\mathbf{\Psi}$ denotes the $q \times q$ covariance matrix for the random effects.
- $\epsilon \sim \mathbf{N}(\mathbf{0}, \sigma^\mathbf{2}\mathbf{\Lambda})$ is the error term where $\mathbf{\Lambda}$ is the $N \times N$ covariance matrix for errors.

The Laird-Ware formulation for single level linear mixed model (5.3) can be extended to multilevel models, one level nested within the other. When there are

two levels of random effects, the response variable for the lowest level is denoted as:

$$\mathbf{y_{ij}} = \mathbf{X_{ij}}\beta + \mathbf{Z_{i,j}}\gamma_{\mathbf{i}}(\mathbf{t}) + \mathbf{Z_{ij}}\gamma_{\mathbf{ij}}(\mathbf{t}) + \epsilon_{\mathbf{ij}}, i = 1, ...s, j = 1, ...r_i, \tag{5.4}$$

where s denotes the number of subjects or individuals and r_i is the number of replicates in the i^{th} subject. Here $\gamma_{\mathbf{i}}(\mathbf{t}) \sim \mathbf{N}(\mathbf{0}, \mathbf{\Psi_1})$, $\gamma_{\mathbf{ij}}(\mathbf{t}) \sim N(0, \mathbf{\Psi_2})$ and $\epsilon_{\mathbf{ij}} \sim \mathbf{N}(\mathbf{0},\sigma^2\mathbf{I})$. The first level of random effects $\gamma_{\mathbf{i}}(\mathbf{t})$ are assumed to be independent for different i. Similarly the second level of random effect $\gamma_{\mathbf{ij}}(\mathbf{t})$ is assumed to be independent for i and j and also of the first level. The error term $\epsilon_{\mathbf{ij}}$ is independent for all i, j and of the random effects.

Several methods are available for parameter estimation in linear mixed effects models (Searle et al., 2006, Vonesh and Chinchilli, 1997), two of which are the Maximum Likelihood (ML) method and the Restricted (or Residual) Maximum Likelihood (REML) method. For model (5.3) the parameters are β, σ, and a set of parameters θ used to determine the variance-covariance parameters. The likelihood function is then probability density of the data given the parameters, regarded as a function with the data fixed. So:

$$\mathcal{L}(\beta, \theta, \sigma^2|\mathbf{y}) = p(\mathbf{y}|\beta, \theta, \sigma^2).$$

Here, $\mathcal{L}$ is the likelihood, p is the probability density and y denotes the entire response vector. ML estimates of the variance components (such as σ^2 and $\mathbf{\Psi}$) tend to underestimate these parameters (for discussion see Pinheiro and Bates, 2000). REML (Harville, 1977, Patterson and Thompson, 1971) gives an unbiased estimator of the variance components taking into account the number of fixed effects estimated, losing 1 degree of freedom for each. This is achieved by applying maximum likelihood to the least squares residuals, which are independent of the fixed effects. REML criterion as given by Laird and Ware (1982) is defined as:

$$\mathcal{L}_R(\theta, \sigma^2|\mathbf{y}) = \int \mathcal{L}(\beta, \theta, \sigma^2|\mathbf{y})d\beta.$$

The linear mixed effects models are fitted using the `lme()` function of the `R nlme`

package by the method of restricted (or residual) maximum likelihood or REML. The following section demonstrates the development of these well established linear mixed models for MEG data and their utility in describing specific brain functions.

5.3 Estimation of Temporal Functions: an application in MEG dipoles

Ventrucci et al. (2014) modelled the dipolar activity in pre-stimulus MEG data using a set of temporal curves - frequency, amplitude and dipolar strength and spatial features - size, location and orientation of the dipole as mentioned in Chapter 3. This work is extended in this chapter by modelling the temporal characteristics in a functional mixed model framework, to study and account for the respective levels of variations within and between subjects.

The dipole models of Ventrucci et al. (2014) give the realisations of the functions as estimated values of the smooth curves at each of the time points where the signals were initially recorded. Since the sampling frequency of the MEG recordings is very dense (127 time points spanning only 0.5 seconds), fitting a full model, even with the smooth estimates, would involve a very large data set demanding very large memory and thus making the model fitting computationally very expensive. To reduce the number of observations per replicate while preserving the features of the functions, smoothed curves of the three temporal parameters are re-fitted using P-splines with a fewer number of splines, and the spline coefficient estimates thus obtained are used as the response variable for the functional mixed effects model.

Models for MEG dipoles described in Chapter 3 produce a set of characteristic curves, for each replicate in a subject. These functional observations are generated for each replicate using the dipole model (Ventrucci et al., 2014) described in Chapter 3. In order to ascertain the general temporal characteristics of the dipoles in the pre-stimulus period, the mean curves of the temporal characteristics

- frequency, amplitude and dipole strength were investigated by Ventrucci et al. (2014). Due to the nature of the experiment and the way in which the dipole model estimates the curves, these smoothed functions are generated on observed data for each replicate in each subject. Then a simple rule is used - two adjacent regions or poles exhibiting similar frequencies and a degree of out-of-phase behaviour detects a dominant dipole occurring in a certain duration of time.

A question of interest then is whether this dipolar behaviour can be characterised by temporal characteristics alone. Ventrucci et al. (2014) describe a dipole model that ascertains the presence of a dipole based on frequency, amplitude and dipole strength. The frequency and amplitude of each replicate is the average frequency and amplitude of the two adjacent regions in the dipole with opposite phase angles called the poles. The functional parameter 'dipole strength' is derived as a curve measuring the degree to which the signals at the two poles are out-of-phase as shown by Ventrucci et al. (2014). Once dipoles are modelled for each replicate, the mean characteristics of the parameters may be investigated by fitting a functional model for all the replicates for the three temporal functions or parameters. If all the estimated values of the curves are considered, the input data for such a model will run into a very large number of observations making it computationally expensive. In order to reduce the number of observations or data dimensionality, smooth functions are re-fitted to each of the curves at each replicate with much fewer number of coefficients using both the B-splines and P-splines. The estimates using the method of P-splines are found to be superior, especially in terms of tracking the curves at the tails. Fig. 5.1 shows the fit using B-splines and P-splines with 6 knots in each case for the dipolar strength curve of a single replicate. It is clearly demonstrated that the P-spline fit is more realistic, as the unintended wiggliness of the B-spline fit can be controlled by the penalty parameter λ in (5.2).

Table 5.1 gives the range and median of the curve values as well as MSEs of their fits using the P-splines for three values of number of knots. The goodness of fit of the curve estimates increase as the number of knots are increased. For the frequency curves the re-estimated curves using P-splines with 13 knots show almost negligible mean squared errors. With only 8 knots, there is a median of

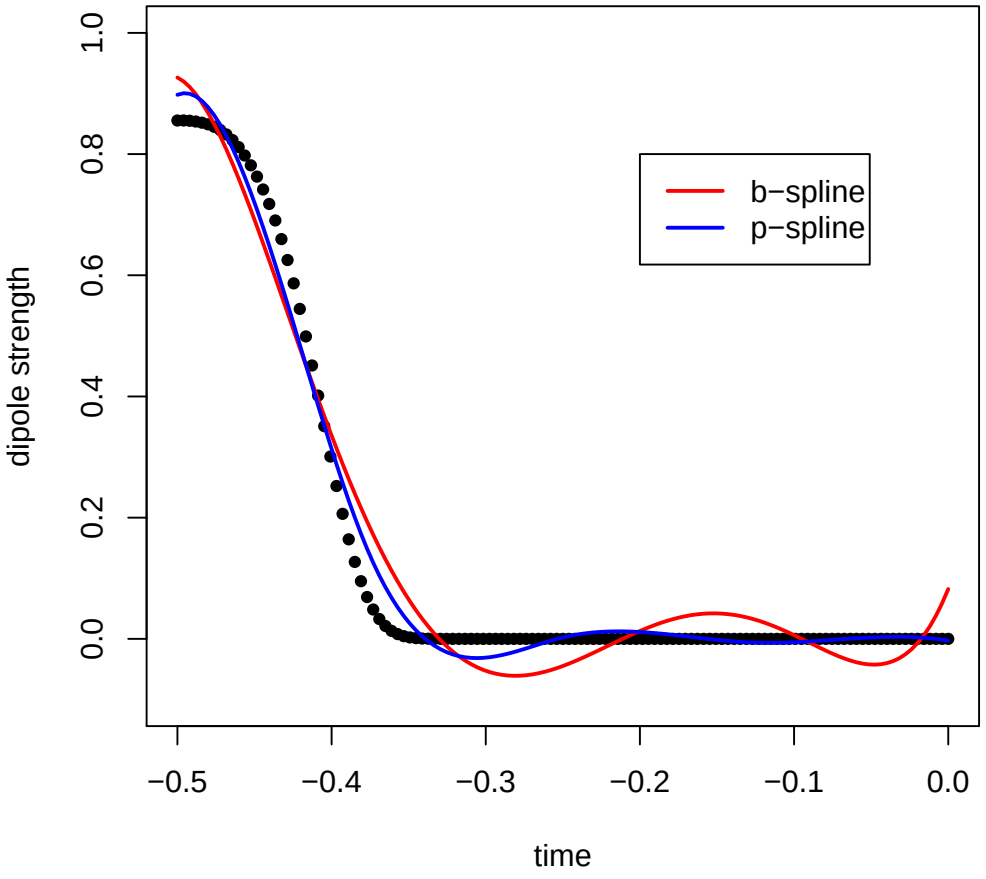

FIGURE 5.1: B-splines and P-splines fits for dipole strength curve in a single replicate using 6 knots

the mean squared error of 0.004 , and 75% of the MSEs in all replicates of 15 subjects are below 0.003. Similar results of low MSE is evident for the fits to the amplitude curves. The maximum value of the MSE for amplitude fit with 13 internal knots is almost negligible at the order of 10^{-04} where as 50% of MSE values are below 1.4307×10^{-06} showing very good fits. Even in case of the lowest considered number of knots, where 8 knots are utilised to fit P-spline smoothed curves to amplitude, the values of the MSEs are comparatively low (a maximum value of 0.0317 with 50% of the MSE values lying below 0.0002).

In order to fix the number of knots to estimate the functional data, mean squared errors for the three curves across all replicates are demonstrated for models using

Curve Fit	Min	Max	Median
Frequency	4.99	30.55	12.18
MSE p=8	< 0.001	0.52	0.004
MSE p=9	< 0.001	0.12	< 0.001
MSE p=13	< 0.001	0.003	< 0.001
Amplitude	0.02	17.68	1.35
MSE p=8	< 0.001	0.03	< 0.001
MSE p=9	< 0.001	0.004	< 0.001
MSE p=13	< 0.001	< 0.001	< 0.001
Dipole strength	$<< 0.001$	1.00	0.05
MSE p=9	$<< 0.001$	0.03	0.001
MSE p=13	$<< 0.001$	0.03	< 0.001
MSE p=15	< 0.001	0.02	< 0.001

TABLE 5.1: Summary statistics for temporal curves obtained from the dipole model estimates and MSE of model fits of the temporal curves for varying number of knots for all replicates in 15 subjects.

varying number of knots for all the 15 subjects. These values of MSE are computed for amplitude and frequency functions of all replicates in 3 subjects (AHE08, MME25 and TMR04) here using 8, 9 and 13 internal knots (9, 10 and 14 spline coefficients) and are summarised in Fig. 5.2 and Fig. 5.3 respectively. The MSE for all replicates in the 3 selected subjects for dipole strength fits with 9, 13 and 15 internal knots (10, 14 and 16 spline coefficients) using the P-spline method are presented in Fig. 5.4.

Frequency and amplitude curves can thus be reasonably approximated using 8 internal knots. For the dipole strength model, the maximum MSE for 9 knots is 0.03 where as the curve values only range between 0 and 1. A higher number of knots are required to provide a good fit for dipole strength, especially to control for unintended wiggly fit where the curve itself is flat at 0 or at very low values (similar to Fig. 5.1. For both the frequency and amplitude models, 8 knots yielding 9 P-spline coefficients are used to estimate each function at the replicate level. For the dipolar strength model, 13 knots yielding 14 P-spline coefficients are used.

Fig. 5.2 to Fig. 5.4 illustrate the distributions of MSEs for varying number of knots (and hence P-spline coefficients) in 3 subjects for frequency, amplitude and dipole strength fits respectively. It has already been established that when the number of internal knots is $p = 8$, the estimated curves have low MSEs (Table 5.1,

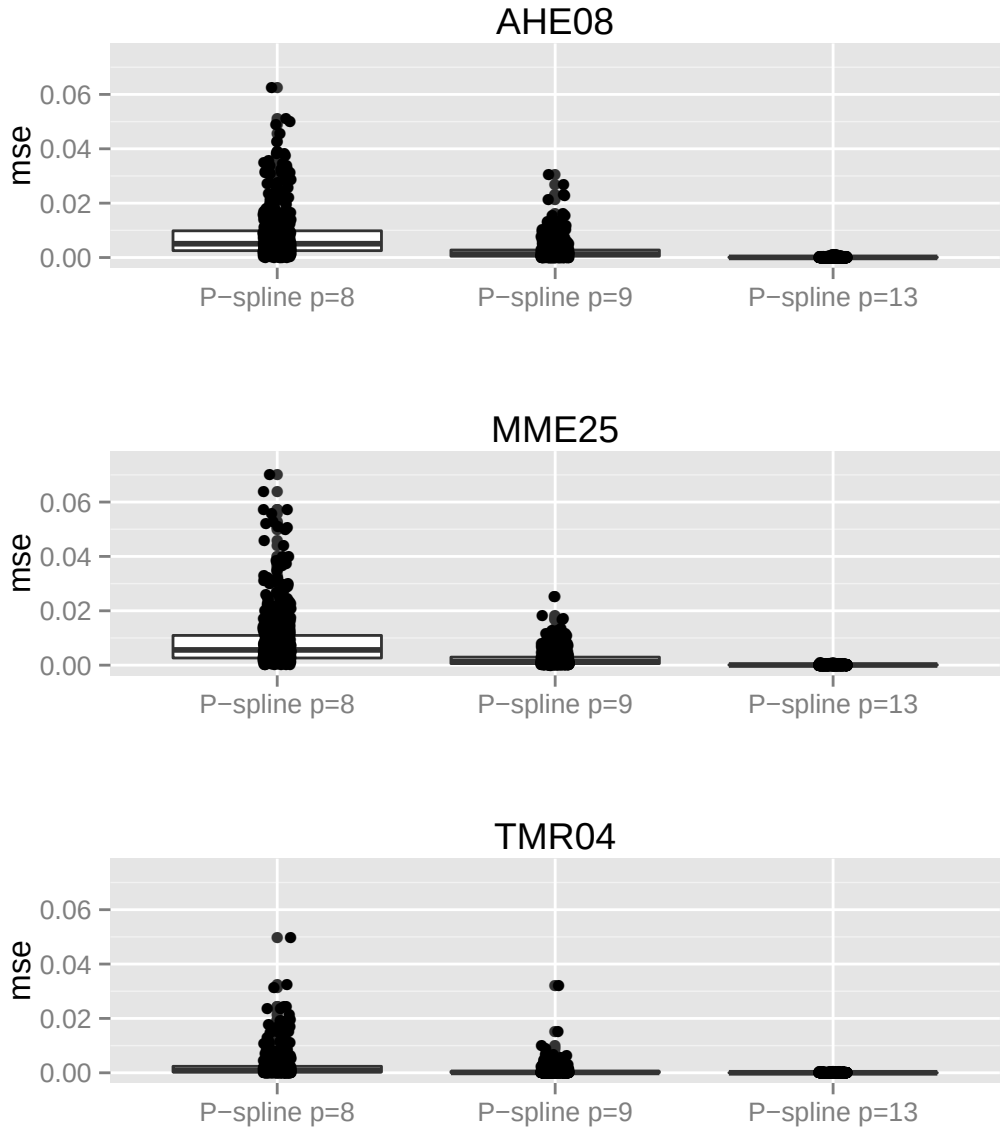

FIGURE 5.2: Distribution of mean squared errors of p-spline (8, 9 and 13 knots) fits of frequency

rows 2 and 5) in relation to the values of the curves (Table 5.1, rows 1 and 4) for frequency and amplitude functions. For dipolar strength, 13 internal knots are chosen to increase the goodness of fit of the curves. From the plots of distribution of the MSEs for 3 subjects (Fig. 5.4), it can be seen that the MSE and hence the fit in each subject remain similar. It should be noted here that the first P-spline coefficient estimates the mean of the curve and the remaining 8 P-spline coefficients estimate the fluctuations with respect to the mean. It should also be noted that as the number of P-spline coefficients increase, the variability among

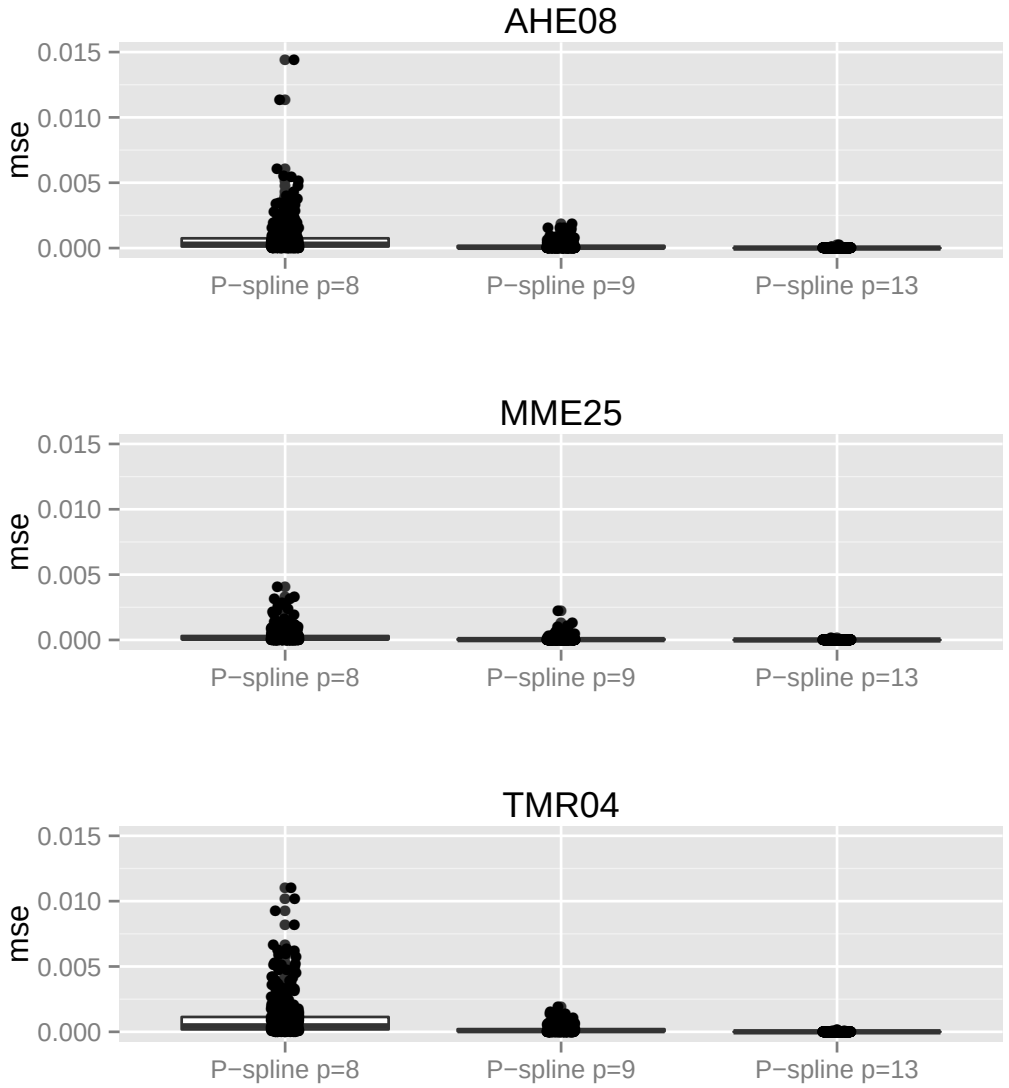

FIGURE 5.3: Distribution of mean squared errors of p-spline (8, 9 and 13 knots) fits of amplitude

the spline coefficients themselves decrease, due to increase in smoothing.

5.4 Functional Mixed Effects Model for MEG data

The temporal functions derived from the dipole models are now summarised as P-spline coefficients that describe the curves (Section 5.3). This reduces the data

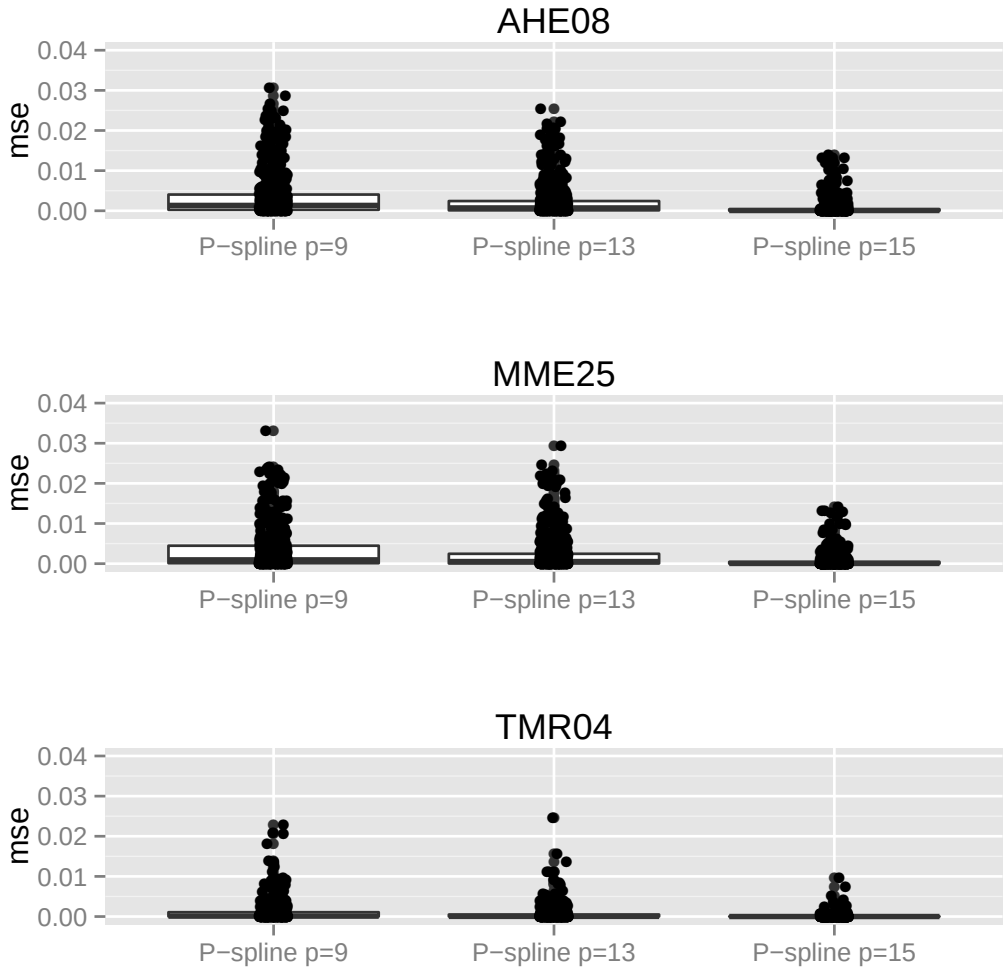

FIGURE 5.4: Distribution of mean squared errors of p-spline (9, 13 and 15 knots) fits of dipole strength

for each curve from 127 time points in the pre-stimulus data to 9 coefficients for frequency and amplitude, and 14 coefficients for dipolar strength. It has been noted before (in Chapter 3) that there is variability present at the subject level and also at the replicate within subject level. Once the P-spline coefficients are estimated, functional mixed effects models are fitted to assess these variations.

The model equation (5.3) looks similar to (4.1) while modelling repeated responses in the EEG data set in Chapter 4. One key distinction is in the specification of the responses $\mathbf{Y}(\mathbf{t})$. In the case of the EEG data, the responses at each replicate are the average value at four repeated segments of the curves. In this case, the $p + 1$ P-spline coefficients obtained from smoothing the characteristic functions

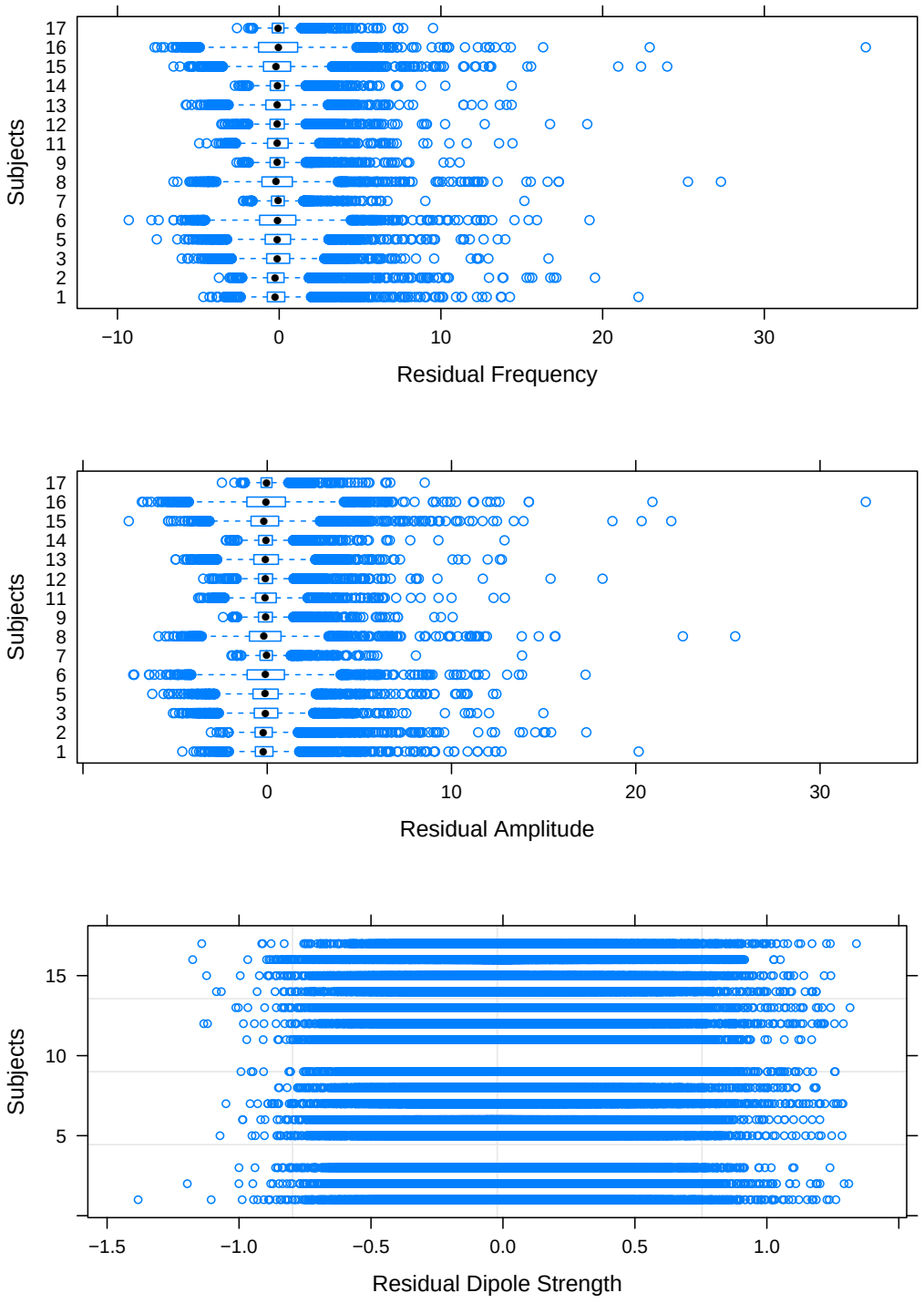

FIGURE 5.5: Residuals per subject for frequency, amplitude and dipole strength models

are treated as responses. The responses are the value of the coefficients and the fixed covariates are the P-spline coefficient indices (1-9 in case of frequency and amplitude and 1-14 in case of dipolar strength) denoted as `param`. The random covariates are the subjects denoted as `subj` and replicates denoted by `repl` both of which are treated as factors.

Three separate functional mixed effects models are considered to estimate the mean functions describing the mean frequency, amplitude and strength of dipoles occurring in the pre-stimulus period of the MEG experiment. Multiple replicates within each subject as a random effect and subject itself as a random effect are the two random effects to be accounted for. When considering the mean curve for frequency, amplitude and dipolar strength both random effects are of interest. The P-splines coefficients for the smooth curves obtained from the dipole model are treated as the observed functional responses in this model.

The mixed model fitted to each of the functions can be represented as follows.

$$y_{ijp} = \beta_0 + \beta p + b_{ij} + b_i + \epsilon_{ijp}, \tag{5.5}$$

- β_0 is the overall mean effect of the dipolar frequency curves, dipolar amplitude curves or dipolar strength curves, for the three mixed models fitted to the three temporal characteristic functions.
- y_{ijp} is the coefficient associated to the i^{th} subject and j^{th} replicate for the p^{th} P-spline coefficient, where $p = 1, 2, ..., 9$ in case of dipolar frequency and amplitude models and $p = 1, 2, ..., 14$ for the mixed model fitted to dipolar strength.
- β_p is fixed effect coefficient associated with the pth level of the the P-spline factor denoted as `param`, p taking values 1 through 9 for both the mean dipolar frequency and mean dipolar amplitude models and values 1 through 14 for the dipolar strength model.
- b_i is the coefficient associated with the ith element of the random subject effect.

- $b_{i=k} \sim \mathrm{N}(0, \psi_k^2)$, $\mathrm{Cov}(b_{i=k}, b_{i=k'}) = \psi_{kk'}$
  $\epsilon_{ijp} \sim \mathrm{N}(0, \sigma^2\lambda_{ijp})$, $\mathrm{Cov}(\epsilon_{ijp}, \epsilon_{(ijp)'}) = \sigma^2\lambda_{(ijp)(ijp)'}$.

In all the cases, the covariance matrices of the error terms $\mathbf{\Lambda}$, are assumed to be identity matrices I of the appropriate order at this stage, treating the distributions of the errors as Normal. The output of the standard deviations from the mixed effects model of frequency show very small variations for the replicate within subject effect (4.4988×10^{-05}) and is dominated by standard deviation of the residuals (2.1246). There is a small effect of the random subject covariate ($sd = 0.1418$). The fixed effect (Level of the P-spline coefficient denoted by the factor `param` with 9 levels) has a standard error of 0.0448 and a correlation of 0.669. All the coefficient estimates of the levels of the fixed effect `param` are significant at 5% level of significance (p-value < 0.05), except level 7 (t-statistic = 0.32753, p-value = 0.7433).

Again, for the mixed effects model for amplitudes, the standard deviation of the random effect replicates within subject is very low (6.3094×10^{-05}). This is further dominated by the variation in the residuals ($sd = 1.3918$). The random subject effect has a standard deviation of 0.0659. The fixed effect `param` denoting the P-spline indices of the amplitude model has a standard deviation of 0.0239 and a correlation of 0.505. All the coefficient estimates (9 levels of the fixed effect) are significant at 5% level of significance (p-value < 0.05).

There are 14 levels of the fixed effect `param` for the mixed effects model for dipole strength, two of which have non-significant estimates as computed by the mixed model for dipolar strength (level 5, t-statistic = 1.4499, p-value = 0.1471; level 11, t-statistic = 0.1054, p-value = 0.9161). The standard deviation of the random effect due to replicates within subjects is very negligible at 4.5917×10^{-06}, masked by the variability remaining in the residuals ($sd = 0.2782$).

Estimated mean and standard deviation functions frequency and amplitude in three subjects AHE08, MME25 and TMR04 are shown in Fig. 5.6 and Fig. 5.7 respectively. The mean functions (red curve) of the frequency for all the three

subjects are relatively flat, and occur at the same level of frequency. The 2σ bands around the mean depicted by the blue dotted lines are also similar. Comparing this to the Fig. 3.8, it is shown that the variation between subjects and within subjects have been accounted for.

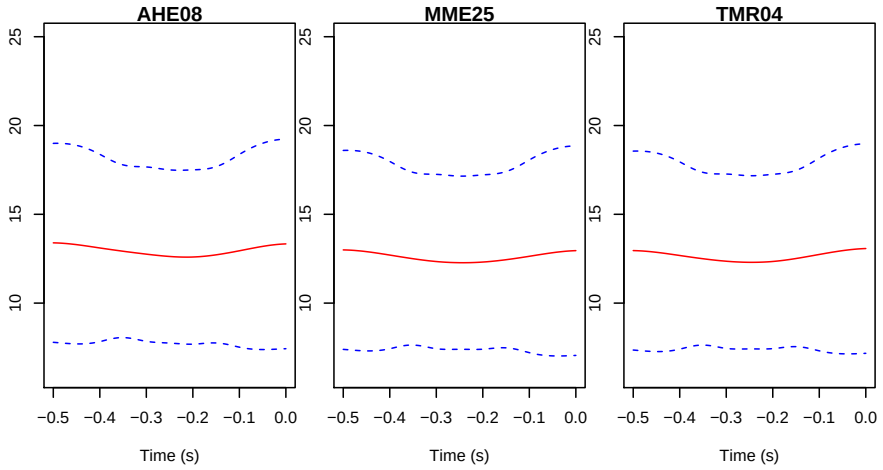

FIGURE 5.6: Estimated mean (red solid line) and 2 standard deviations around the mean (blue dotted line) functions of the frequency for 3 subjects AHE08, MME25 and TMR04.

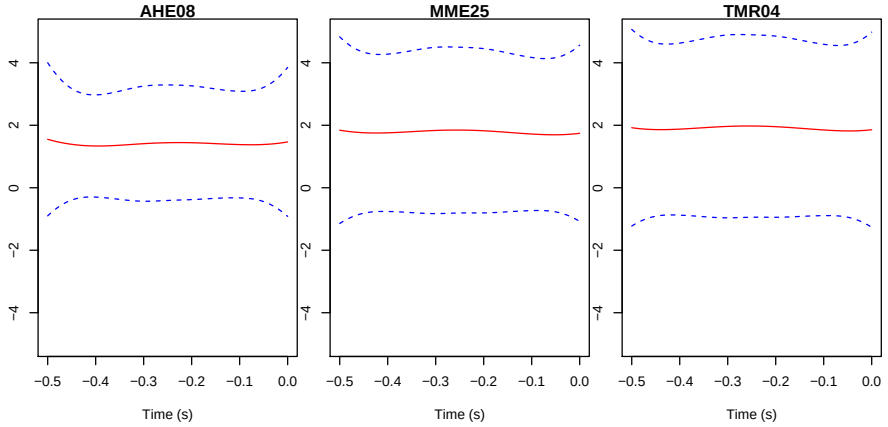

FIGURE 5.7: Estimated mean (red solid line) and 2 standard deviations around the mean (blue dotted line) functions of the amplitude for 3 subjects AHE08, MME25 and TMR04.

Assumptions for the linear mixed effects models were also examined, to assess the plausibility of these models. Normality of the within subject residuals were checked using the QQ plots for residuals. Three different plots were obtained for the three curves and are plotted in Fig. 5.8. They show that the normality

assumption is valid for overall frequency and dipole strength curves. However, amplitude functions need to be transformed to meet the normality criterion.

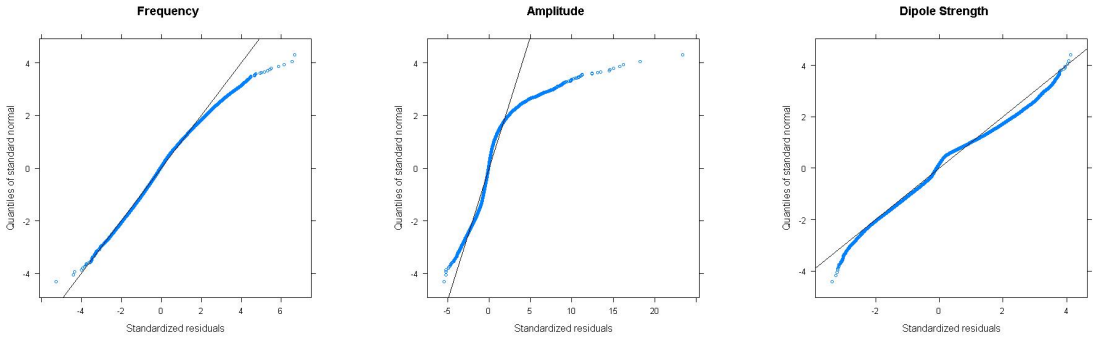

FIGURE 5.8: qq plots for (a) frequency (left), (b) amplitude (centre) and (c) dipole strength (right).

The errors are assumed to be independently and identically normally distributed with 0 mean and a constant variance for all the models. The plots of standardised residuals against the fitted values from the models for frequency, amplitude and dipolar strength as shown in Fig. 5.9 - Fig. 5.11 are visually analysed to check this assumption.

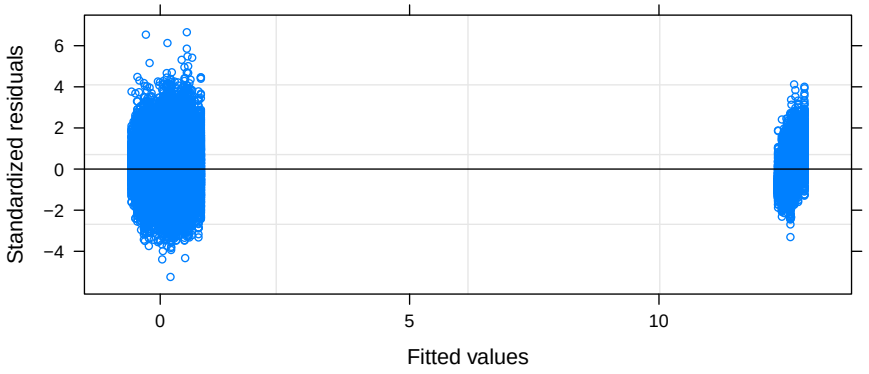

FIGURE 5.9: Standardised residuals against fitted values of the 9 p-spline coefficients from the functional mixed effects model of the average dipolar frequency functions of MEG data from 15 subjects

It can be seen that the standardised residuals are symmetrically distributed around 0 for all the three models. Hence the normality assumption with mean 0 seems plausible for the functional mixed models for the temporal characteristics. For the purpose of this research, based on approximately equal spread of the residuals around the 0 line, it is also accepted that the residuals have near equal variances.

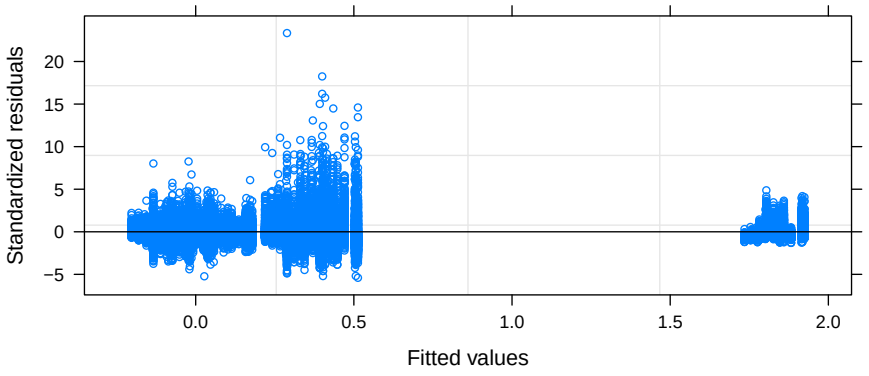

FIGURE 5.10: Standardised residuals against fitted values of the 9 p-spline coefficients from the functional mixed effects model of the average dipolar amplitude functions of MEG data from 15 subjects

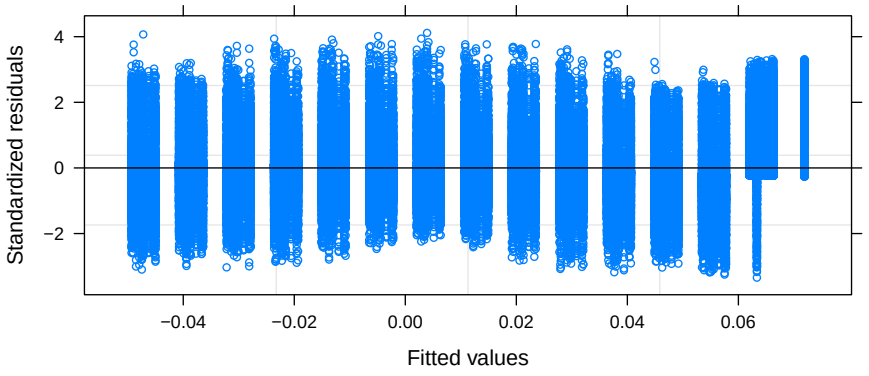

FIGURE 5.11: Standardised residuals against fitted values of the 14 p-spline coefficients from the functional mixed effects model of the average frequency functions of MEG data from 15 subjects

However, it may be argued that some heteroscedasticity may be present and this must be accounted for in order to obtain precise and correct inferences from the models. Many methods have been proposed in the current statistical literature to model the variance and covariance functions. These are discussed as part of the future work to improve the existing model fit, in chapter 6.

5.5 Discussion

P-spline coefficients were constructed for data on temporal functions obtained from the dipole models (Ventrucci et al., 2014) and mixed effects models were

Function	No. of P-spline coefficients	`subj`	`repl` in `subj`	residual
frequency	9	0.1418	4.4988×10^{-05}	2.1246
amplitude	9	0.0659	6.3094×10^{-05}	1.3918
dipolar strength	14	0.0038	4.5917×10^{-06}	0.2782

TABLE 5.2: Standard deviations of random effects and residuals in the mixed effects models

developed for the pre-stimulus segments of temporal functions using the P-spline coefficients as responses and the coefficient indices or levels as the fixed covariate, after accounting for random effects of subjects and replicates within subjects. It was found that the variability associated with the random effect of replicates within subjects were negligibly small and dominated by the residuals for all the three models. (Table 5.2 provides a summary of the standard deviations of the random effects and residuals from the three models). This may be due to assuming a constant shift across all values of `param` simultaneously when the random effect of replicate within subjects is fitted and it being estimated as 0 (or very small values) for noisy data. Further, from the distributions of the residuals for the three models shown in Fig. 5.5, it is evident that the residuals lie in the range similar to the data.

In conclusion, mixed modelling strategies for functional data proposed here for neurological studies provide a flexible framework to address the variability between and within subjects in characterised signals for single trials. Characterisation and further smoothing to obtain the coefficient estimates provide the dimension reduction methods for increasing computational efficiency of the analysis. Once the variations are accounted for using the mixed model framework, the fitted data may be used to study the features of the signals. Similar models may be fitted for the post-stimulus period in the experiment and the two groups can be compared to assess if the stimulus leads to an actual change in the temporal characteristics. A further fixed effect for conditions will estimate the differences of the frequency, amplitude and dipole strength based on the experimental conditions. As the models are developed based on observations at each replicate, this provides a powerful framework for modelling single trial data.

Chapter 6

Conclusion

Single replicate (or single trial) analysis of neuroimaging data has gained focus because of the benefits obtained through investigating the features present in a signal instead of averaging these effects out over multiple replicates. The research in this thesis was conducted to systematically develop flexible regression models for single trial analysis of specific brain activities using EEG and MEG signals collected for a number of replicates in many subjects. With this objective three key areas of interest were outlined in Section 1.4. Section 6.1 outlines the main contributions of this thesis in context of these specific research aims. Section 6.2 discusses some directions of future work based on this research.

6.1 Discussion and Key Contributions

One of the main research areas of interest for single trial analysis in neuroimaging is improving signal to noise ratio. Therefore, estimation and elimination of noise and artefacts requires rigorous pre-processing before model fitting. This is addressed in Chapter 2 where a novel pre-processing *artefact rejection* step in TMS-EEG analysis to remove noise and artefacts and estimate signals is introduced using an additive model framework applied on the TMS-EEG data for illustration. Results from the TMS-EEG experiment have already been published in Thut et al. (2011a)

using an ad-hoc method of eliminating artefacts. In the published article, data from each trial - where the spike artefacts with high amplitude and frequency occurred in the TMS-EEG data due to the pulses - were discarded, and then the signal was interpolated to estimate the missing data. In Chapter 2 of this thesis, the artefact correction of signals was achieved by fitting an additive model framework to estimate the artefacts and signal as components of the model. This artefact correction step is introduced as an estimation step where the artefacts and signals of interest are estimated as additive components in the model, instead of estimating the signal using interpolation as discussed in Thut et al. (2011a) and thus it provides a more elegant solution to the problem.

When estimating the artefacts for the TMS-EEG data using the additive model framework, it was found that the spikes generated had variable duration. The duration was found to vary from trial to trial and also between different channels. An estimate of the variable span for the spike duration was required and included in the model. This led to the development of two algorithms - both of which track and estimate the spike only over the period where it occurs. The first algorithm is model based and estimates the spike duration based on the partial residuals computed by the model. The algorithm assumes that the standard deviation of the partial residuals in consecutive 5ms time frames should be close to each other. The second algorithm is data based, and estimates a threshold signal value from the signal trace where the stimulus has not yet been applied (the pre-stimulus period). It then compares the signal after the TMS pulse is applied, and detects the point in time after which the signal trace is always lower than the maximum amplitude reached in the pre-stimulus period. There algorithms provide two different methods to track and measure the span of the spikes and produce very similar results. The data based method was found to be computationally more efficient since the model was required to be fitted only once.

Introducing additive models and defining the structures of the artefacts (spike, mains signal and long-term trend) to estimate the underlying brain signal makes *artefact correction* a modelling step. After correcting for the spike, mains current and long-term trend estimated by the additive model, in the TMS-EEG example

the remaining component is assumed to be the 'brain' signal of interest. This method based on additive models has several advantages over the standard ad-hoc method used in the neuroimaging literature, as listed below:

- The flexible framework of additive models allows for any known and estimable artefacts to be included in the model as additional components.
- Smooth flexible patterns induced by the artefacts can be included during this modelling step using the backfitting algorithm. For example, the artefact due to the background apparatus noise arising from the 50 Hz mains current is estimated by a 50 Hz cosine function as an additive component in the model.
- Neuroimaging data often have linear and non-linear long-term trend present in the data. This trend varies from replicate to replicate, and may be present in some cases and absent in others. By treating trend as one of the smooth additive components of the model, this component is simultaneously estimated and accounted for.
- By using appropriate smoothing parameters, signals of a particular frequency may be extracted. For example, appropriate smoothing parameters used for estimating the 'brain' signal of interest in the TMS-EEG example, predetermined using a sensitivity analysis, were able to extract the signal at the α band frequencies that are of interest in the particular experiment.

The previously pre-processed neuroimaging signals from the MEG experiment and the artefact corrected signals from the EEG experiment at the trial level contain data for a number of channels or sensors for a time span with a high sampling rate. However, since entrainment is a mainly temporal phenomena, and dipolar activity can be defined as a temporal phenomena once the location of the dipole has been fixed to a group of sensors on the scalp, solving the problem of high resolution in the temporal scale is of particular significance in both the cases. This issue of high dimensionality or temporal resolution is dealt with in this work, by use of a characterisation method using characteristic functions based on Euler's formula (Eilers, 2010). This method is a novel way to characterise signals at the replicate

level and has been used for the first time to establish evidence of neurological phenomena such as entrainment and dipolar activation. Several advantages of this characterisation technique can be noted:

- This characterisation method is based on computing the zero-crossings of each signal over time. These set of points along with the maxima of absolute amplitude values are much smaller in size compared to the signal data of the entire time trace. This reduces the number of data points while retaining the features of the signal that are of interest, thereby increasing computational efficiency.
- The evaluation of zero-crossings can easily lead to smoothed phase, instant frequency and amplitude curves and be readily used to compute their functions, which are important characteristic curves to investigate neurological phenomena such and entrainment and dipolar activity.
- Data from signals stored as functional curves provide the basis for functional models as proposed in the final chapters of this thesis.
- Smoothing can be easily applied to the characterised data, to retain the long-term features of the curves while minimising noise.

For the EEG data, the artefact corrected 'brain' signals of interest are characterised as temporal functions - frequency, amplitude and phase curves. The summary of these functions along with their functional mean and standard deviations for each subjects can be computed. Three of these subjects are reported as examples in Chapter 3. Data from remaining subjects are presented as part of the Appendix. These functional curves are then used to model entrainment of signals in Chapter 4. By definition it is known that entrainment of the brain signal refers to changing to a particular frequency and remaining at that frequency for at least one complete oscillation. It may also be accompanied by an enhancement of amplitude once the signal has picked up the entrainment frequency. It is further suggested that the phase of the signal at which the first TMS pulse is administered can influence

the entrainment of the signal. To assess these properties of entrainment, separate models are proposed for each, the frequency, amplitude and phase coefficient. Since the data are collected for several subjects and replicates for each subject, a mixed effects model framework is proposed to estimate the variation between and within subjects in such data sets. Moreover, the nature of the stimulus in the TMS-EEG experiment provided 4 repeated observations in-between 5 consecutive TMS pulses leading to a repeated measures mixed effects model. This flexible regression modelling framework to model entrainment can address multiple features of the problem in the TMS-EEG experiment setting simultaneously:

- In the TMS-EEG experiment, 5 consecutive pulses are applied at specific intervals. Hence the measurements between successive pulses provide repeated observations. The proposed modelling framework naturally takes into account the repeated nature of the stimulus.
- Average measurements of the temporal parameters - frequency, amplitude and phase coefficient in the time duration between two pulses are modelled. Here the mixed effects model framework provides the estimated frequency, amplitude and phase coefficient and ensures that the two sources of random variation between subjects and between replicates, are accounted for.
- Experimental condition (TMS pulses and three other conditions) for which the replicate has been recorded is introduced as a fixed categorical covariate in the model, and hence the estimates of frequency, amplitude and phase can be compared across these conditions, using the model coefficients.
- The phase of the signal at the onset of the stimulus is also included as a fixed effect, and is used to assess how phase-at-onset influences entrainment pattern.

When the stimulus is not repeated in nature, but occurs at an instant in time, the mixed models framework can be adapted to explain neurological phenomena before and after stimulation. An example is the MEG study investigated as a part of this

thesis. Here the neurological phenomena of dipolar activation at α frequency in the brain is of interest and has been modelled in the pre-stimulus period. The MEG data consists of signals before and after the visual stimulus. A dipole model based search optimisation method proposed by Ventrucci et al. (2014) is applied to this data to elicit temporal and spatial features features. Temporal functions such as frequency and amplitude at the two poles of a detected dipole and an associated dipolar strength during the pre-stimulus period are obtained. Spatial characteristics such as location, size and orientation of the dipole during this period are also estimated. These modifications are explained and summarised in Chapter 3. In the mixed model set up, only the temporal characteristics are considered to assess the variations at the subject and replicate levels before stimulus. Chapter 5 gives a description and illustration of how this modelling step may be implemented for such data sets. Experimental conditions are not considered in this model because the analysis done here is based on data from before the stimulation was applied. The estimated functional curves associated with the temporal features have the same sampling rate as the signal. In order to reduce the resolution, smoothing based on P-splines is applied to approximate the curves and a smaller number of P-spline coefficients are utilised as the response variable in the mixed model.

Dipole activity in the brain is a complex spatiotemporal phenomena. However, characterisation of the signals as temporal and spatial characteristics provides a simplification that can be then utilized to describe the phenomena. Using an optimal search algorithm, the location of the dipole may be fixed to a group of sensors. Modelling the prestimulus temporal functions provide insights about the general features of the dipole based on their temporal functions. The mixed model setting accounts for the random variations at the subject and replicates within subject levels.

6.2 Future Work

A number of areas of future work have been identified stemming from the work presented in this thesis and these areas are discussed below.

6.2.1 Estimating signals using P-splines

Additive models provide a flexible framework to identify and model the various artefact components and estimate the 'brain' signal of interest. However one of the limitations in the additive model is the precise identification of the signal and distinguishing it from the noise. In the particular example of the TMS-EEG data set, the spike component due to the TMS pulses, when the initial duration of the spike is fixed, leads to over or under estimation of the spike component, since the duration of TMS pulse is also variable. When the assumed time duration of the spike is longer than the duration that the spike effect actually lasts, it is reflected in the near zero values of the partial residuals corresponding to the errors, where the backfitting algorithm estimates a spike effect which is longer than necessary. On the other hand, the under estimation of the time duration may lead to dampened effects of the spike component remaining embedded in the signal.

To overcome this problem, two methods have been proposed in Section 2.3.3 that estimate the time span for spikes at each replicate. Another approach may be to adjust the estimated signal component itself. Harmonic penalties for quasi-periodic signals discussed in Eilers (2010) are a powerful technique to estimate a signal of varying frequency and amplitude where the data is missing and may be used to estimate the phase for this scenario. The estimated signals give a good starting point for the signal. Further, as shown by the author, using P-splines with harmonic penalties $\theta_j - 2q\theta_{j-1} + \theta_{j-2}$ where $q = \cos(2\pi d/P)$, d is the distance between knots and P is the period, instead of second order differences $\Delta^2\theta_j = \theta_j - 2\theta_{j-1} + \theta_{j-2}$ (Eilers and Marx, 1996), good estimates of the phase may be obtained in the region where the identification of the signal from the noise and artefacts is ambiguous. This can be achieved by simply treating the signal

estimates in that time span as missing and substituting the expression for q as $\cos(2\pi d/P)$, with P as the time period observed in the remaining signal.

Obtaining precise estimate of the signal in terms of the amplitude is also particularly important in the region of the TMS spikes, because any actual enhancement of the amplitude must be captured in the signal estimates to account for entrainment. In this context, a P-splines based varying coefficients may be explored to obtain more refined estimates of the amplitude. (Eilers and Marx, 2002).

6.2.2 Variance covariance structures

The mixed models for the repeated measurements as well as the functional responses require to be further explored using different variance-covariance structures to improve model inference. In both the scenarios, the random effect of replicates within subjects b_{ij} are are assumed to be independent of different i and j, the random effect of subjects b_i are assumed to be independent of different i and the errors ϵ_{ij} have been assumed to be independent and identically Normally distributed with 0 mean, equal variances and 0 covariances. However, inference can be misleading if the homoscedasticity or equal variance assumption is violated. So appropriate variance covariance structures for the data are required to be investigated and applied to improve model fit and inference as accurate estimation of a covariance function leads to efficiency gain in estimating the mean functions and fixed effects parameters (Fan et al., 2007). There is a lot of methodological research in the area of variance covariance structures to address the problem of heteroscedasticity. Model misspecification using parametric methods have led to more flexible semiparametric and nonparametric approaches gaining popularity.

In longitudinal studies, some of the main nonparametric methods of estimation of covariance structures are using local polynomials to smooth various moment estimators of the variance and covariance functions (Diggle and Verbyla, 1998) and using Cholesky decomposition for large variance covariance matrices (J.Z.

et al., 2006, Wu and Pourahmadi, 2003). In the functional data analysis framework, some of the leading methods include a Kalman filtering algorithm introduced by Guo (2002) to handle large matrices in the mixed model setting of smoothing splines, Bayesian penalized spline to model variance function of heteroscedastic errors (Crainiceanu et al., 2007), a smoothing spline based varying coefficient model with an iterative reweighted least square procedure to fit the model (Krafty et al., 2008), regression spline based methods (Rice and Wu, 2001) and a semiparametric method for the error covariance function with a local polynomial based method to estimate the variance function and correlation modelled parametrically (Fan et al., 2007). Chen and Wang (2011) propose a method to decompose functional outcomes as a sum of several terms in the mixed model setting and estimation of covariates with time-varying coefficients. An alternative approach is to use functional principal components to reduce dimensionality and subsequently model the covariance function. Important contributions in this area are from Ramsay and Silverman (2005), Kauermann and Wegener (2011), Yao et al. (2005, 2006) for longitudinal data and Di et al. (2009), Staicu et al. (2010) for multi-level functional data.

6.2.3 Extending the functional model framework for dipoles

A natural extension of the functional mixed models developed for pre-stimulus MEG data will be to apply similar methods for modelling the post-stimulus MEG data. It is of interest to see the differences in the temporal characteristics - average dipolar frequency, average dipolar amplitude and dipole strength - before and after the visual stimulus to investigate if there is evidence of more pronounced dipolar brain activation at α frequencies after stimulation. This can be assessed by changes in patterns of mean frequency functions and the curves based on 2 standard deviation converging towards the α frequencies. A significant change in the duration and dipolar strength of the strongest dipole in the post-stimulus period is also of interest and increase in both these characteristics is a desirable result.

Further, dipolar activity in the brain is a spatiotemporal phenomena and the spatial characteristics such as location, size and orientation of the dipoles have variation between subjects and replicates. Another extension of the functional mixed model framework would be to incorporate the spatial and temporal characteristics simultaneously, after accounting for random effects of subjects and replicates within subjects, to fully describe dipolar activity.

Appendix A

Supplementary Results

In chapter 3, characterisation functions of selected subjects are summarised for both the EEG and MEG data sets to illustrate the characterisation method proposed. Particularly in the TMS-EEG experiment, the subject S02 has been used to illustrate characterisation and summary of the EEG signals. Five additional subjects (S01, S03, S09, S10 and S11) are used to model the data in Chapter 4. Similarly only three subjects (AHE08, MME25 and TMR04) from the MEG data set have been used to depict the characterisation and summary of their characteristic functions to study dipolar activity. Further, data from 12 more subjects have been used in the functional mixed models described in Chapter 5. Characterisation and summary results from these additional subjects in the EEG and MEG setting are reported in sections A.1 and A.2 respectively.

A.1 Characterisation and Summary of additional subjects in the TMS-EEG data

The estimated signals (using the additive model described in Chapter 2) from the remaining 7 subjects in the EEG data set are visually inspected. It should be noted here that only 5 of these 7 subjects have been used in the model since the subjects S12 and S13 have been deleted from further analysis due to erronous data and a

systematic artefact not accounted for in the model respectively. Fig. A.1- Fig. A.5 shows the estimated 'brain' signals of interest for the five additional subjects that were used for the characterisation and modelling of the EEG data.

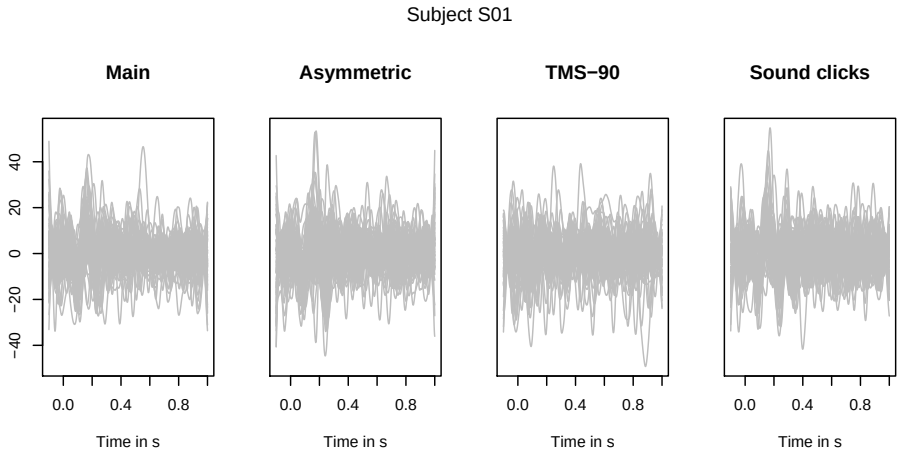

FIGURE A.1: Estimated 'brain' signals of interest by each experimental condition for subject S01

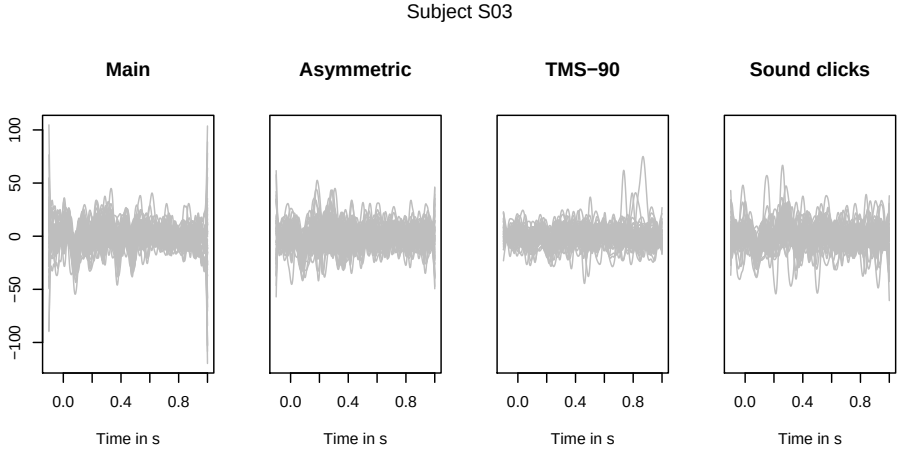

FIGURE A.2: Estimated 'brain' signals of interest by each experimental condition for subject S03

It should also be noted that one replicate each from the following sets - subject S03 TMS-90, subject S03 sound clicks and subject S10 main condition - were eliminated from the analysis due to being estimated as anomalous signals with very large amplitudes.

The visual inspection of the estimated 'brain' signals of interest from the EEG data set is followed by the characterisation of these signals into phase, frequency and

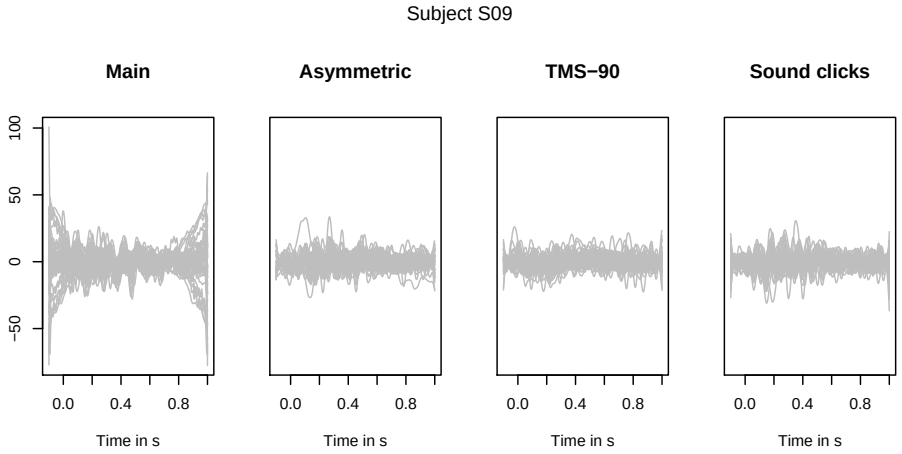

FIGURE A.3: Estimated 'brain' signals of interest by each experimental condition for subject S09

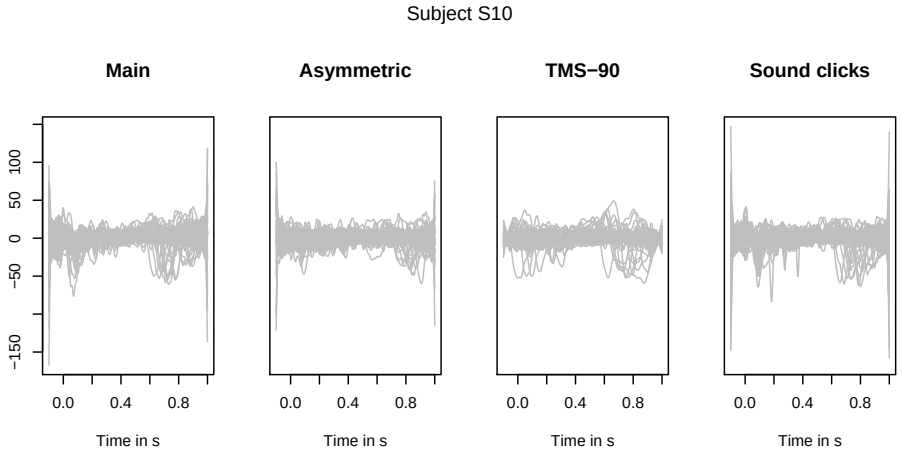

FIGURE A.4: Estimated 'brain' signals of interest by each experimental condition for subject S10

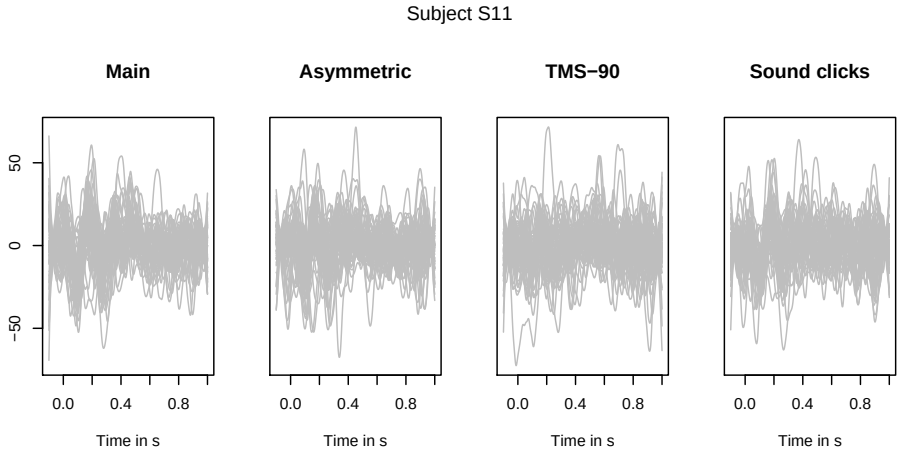

FIGURE A.5: Estimated 'brain' signals of interest by each experimental condition for subject S11

amplitude curves. Fig. A.6, Fig. A.7 and Fig. A.8 illustrate these characteristic functions respectively along with the mean functions (by a red solid line) and estimates of confidence curve, 2 standard deviations around the respective mean curve(by blue dotted lines). The vertical dotted red lines mark the time point where the 5 TMS pulses are administered.

The mean phase curves show mean oscillations between 10 and 11 Hz in a span of 1.1s as a gradually increasing almost linear function. So the signals are on an average in the α band of frequencies for all the experimental conditions in all subjects (see Fig. A.6 and Fig. A.7). However, the standard deviation curves around the functional mean tend to come closer to the mean curve, during or immediately after the stimulus is administered, especially for the main experimental condition. This observation leads to the mixed model for testing if the average standard deviations around mean frequencies decrease with stimulation, after accounting for random effect of subjects. The amplitude functions in Fig. A.8 do not clearly show enhancement of signal amplitude during or after the TMS stimulus in any of the subjects. The values of the average amplitude between two TMS pulses are treated as repeated measurements in the mixed models setting to test for further evidence of enhancement of signals accounting for differences due to experimental conditions and phase as the onset of the TMS stimuli. These models based on the data from S02 (illustrated in Chapter 3) and the 5 subjects summarised here to explain entrainment are fully described and reported in Chapter 4.

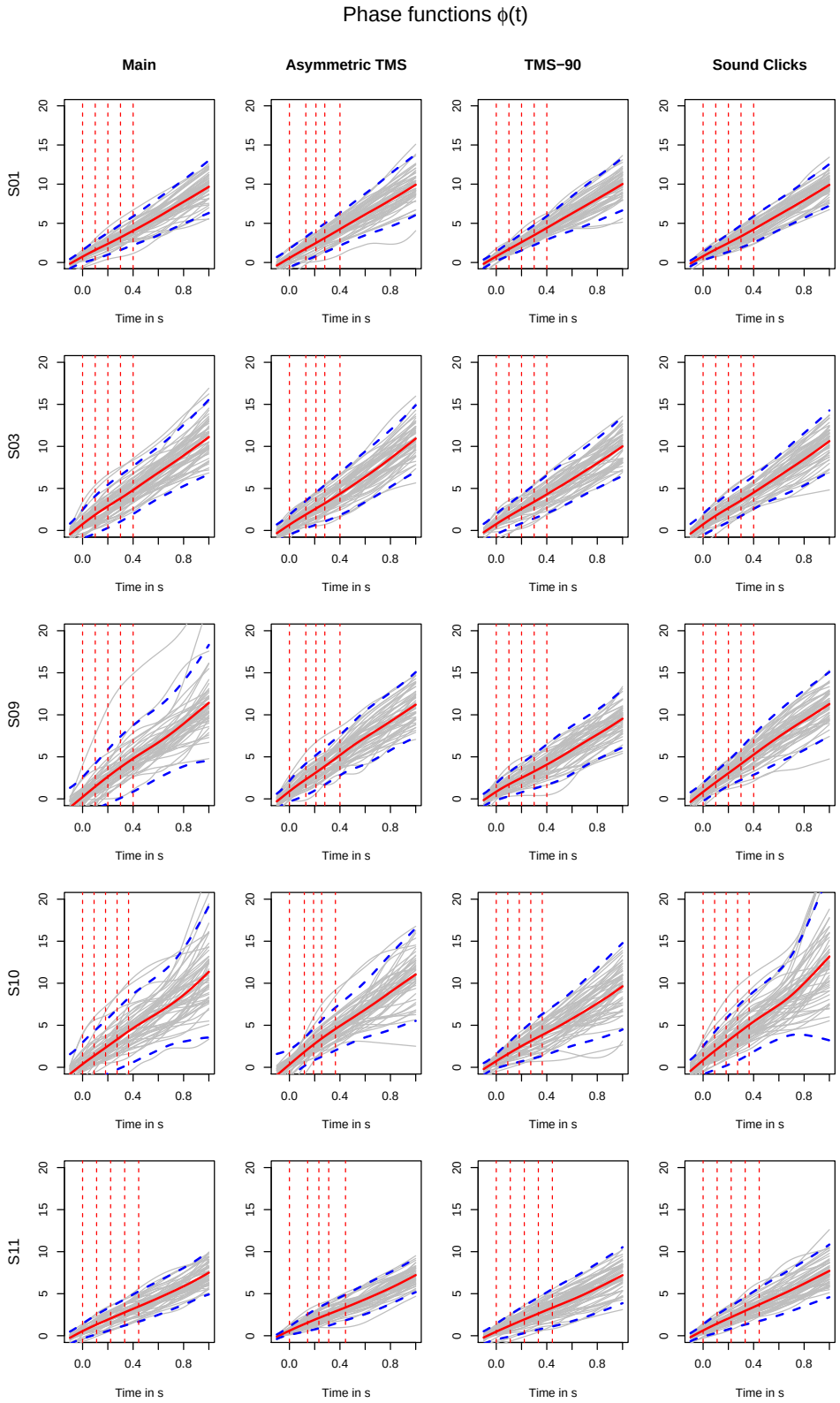

FIGURE A.6: Estimated phase functions by each experimental condition for subjects S01, S03, S109, S10 and S11 with corresponding functional mean (red) and functional standard deviation functions (blue dotted). The vertical red dotted lines represent the time points where the 5 TMS pulses occurred.

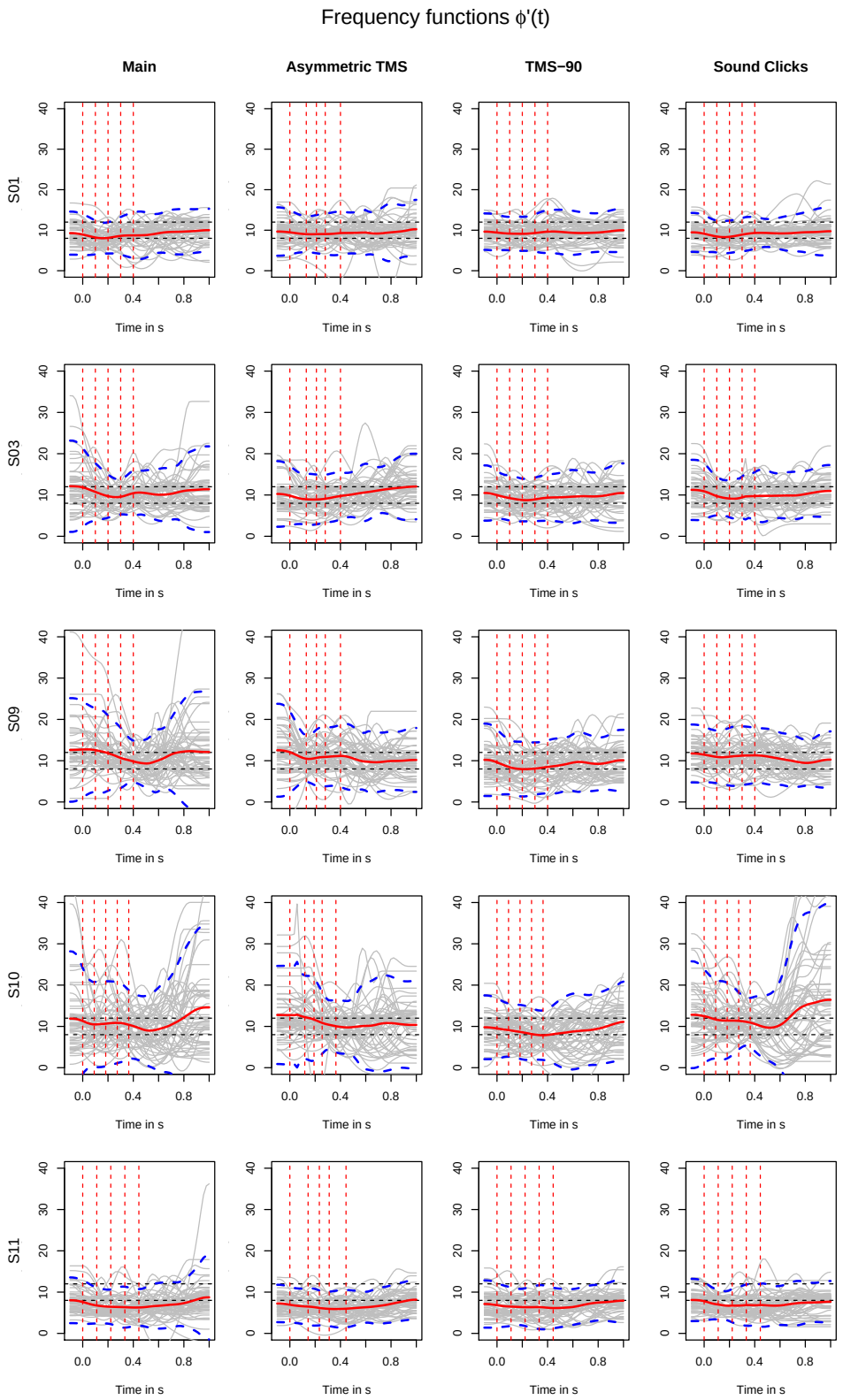

FIGURE A.7: Instantaneous frequency functions (estimated as the first derivative of the phase functions) by each experimental condition for subjects S01, S03, S109, S10 and S11 with corresponding functional mean (red) and functional standard deviation functions (blue dotted). The vertical red dotted lines represent the time points where the 5 TMS pulses occurred.

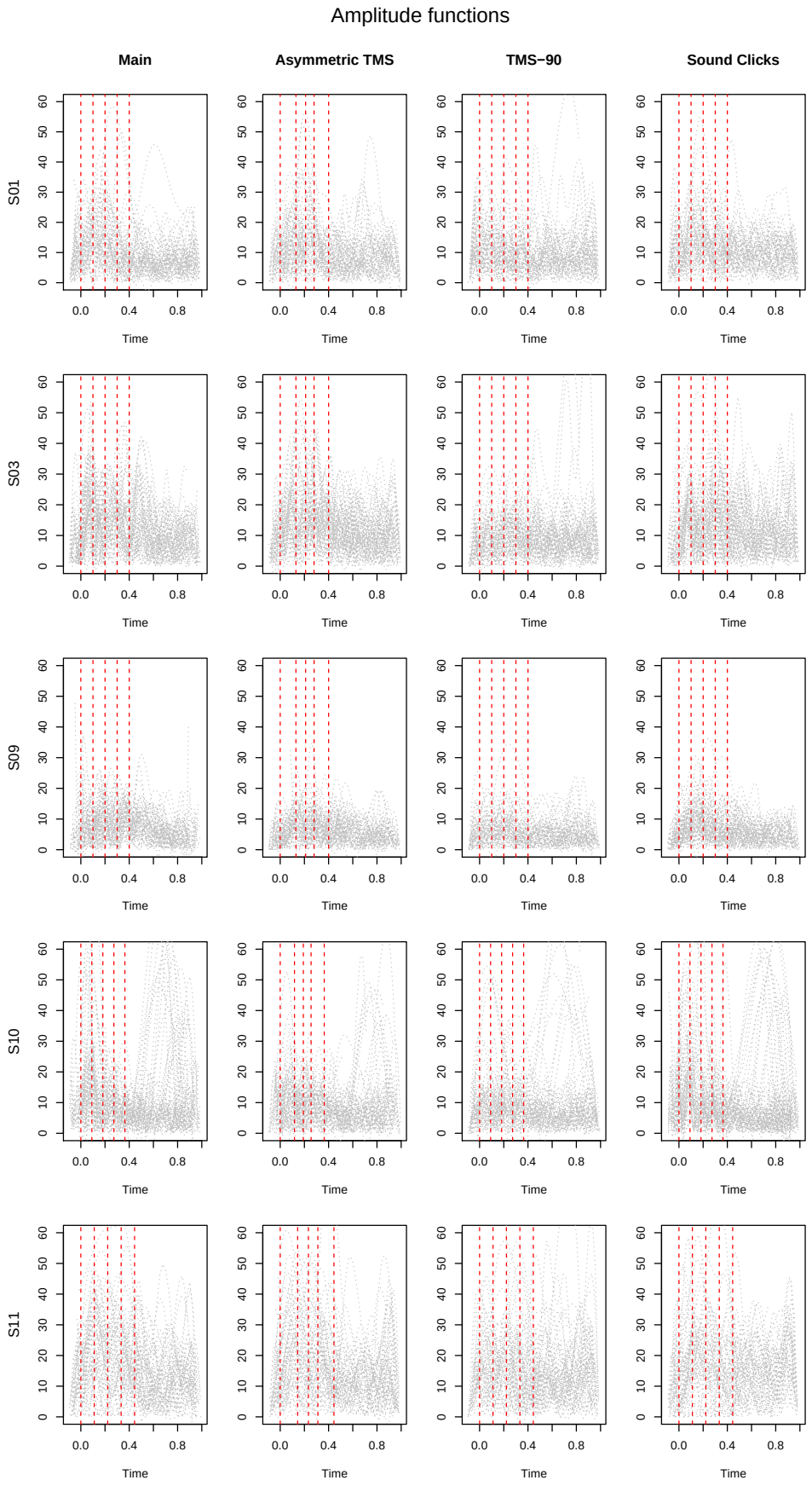

FIGURE A.8: Amplitude functions by each experimental condition for subjects S01, S03, S109, S10 and S11. The vertical red dotted lines represent the time points where the 5 TMS pulses occurred.

A.2 Characterisation and Summary of additional subjects in the pre-stimulus MEG data

Estimated curves for the functional mean frequency of the two poles for the additional 12 subjects are summarised in Fig. A.9 along with their corresponding functional mean (red solid line) and 2 standard deviations around the functional mean (blue dotted lines) for each subject in the pre-stimulus data. The mean amplitude function of the two poles from each dipole is also summarised for each remaining subject in Fig. A.10. The red solid line represents the functional mean curves of all the replicates of each subject, and the blue dotted curves represent the functional curves spanning 2 standard deviations around this mean.

It can be seen that the mean frequency curves in the pre-stimulus period lie in the α band of frequencies ($8 - 12$ Hz) in all the subjects. However, the curves corresponding to 2 standard deviations around the mean frequencies lie outside the α range in all the subjects which corroborate with the results from the other three subjects illustrated in Chapter 3. A possible explanation of this is the fact that this is data from the pre-stimulus period of the study. So it may be expected that the frequency of the dipole detected is not necessarily bound to the α band during this time scale. There is not a lot of variation evident on visual inspection in the frequency curves between subjects. However, within each subject, the instantaneous frequency seems to vary between 5 and 30 Hz. There is considerable variation in amplitude both within subjects (from replicate to replicate) as well as between subjects. For example, subjects JOE22, RBE13 and VIA12 have very low mean amplitude curves and narrow 2SD confidence bands around mean amplitudes as compared subjects CDE04 and DBD12. These patterns of variation between and within subjects conforms to the findings from the illustrative subjects used in Chapter 3 and are accounted for in the mixed model framework proposed for analysing this data set, as detailed in Chapter 5.

Fig. A.11 summarises the spatial features of the dipoles in terms of their location, sizes, strength and orientation. The greyscale is indicative of the dipolar strength,

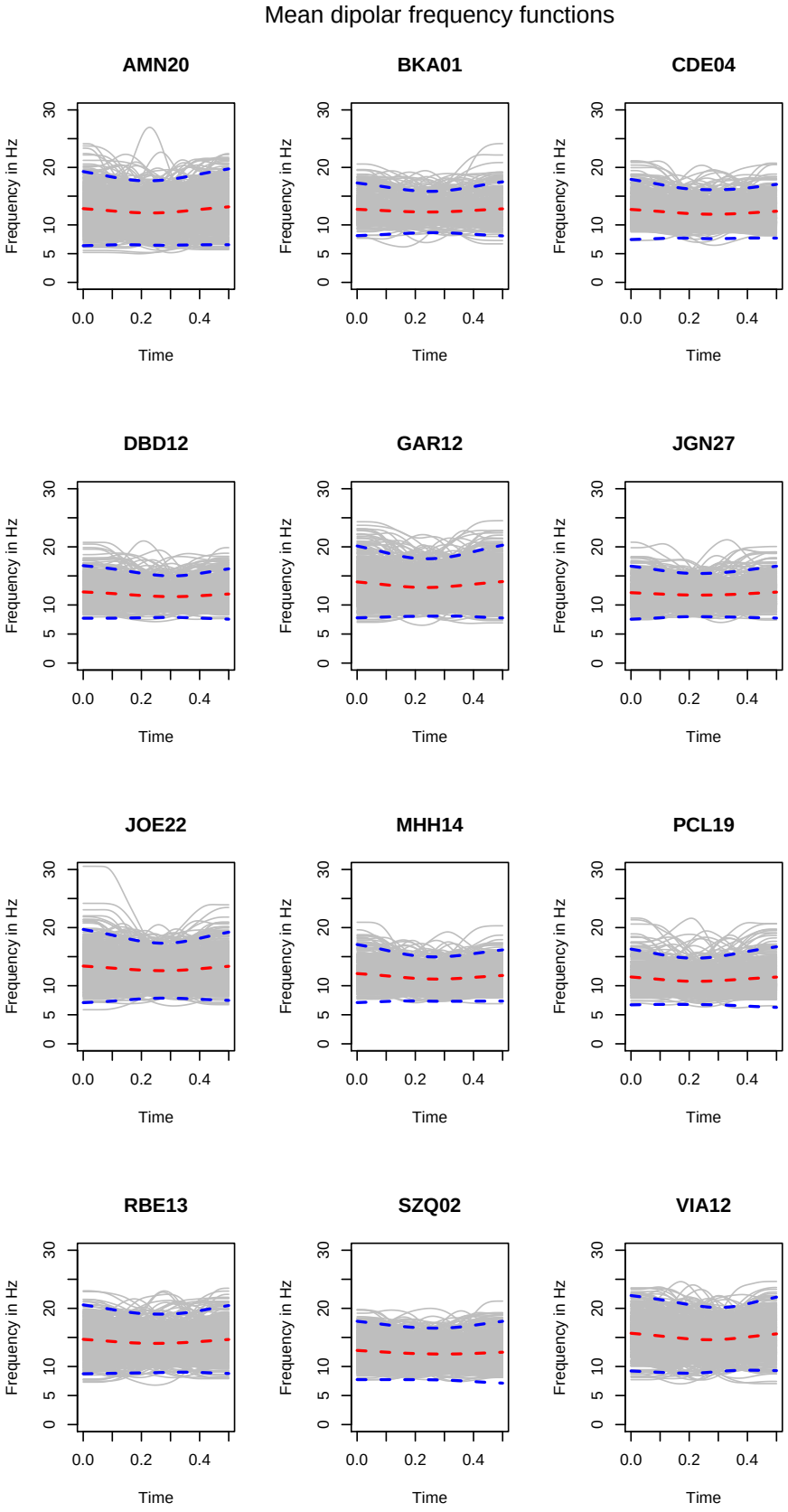

FIGURE A.9: Mean frequency functions for each dipoles for all replicates in 12 subjects from the MEG data set with corresponding functional mean (red solid line) and 2 standard deviations around the functional mean (blue dotted line)

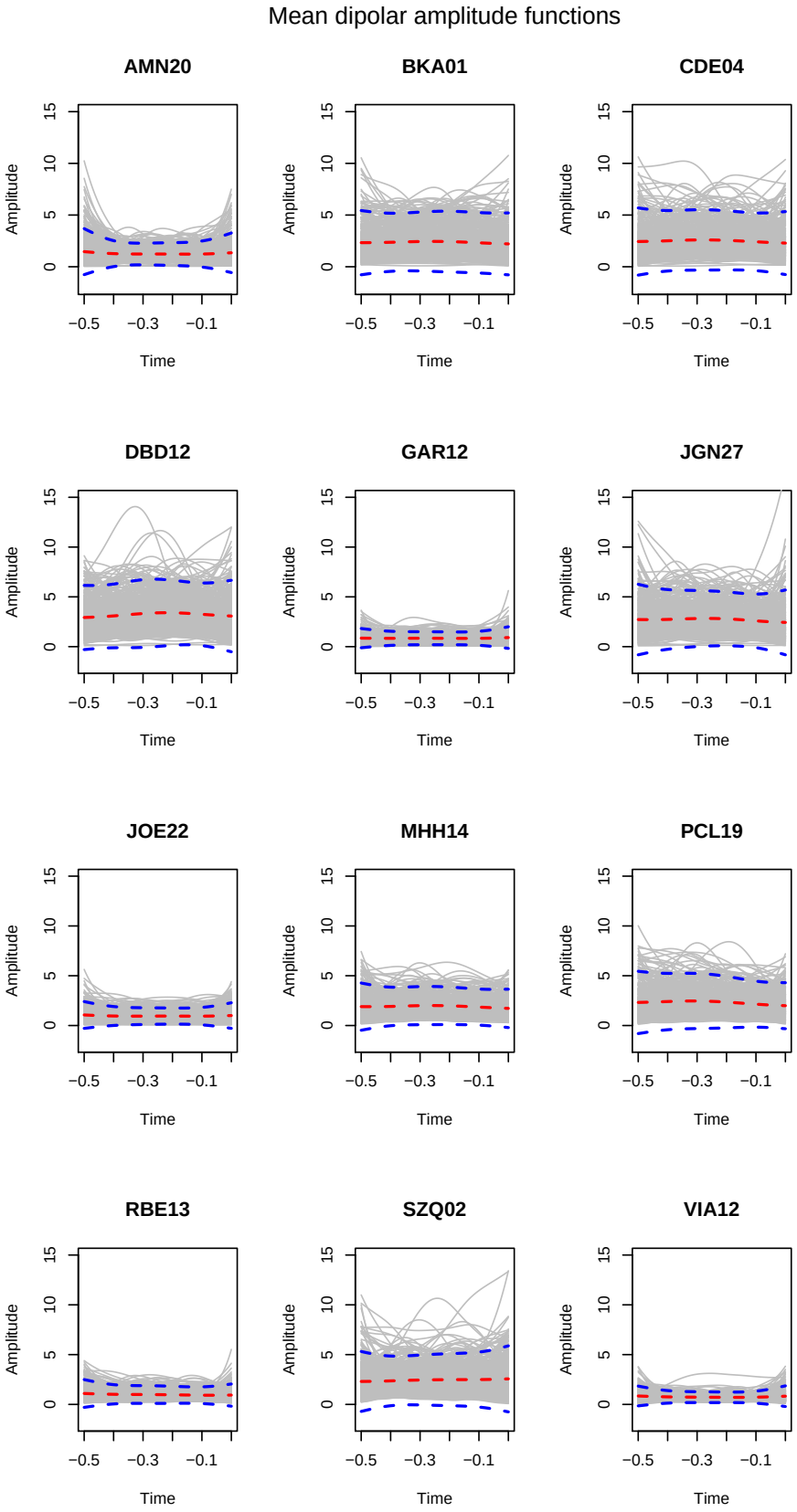

FIGURE A.10: Mean amplitude functions for each dipoles for all replicates in 12 subjects from the MEG data set with corresponding functional mean (red solid line) and 2 standard deviations around the functional mean (blue dotted line)

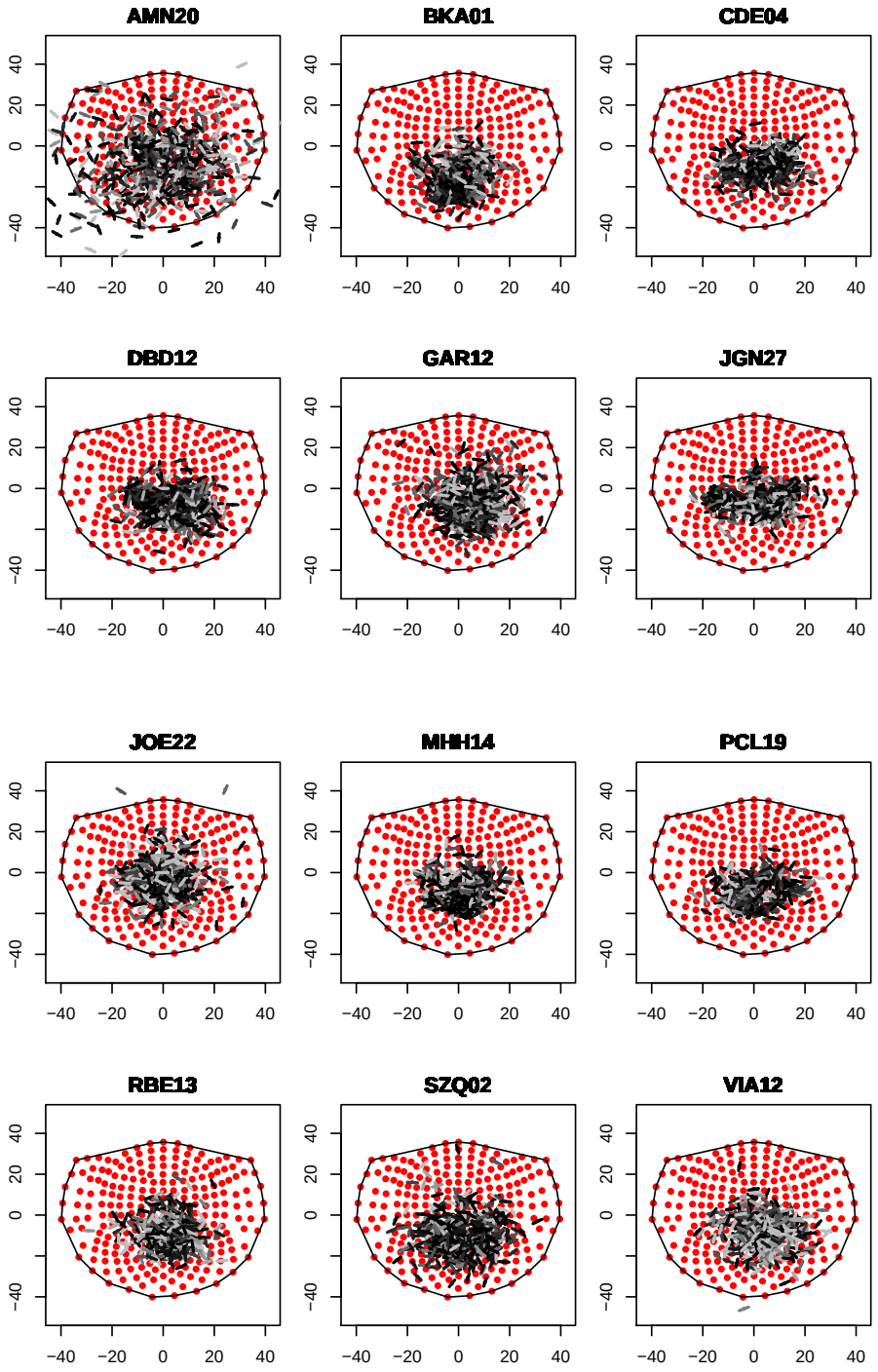

FIGURE A.11: Spatial distribution of dipoles in all replicates for additional 12 subjects with greyscale indicating strength of the dipoles, length indicating the size of the dipoles and the tilt indicating the orientation of one pole relative to the other.

with black showing strong and pale grey depicting a weak dipolar activity. The slant or tilt of the dipoles indicates the orientation of one pole relative to the other. The location of the dipole is demonstrated by the position with reference to the outline of the human head. The length of the line captures the size of the dipole and is a measured by the span of the number of sensors in the region that detects dipolar activity. It can be seen that some of the estimated locations of the dipoles lie outside the head. This is especially prominent in subject AMN20 and need further investigation and refinement of the search algorithm as proposed in the future work outlined in Chapter 6.

Dipolar strength of the dipoles detected in the pre-stimulus period vary in magnitude as well as over time. These variations in magnitude are summarised in Fig. A.12 and the variability over time are depicted in Fig. A.13, with a dotted red line tracing the smooth mean curve of the dipolar strength. It can be seen that the mean and standard deviations of the dipolar strength of the strongest dipole detected for each replicate varies between subjects (Fig. A.12). The mean strength of the dipoles is stronger for some subjects than others. This variation is accounted for in the mixed model for dipole strength described in Chapter 5, while controlling for random effect due to subject. The distribution over time of the occurrence of dipoles varies randomly (Fig. A.13) in all subjects, although very small peaks are visible in some of the mean curves (e.g., between 0.1 and 0.2s in RBE13) indicating that the dipoles in these regions are stronger.

The average dipolar frequency, average dipolar amplitude and dipolar strength curves are modelled in a functional mixed model setting as described in Chapter 5.

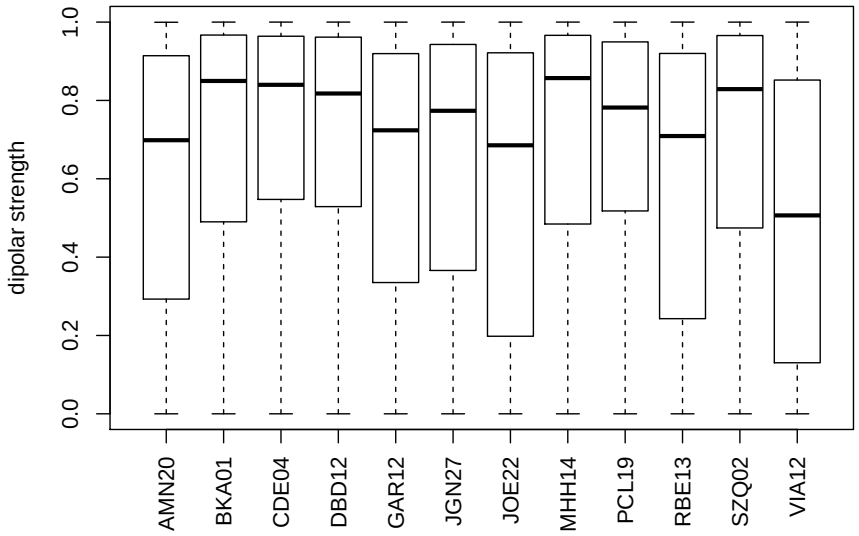

FIGURE A.12: Distribution of maximum dipolar strength across all replicates for the 12 subjects

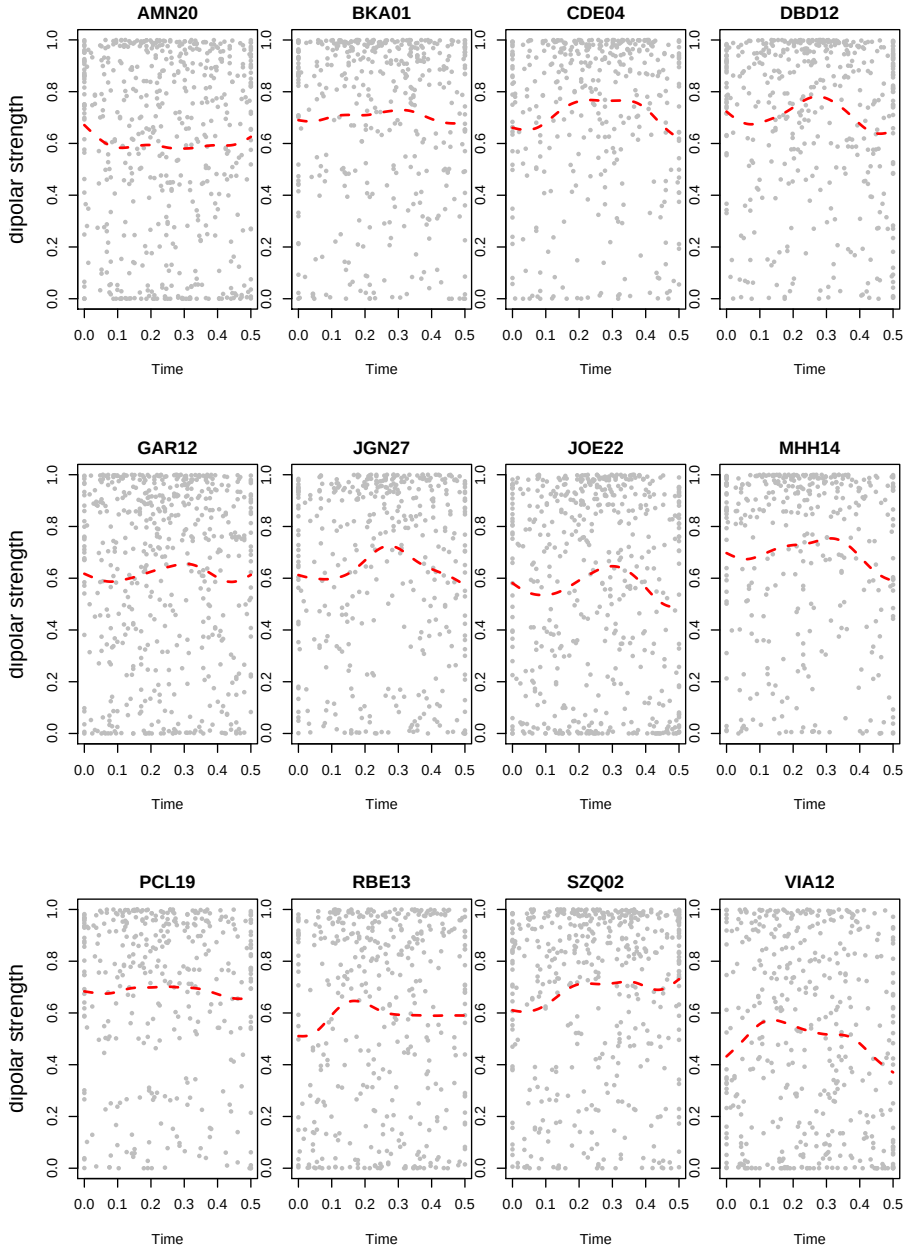

FIGURE A.13: Spread of the maximum dipolar strength over time across all replicates for the 12 subjects;

Bibliography

Antoniadis, A. and Sapatinas, T. (2007). Estimation and inference in functional mixed-effects models. *Computational Statistics and Data Analysis*, 51(10):4793 – 4813.

Barker, A., Jalinous, R., and Freeston, I. (1985). Non-invasive magnetic stimulation of human brain cortex. *The Lancet*, 325(8437):1106 – 1107. Originally published as Volume 1, Issue 8437.

Boashash, B. (1992). Estimating and interpreting the instantaneous frequency of a signal - part i: Fundamentals. *Proceedings of the IEEE*, 80(4):520–538.

Bosq, D. (2000). *Linear processes in function spaces. Lectures notes in Statistics.* Springer Verlag.

Bowman, A. W. and Azzalini, A. (1997). *Applied Smoothing Techniques for Data Analysis : The Kernel Approach with S-Plus Illustrations: The Kernel Approach with S-Plus Illustrations.* Oxford University Press, Oxford.

Bowman, A. W. and Azzalini, A. (2003). Computational aspects of nonparametric smoothing with illustrations from the sm library. *Comput. Stat. Data Anal.*, 42(4):545–560.

Bugli, C. and Lambert, P. (2006). Functional anova with random functional effects: an application to event-related potentials modelling for electroencephalograms analysis. *Computational Statistics and Data Analysis*, 25(21):3718–3739.

Cardoso, J. (1998a). Blind signal separation: statistical principles. *Proceedings of the IEEE*, 9(10):2009–2015.

Cardoso, J. (1998b). Multidimensional independent component analysis. *In Proc. ICASSṔ98, Seattle, WA*.

Carreira-Perpiñán, M. (1997). Density networks for dimension reduction of continuous data: Analytical solutions. *Technical report CS-97-09, Dept. of Computer Science, University of Sheffield, UK*.

Catherine E. Davey, David B. Grayden, G. F. E. L. A. J. (2013). Filtering induces correlation in fmri resting state data. *NeuroImage*, 64:728–740.

Chen, H. and Wang, Y. (2011). A penalized spline approach to functional mixed effects model analysis. *Biometrics*, 67(3):861–870.

Chiou, J., Müller, H., and Wang, J. (2003). Functional quasi-likelihood regression models with smooth random effects. *Journal of the Royal Statistical Society, Series B*, 65:405–423.

Cleveland, W. (1979). Robust locally weighted regression and smoothing scatterplots. *J. Amer. Statist.Assoc.*, 74:829–836.

Comon, P. (1994). Independent component analysis - a new concept? *Signal Processing*, 36:287–314.

Crainiceanu, C. M., Ruppert, D., Carroll, R., Adarsh, J., and Goodner, B. (2007). Spatially adaptive penalized splines with heteroscedastic errors. *Journal of Computational and Graphical Statistics*, 16(2).

Craven, P. and Wahba, G. (1979). Smoothing noisy data with spline functions. estimating the correct degree of smoothing by generalized cross-validation. *Numerische Mathematik*, 31:377–403.

De Boor, C. (1978). *A Practical Guide to Splines*. Spring Verlag, New York.

De Graaf, T. A., Gross, J., Paterson, G., Rusch, T., Sack, A. T., and Thut, G. (2013). Alpha-band rhythms in visual task performance: Phase-locking by rhythmic sensory stimulation. *PLoS ONE*, 8(3):e60035.

Delicado, P., Giraldo, R., Comas, C., and Mateu, J. (2010). Statistics for spatial functional data: some recent contributions. *Environmetrics*, 21(3-4):224–239.

Di, C., Crainiceanu, C., Caffo, B., and Punjabi, N. (2009). Multilevel functional principal component analysis. *Ann Appl Stat*, 3(1):458–488.

Diggle, P., Heagerty, P., Liang, K.-Y., and Zeger, S. (2002). *Analysis of Longitudinal Data*. OUP, Oxford, UK, 2 edition.

Diggle, P. J. and Verbyla, A. P. (1998). Nonparametric estimation of covariance structure in longitudinal data. *Biometrics*, 54(2):401–415.

Eilers, P. H. (2010). The smooth complex logarithm and quasi-periodic models. In Kneib, T. and Tutz, G., editors, *Statistical Modelling and Regression Structures*. Physica-Verlag HD, Berlin Heidelberg.

Eilers, P. H. and Marx, B. D. (1996). Flexible smoothing with b-splines and penalties. *Statistical science*, pages 89–102.

Eilers, P. H. and Marx, B. D. (2002). Generalized linear additive smooth structures. *Journal of Computational and Graphical Statistics*, 11:735751.

Fan, J. (1993). Local linear regression smoothers and their minimax efficiencies. *Ann. Statist.*, 21:196216.

Fan, J. and Gijbels, I. (1992). Variable bandwidth and local linear regression smoothers. *Ann. Statist.*, 20:2008–2036.

Fan, J., Huang, T., and Li, R. (2007). Analysis of longitudinal data with semiparametric estimation of covariance function. *Journal of the American Statistical Association*, 102:632641.

Fan, J. and Marron, J. (1994). Fast implementations of nonparametric curve estimators. *J. Comput. Graph. Statist.*, 3:3556.

Friston, K., Josephs, O., Zarahn, E., Holmes, A., Rouquette, S., and Poline, J. (2000). To smooth or not to smooth?: Bias and efficiency in fmri time-series analysis. *NeuroImage*, 12(2):196–208.

Golub, G. H., Heath, M., and Wahba, G. (1979). Generalized cross-validation as a method for choosing a good ridge parameter. *Technometrics*, 21(2):215–223.

Gonzalez-Moreno, A., MAurtenetxe, S., Lopez-Garcia, M.-E., Pozob, F. d., Maestu, F., and Nevado, A. (2014). Signal-to-noise ratio of the meg signal after preprocessing. *Journal of Neuroscience Methods*, 222:56–61.

Guo, W. (2002). Functional mixed effects models. *Biometrics*, 58(1):121–128.

Hallett, M. (2000). Transcranial magnetic stimulation and the human brain. *Nature*, 406(6972):147 – 150.

Härdle, W. (1987). Algorithm as 222: resistant smoothing using the fast fourier transform. *Appl. Statist.*, 36:104111.

Härdle, W. and Scott, D. (1992). Smoothing by weighted average of rounded points. *Comput. Statist.*, 7:97128.

Harville, D. (1977). Maximum likelihood approaches to variance component estimation and to related problems. *Journal of the American Statistical Association*, 72:320–340.

Hastie, T. and Tibshirani, R. (1986). Generalized additive models. *Statistical Science*, 1(3):297–310.

Haufe, S., Dähne, S., and Nikulin, V. V. (2014). Dimensionality reduction for the analysis of brain oscillations. *NeuroImage*, 101:583–597.

Herrmann, C. S. (2001). Human eeg responses to 1100 hz flicker: resonance phenomena in visual cortex and their potential correlation to cognitive phenomena. *Experimental Brain Research*, 137(3-4):346–353.

Hurvich, C. M., Simonoff, J. S., and Tsai, C.-L. (1998). Smoothing parameter selection in nonparametric regression using an improved akaike information criterion. *Journal of the Royal Statistical Society. Series B (Statistical Methodology)*, 60(2):271–293.

Hyvärinen, A. (1999a). Fast and robust fixed-point algorithms for independent component analysis. *IEEE Transactions on Neural Networks*, 10(3):626634.

Hyvärinen, A. (1999b). The fixed-point algorithm and maximum likelihood estimation for independent component analysis. *Neural Processing Letters*, 10(1):1–5.

Hyvärinen, A. (1999c). Survey on independent component analysis. *Neural Computing Surveys*, 2:94–128.

Hyvärinen, A. and Oja, E. (1997). A fast fixed-point algorithm for independent component analysis. *Neural Computation*, 9(7):1483–1492.

Ilmoniemi, R. J., Virtanen, J., Ruohonen, J., Karhu, J., Aronen, H. J., Ntnen3, R., and Katila, T. (1997). Neuronal responses to magnetic stimulation reveal cortical reactivity and connectivity. *NeuroReport*, 8:3537–3540.

James, G. (2002). Generalized linear models with functional predictors. *Journal of the Royal Statistical Society, Series B*, 64:411–432.

James, G., Hastie, T., and Sugar, C. (2001). Principal component models for sparse functional data. *Biometrika*, 87:587–602.

Jones, M., Marron, J., and Sheather, S. (1996). A brief survey of bandwidth selection for density estimation. *Journal of the American Statistical Association*, 91(433):401–407.

Jutten, C. and Herault, J. (1991). Blind separation of sources, part i: An adaptive algorithm based on neuromimetic architecture. *Signal Processing*, 24:1–10.

Jutten, C., Herault, J., and Guerin, A. (1988). *IN.C.A: an independent component analyzer based on an adaptive neuromimetic network*. Manchester Press.

J.Z., H., Liu, N., Pourahmadi, M., and Liu, L. (2006). Covariance matrix selection and estimation via penalized normal likelihood. *Biometrika*, 93:8598.

Kauermann, G. and Wegener, M. (2011). Functional variance estimation using penalized splines with principal components analysis. *Statistics and Computing.*, 21:159171.

Komssi, S., Kahkonen, S., and Ilmoniemi, R. J. (2004). The effect of stimulus intensity on brain responses evoked by transcranial magnetic stimulation. *Hum Brain Mapp*, 21:154–164.

Krafty, R., Gimotty, P., Holtz, D., Coukos, G., and Guo, W. (2008). Varying coefficient model with unknown within-subject covariance for analysis of tumor growth curves. *Biometrics*, 64(4):1023–1031.

Laird, N. M. and Ware, J. H. (1982). Random-effects models for longitudinal data. *Biometrics*, 38(4):pp. 963–974.

Mathewson, K. E., Prudhomme, C., Fabiani, M., Beck, D. M., Lleras, A., and Gratton, G. (2012). Making waves in the stream of consciousness: Entraining oscillations in eeg alpha and fluctuations in visual awareness with rhythmic visual stimulation. *Journal of Cognitive Neuroscience*, 24(12):2321 – 2333.

McCulloch, C. E. and Searle, S. R. (2005). *Generalized, Linear, and Mixed Models*. John Wiley and Sons, Inc.

McLean, R., Sanders, W., and Stroup, W. (1991). A unified approach to mixed linear models. *The American Statistician*, 45:54–64.

Miniussi, C. and Thut, G. (2009). Combining tms and eeg offers new prospects in cognitive neuroscience. *Brain Topogr*, 2:58–80.

Moskowitz, M. A. (2002). *A Course in Complex Analysis in One Variable*. World Scientific Publishing Co.

Müller, H. and Stadtmüller, U. (2005). Generalized functional linear models. *The Annals of Statistics*, 33(2):774–805.

Naeem, M., Brunner, C., and Pfurtscheller, G. (2009). Dimensionality reduction and channel selection of motor imagery electroencephalographic data. *Computational Intelligence and Neuroscience*, 2009.

Nikulin, V., Nolte, G., and Curio, G. (2011). A novel method for reliable and fast extraction of neuronal eeg/meg oscillations on the basis of spatio-spectral decomposition. *Neuroimage*, 55(4):1528–1535.

O'Sullivan, F. (1986). A statistical perspective on ill-posed inverse problems. *Statistical Science*, 1:505527.

Park, B. and Turlach, B. (1992). Practical performance of several data driven bandwidth selectors. *Computational Statistics*, 7:251–270.

Patterson, H. and Thompson, R. (1971). Recovery of inter-block estimation when block sizes are unqual. *Biometrika*, 58:545–554.

Pernet, C., Sajda, P., and Rousselet, G. (2011). Single-trial analyses: why bother? *Front. Psychology*, 2:322.

Pinheiro and Bates (2000). *Mixed Effects Models in S and S-Plus*. Springer.

Ramsay, J. and Dalzell, C. (1991). Some tools for functional data analysis. *Journal of the Royal Statistical Society. Series B (Methodological)*, 53:539–572.

Ramsay, J. and Silverman, B. (1997). *Functional Data Analysis*. Springer.

Ramsay, J. and Silverman, B. (2002). *Applied functional data analysis - methods and case studies*. Springer, New York.

Ramsay, J. and Silverman, B. (2005). *Functional Data Analysis*. Springer, New York, 2 edition.

Rice, J. and Wu, C. (2001). Nonparametric mixed effects models for unequally sampled noisy curves. *Biometrics*, 57:253259.

Romei, V., Gross, J., and Thut, G. (2010). On the role of prestimulus alpha rhythms over occipito-parietal areas in visual input regulation: Correlation or causation? *The Journal of Neuroscience*, 30(25):8692–8697.

Ruppert, D. (2002). Selecting the number of knots for penalized splines. *J. Comput. Graph. Stat.*

Ruppert, W. and Carroll (2003). *Semiparametric Regression*.

Salehin, S. and Abhayapala, T. (2010). Time-frequency domain fundamental frequency estimation and localization of quasiperiodic, pulsatic signal in a correlated mixture. In *Signal Processing and Communication Systems (ICSPCS), 2010 4th International Conference on*, pages 1–4.

Schnitzler, A. and Gross, J. (2005). Normal and pathological oscillatory communication in the brain. *Nature Reviews Neuroscience*, 6(4):285296.

Searle, S. S., Casella, G., and McCulloch, C. E. (2006). *Variance Components*. John Wiley and Sons, Inc.

Silverman, B. (1982). Algorithm as 176: kernel density estimation using the fast fourier transform. *Appl. Statist.*, 31:9399.

Spaak, E., de Lange, F. P., and Jensen, O. (2014). Local entrainment of alpha oscillations by visual stimuli causes cyclic modulation of perception. *Journal of Neuroscience*.

Staicu, A.-M., Crainiceanu, C., and Carroll, R. (2010). Fast methods for spatially correlated multilevel functional data. *Biostatistics*, 8:129.

Stone, M. (1974). Cross-validatory choice and assessment of statistical predictions. *Journal of the Royal Statistical Society. Series B (Methodological)*, 36(2):111–147.

Tanabe, J., Miller, D., Tregellas, J., Freedman, R., and Meyer, F. G. (2002). Comparison of detrending methods for optimal fmri preprocessing. *NeuroImage*, 15(4):902–907.

Thut, G., Schyns, P. G., and Gross, J. (2011a). Entrainment of perceptually relevant brain oscillations by non-invasive rhythmic stimulation of the human brain. *Frontiers in psychology*, 2.

Thut, G., Veniero, D., Romei, V., Miniussi, C., Schyns, P. G., and Gross, J. (2011b). Rhythmic tms causes local entrainment of natural oscillatory signatures. *Current Biology*, 21:1176–1185.

Ventrucci, M., Bowman, A. W., Miller, C., and Gross, J. (2014). Quasiperiodic spatiotemporal models of brain activation in single-trial meg experiments. *Statistical Modelling*, 14(5):417–437.

Ventrucci, M., Miller, C., Gross, J., Schoffelen, J.-M., and Bowman, A. W. (2011). Spatiotemporal smoothing of single trial {MEG} data. *Journal of Neuroscience Methods*, 200(2):219 – 228.

Vonesh, E. and Chinchilli, V. (1997). *Linear and Non linear Models for the Analysis of Repeated Measures.* Marcell Dekker, New York.

Wand, M. and Jones, M. (1995). *Kernel Smoothing.* Chapman & Hall, London.

Wang, N., Carroll, R., and Lin, X. (1998). Efficient semiparametric marginal estimation for longitudinal/clustered data. *Journal of the American Statistical Association*, 100:147–157.

Wood, S. (2006). *Generalized additive models: an introduction with R.* CRC press.

Wu, W. B. and Pourahmadi, M. (2003). Nonparametric estimation of large covariance matrices of longitudinal data. *Biometrika*, 90:831844.

Yao, F., Müller, H., and Wang, J. (2005). Functional linear regression analysis for longitudinal data. *Journal of the American Statistical Association*, 33:2873–2903.

Yao, F., Müller, H., and Wang, J. (2006). Penalized spline models for functional principal component analysis. *Journal of the Royal Statistical Society. Series B*, 68:3–25.

Zhang, L., Samaras, D., Tomasi, D., Alia-Klein, N., Cottone, L., Leskovjan, A., Volkow, N., and Goldstein, R. (2005). Exploiting temporal information in functional magnetic resonance imaging brain data. *Med Image Comput Comput Assist Interv.*, 8(1):679–687.